Dissertation

PRECLINICAL CHARACTERIZATION OF BIORESORBABLE MAGNESIUM IMPLANTS FOR OSTEOSYNTHESIS

submitted by

Dr.med.univ. Mag.rer.nat Stefan Franz FISCHERAUER

for the Academic Degree of

Doctor of Medical Science

at the

Medical University of Graz

Institute of Orthopaedics and Orthopaedic Surgery

Institute of Trauma Surgery

under the Supervision of

Assoz.-Prof. Priv.-Doz. Dr.med.univ. Annelie-Martina WEINBERG, MBA

Univ.-Prof. Dr.rer.nat. Klaus-Dieter KÜHN

Dr.med.univ. Tanja KRAUS

Graz, 2015

Statutory Declaration

I hereby declare that this dissertation is my own original work and that I have fully acknowledged by name all of those individuals and organisations that have contributed to the research for this dissertation. Due acknowledgement has been made in the text to all other material used. Throughout this dissertation and in all related publications I followed the guidelines of "Good Scientific Practice Date.

Graz, 12.02.2014 *Stefan Franz Fischerauer*

Dedicated to
my parents and Sandra

Preface

"A biomaterial is a nonviable material used in a medical device, intended to interact with biological systems." (Williams, 1987)

In early days, natural materials that were available in the environment were used as biomaterials. In the first known description of medical fracture management (the Edwin Smith Papyrus of Ancient Egypt, circa 2600_{BC}), a splint and bandage with honey, grease, and lint were used for a humerus fracture stabilization [1]. About 2000 years ago, the Chinese, Aztecs and Romans were already using soft and malleable gold to fill tooth cavities, and high strength, relatively lightweight wood for limb and tooth prosthetics [2]. Some of this treatment protocols remained for over 4000 years. The oldest implants for internal fixation of fractures were made from various materials (ivory, bone, and metals of bronze, lead, gold, copper, silver, brass, steel, and aluminum alloys) [3]. With ivory and bone used as pegs for intramedullary fixation, also the first materials that showed the ability to be reabsorbed by the body have been applied [4, 5]. Nicholas Senn, an American surgeon, who performed pioneering work on the application of ivory and bony fixation devices, can in that regard be called the father of biodegradable implants [6, 7]. Just in the last 150 years the advancement of techniques and technology and the effort of several important surgeons were responsible for further development and improvement of biomaterial devices. Naturally occurring biomaterials were ousted by synthetically produced polymers, alloys, and composites. These novel materials had numerous advantages, including enhanced mechanical, chemical and biological performance, improved functionality, and high reproducibility [2]. The first study of metallurgy in internal fracture fixation was performed by H.S. Levert in 1829. Levert studied platinum, lead, silver, and gold in vivo to understand the biocompatibility of each metal [8]. The inventions of anaesthesia (William Thomas Green Morton 1846), antisepsis (Joseph Lister 1865) and X-rays (Wilhelm Conrad Röntgen 1895) were mainly responsible for further influences of operative treatment methods of fractures [7]. Developments of all kinds of osteosynthesis, i.e. plates (Hansmann 1886), external fixation (Parkhill 1897) and intramedullary nails (Schöne 1913) followed [7]. In that consent the first textbook to deal

with osteosynthesis "Traité de l'immobilisation directe des fragments osseux dans lesfractures" was published in 1870 by Laurent Jean Baptiste Bérenger-Féraud [9].

The most influential pioneer of using magnesium (Mg) as a biomaterial was the physician Erwin Payr from Graz, Austria whose versatile clinical applications and reports inspired many other clinicians to advance the field of biodegradable magnesium implants to various surgical areas [10]. Erwin Payr performed his first experiments on Mg resorption in 1892 [11]. In 1898, Payr was supplied with barely available biodegradable devices in forms of pure Mg sheets and plates, pins, spheres, wires, pegs, cramps and nails from the company I. Rohrbeck in Vienna, Austria for animal and human trials [11, 12]. It was Lambotte and Verbrugge, who recommended the use of Mg implants for osteoynthetic applications in several clinical areas including supra- and condylar fractures in children, lower arm diaphyseal fractures, malleolus fractures, and phalanx and metacarpal fractures, after performing clinical investigations in children around 1906 [13, 14] (notable that the same clinical indications are discussed nowadays again). However, as controlling mechanism of corrosion behavior of Mg in vivo had not been resolved, Mg was pushed into the background parallel to the development of vanadium steel (William O'Neil Sherman, 1912) [15], corrosion resistant stainless steel (1931) [16], cobalt alloys (Charles Scott Venable and Walter Goodloe Stuck in 1936) [17], and titanium alloys (Gottlieb Leventhal in 1951) [18]. Mg was as a consequence no longer investigated as a material for medical application [19].

Rapid advancements in material synthesis, fabrication and modification techniques, the molecular biology revolution of the 1970s and advances in genomics and proteomics in the 1990s and 2000s, and the demand for extended improvement of the health and wellbeing of humankind have paved the way for a rapidly expanding market and the fully potential of biomaterials development [2]. Modern materials are required to enhance device performance, to improve function, deliver biactive compounds and achieve the goal of tissue regeneration [20]. These demands transitioned the biomaterials science from a practitioner-driven discipline to a multidisciplinary field of science [2]. Biomaterials are nowadays investigated and developed in an interdisciplinary manner according to their complex relationship between chemical and physical properties and the biological response they illicit in vitro and in vivo [2].

The demand for short-term, non-permanent implants is set especially in children, but also as the general population ages. Furthermore, there are expectations in the advancement of implant-materials from bioinert to biocompatible/bioabsorbable to those designed to

stimulate/promote tissue responses [20]. The "re"-development of biodegradable magnesium implants is one of such emerging biomaterials. The Laura Bassi Center "Bioresorbable Implants for Children - BRIC" comprised multidisciplinary expertise for the development and investigation of new functional biomaterials. BRIC's overall aim is the improvement of fracture healing in infants and reduction of invasive surgery by the development of a bioresorbable Mg-based implant, which provides functional support and biodegrades after fracture healing, making a second operation for implant removal unnecessary. This thesis highlights the multidisciplinary development process of an innovative implant that takes into account the characteristics of a growing metabolism, and defines material specifications in biodegradation, mechanical performance, biocompatibility and biofunctionality.

This thesis would not have been possible without the financial support from the Laura Bassi Center of Expertise BRIC (FFG – Austria). Many thanks to all collaborators, colleagues, industry and university partners, as their expertise and stimulating discussions have contributed significantly to the quality of this work. I am particularly grateful to Prof. Annelie Weinberg, who leaded the project in an inimitable enthusiastic manner. Last but not least I would like to acknowledge the staff at the "Hahnhof" (Institute of Biomedical Research, Medical University of Graz) for their years and years of great collaboration and support.

Stefan Franz Fischerauer

Table of Contents

German Abstract

Die Anforderungen an Biomaterialien für eine osteosynthetische Anwendung sind stark gestiegen: Neue Biomaterialien sollten mit dem Körper interagieren und Eigenschaften wie Bioaktivität und Biofunktionalität besitzen. Sie sollten den Heilungsprozess steuern und unterstützen, und in einigen speziellen klinischen Indikationen (z.B. Trauma) sollten sie nach vollbrachter Funktionsarbeit zunehmend degradieren, in den Körper aufgenommen, oder über natürlichem Weg wieder ausgeschieden werden. Diese Anforderungen öffneten ein neues Forschungsfeld, welches in den letzten Jahren ein zunehmendes weltweites Interesse von Materialwissenschaftlern, wie auch Molekularbiologen und Ärzte erfuhr. Aktuelle klinische Anwendungsgebiete für solche biodegradierbaren Materialien, welche mechanische Voraussetzungen und biologische Anforderungen mit einander verbinden, ergeben sich für kardiovaskuläre Stents und orthopädische Implantate.

Magnesium ist eines dieser vielversprechenden Materialien, da es nicht nur ein essenzielles Element im menschlichen Körper stellt, sondern auch als ein Leichtmetall mechanische Eigenschaften beinhaltet, die dem natürlichen Knochen sehr ähnlich sind, und darüber hinaus noch die Fähigkeit besitzen in jeder wässrigen Lösung zu degradieren. Der Fokus dieser Dissertation lag in der Bestimmung von biologischen Eigenschaften von Magnesiumlegierungen, im Speziellen deren Biodegradation, Knochen-Implantat-Interaktion, Biokompatibilität und Biofunktionalität.

Es konnte belegt werden, dass Magnesiumlegierungen alle Voraussetzungen für eine orthopädische Anwendung aufgrund ihrer vielversprechenden mechanischen, elektrochemischen und biologischen Eigenschaften erfüllen. Letztere entscheiden jedoch über die Erfolgsraten in einer klinischen Anwendung. Zukünftige Entwicklungsstrategien von Magnesiumlegierungen sollten daher auf Materialreinheit, körpereigene, unbedenkliche Legierungselemente und auf Strategien für einen homogenen, langsam voranschreitenden Degradationsprozess achten.

Abstract

Nowadays the requirements for biomaterials in osteosynthetic application are very high: New biomaterials should interact with its host and possess properties like bioactivity and biofunctionality. They should support and promote the healing process and in some specific clinical indications (e.g. trauma), they should progressively degrade and be ex- or included by the organism after their work is fulfilled. These requirements opened up a new field of research and gained increasing interest of material scientists as well as molecular biologists and physicians around the world in the last decade. Currently targeted clinical applications for such biodegradable materials that combine mechanical requirements and biological demands are cardiovascular stent application and orthopaedic surgery.

Magnesium is one of those promising materials as it is not only an essential element in the human organism, but also a light metal with mechanical properties that are close to the natural bone with the ability to degrade in any aqueous solution. The focus of this thesis was to examine the biological properties of Mg-alloys with special regard on biodegradation, bone-implant-interface, biocompatibility and biofunctionality.

It has been shown that Mg-alloys can fulfil all requirements for an orthopaedic application due to its promising mechanical, electrochemical, and biological properties. The latter however is the most essential issue for a successful clinical application. Future development strategies of Mg-alloys therefore need to address material purification, non-toxic endogenous alloying elements, and strategies for a homogenous gradual degradation process.

1 Introduction

1.1 General background informations

1.1.1 Basics of fracture healing

Bones represent the only tissue with the ability of full *restitutio ad integrum*, without the formation of scars, once they are damaged. If an adequate vascular support is present, the pattern of fracture repair is dictated by the biomechanical environment [21]. Indeed, sufficient bone healing can only occur subsequently to a restoration of a mechanically stable environment, which can be achieved by a natural process of healing (callus formation), or by the use of external or internal osteosynthetic stabilization techniques. Two types of fracture healing are distinguished, which are determined by the degree of provided mechanical stability.

A fracture fixation with absolute stability without micromotion at the fracture site under physiologic load (interfragmentary deformation less than 2% [21]), results in a primary or direct bone healing by a biological process of osteonal bone remodeling [22]. Absolute stability can only be achieved by surgical intervention with application of rigid, nongliding compression plates or lag screws. In primary bone healing, no callus formation or resorption of fracture ends occurs. Instead, a rigid contact between fracture fragments leads to a direct Haversian remodelling with gradual replacement of irregularly oriented osteons by lamellar longitudinal orientated bone [21]. The bridging of the fracture gap progresses at a rate of 50-100µm/day [23]. If, under absolute stability, a fracture gap remains, the fracture site will be primarily filled by intramembranous bone formation (perpendicular orientated laminar bone formation at gaps less than 800µm to 1mm, and woven bone formation at larger gaps) and secondarily remodelled with longitudinal orientated laminar bone [21, 24].

In a natural bone healing process or under flexible fixation methods, the biomechanical stability is relative (a certain amount of fragment motion occurs). The consequent secondary or indirect bone union is very similar to the process of embryological bone development and includes both intramembranous and endochondral bone formation

[22]. Hunter described four classic stages of natural bone repair occurring after a fracture [25]:

- Inflammation
- Soft callus formation
- Hard callus formation } Repair
- Remodelling

The inflammatory phase begins immediately after the initial trauma. A disruption of the medullary vessels and extravasation of blood results in a hematoma and ischemic necrosis of the bone. The hematoma sets the fundament for the repair phase by releasing growth factors, thereby stimulating angiogenesis and bone formation [21]. Necrotic fracture ends are resorbed by macrophages, which can be seen by a widening of the fracture gap. Studies have shown that the proliferative vascular response and the degree of bone resorption are mainly affected by the condition of the surrounding soft tissues [26].

In the repair phase, the injured bone attains a continuous increase of mechanical stability. With the transformation of hematoma into granulation tissue due to immigration of mononuclear cells and fibroblasts, the mechanical withstand ability against tensile force raises up to 0.1 Nm/mm^2 [27]. In the next step the granulation tissue matures into connective tissue. Due to production of collagen fibres by fibroblasts the ultimate tensile strength lies between 1-60 Nm/mm^2 (elongation at rupture is 17%) and the interfragmentary strain decreases [21]. Mesenchymal stem cells differentiate into chondrocytes or osteoblasts by the guidance of numerous growth factors (e.g. TGF-β, BMPs) [21]. Starting from the endostal and periostal layer an external and internal fibrocartilaginous callus forms and bridges the fracture gap ("bridging callus") [28]. This "soft callus" resists compression, but its ultimate tensile strength are similar to those of connective tissue (4-19 Nm/mm^2; 10-12,8% elongation at rupture) [29]. Callus formation enlarges the cross-sectional diameter of the fracture and increases the resistance to bending [21]. The amount of callus produced depends on compromised vascularization and the stability of the fracture, and increases proportional to fracture instability [21]. Mineralization of the soft callus occurs centripetally and eventually forms a "hard callus" [30]. Further vascularisation and immigration of osteoprogenitor cells form new trabeculae similar to endochondral ossification [21]. The hard callus provides an ultimate tensile strength of 130 Nm/mm^2, but its Young's modulus is high (10,000 Nm/mm^2), and its elongation ability limited to 2% [30]. At the end of the repair phase, bone union is

achieved and the bone has regained enough strength and rigidity to allow low impact exercise [21, 31].

In the final remodelling phase morphological adaption of bone to functional demands takes place by a balanced action of osteoclastic resorption and osteoblastic depostion. Piezoelectric affection of osteoclasts and osteoblasts and the Wolff's law influences the cell activity under loading. Laminar bone remodelling up to the *restitutio ad integrum* may last for 6-9 years depending on the age of a patient [32].

Summarazing, healing under restricted motion, e.g. under the application of intramedullary nails, external fixators, or bridging plates, proceeds intermediately to biological immobilization by a callus formation, whereas a callus-free repair only occurs under absolute rigid stabilization [21]. The type of bone healing can thus be significantly influenced by the type and material of fracture fixation.

The duration of stable fracture consolidation is depending on a patient's age, the type of a fracture, the degree of fracture dislocation and the fracture localization. The younger the patient, the shorter the fracture consolidation time. Fracture consolidation in children under the age of 5 years may take only one week. Metaphyseal fractures heal faster than diaphyseal fractures and diaphyseal transverse fractures slower than oblique fractures [33].

1.1.2 Principals of internal fracture stabilization

The central goals of an injured patient treatment are early mobilization and regain of function. Historical fracture treatment methods include immobilization, traction, amputation and internal fixation. Conservative fracture management with immobilization by casting or extension treatment resulted often in a handicap than in a support of function [22]. In the late 19th century, the concept of open reduction, internal fixation (ORIF) has gained a significant upturn after the invention of anaesthesia, antiseptic prophylaxis and therapy, and X-ray documentation, as well as due to the industrial revolution. The first application of plates, screws, and wires in the 1880s and 1890s, however, were complicated by many obstacles, such as infection, poorly conceived implants and techniques, metal allergy, and a limited understanding of the biology and mechanics of fracture healing [34]. Also, less knowledge about the role of fixation and missing respect for soft tissues impaired the outcome [22]. During the 1950s, Danis and Muller began to evolve the principles and techniques of internal fixation [35]. The subsequent foundation of the Arbeitsgemeinschaft für Osteosynthesefragen

(AO; Assosication for the Study of Internal Fixation (ASIF)) has been a central figure in the exploration of fracture healing, understanding of relevant biological processes, development of technologies and techniques, documentation and interpretation of results, and dissemination during the last half century. Advancements in biological and mechanical science eventually led to contemporary fixation theories and techniques [36].

During a fracture, the bone looses its functionality of bearing weight. By the use of an osteosynthesis this function can be restored immediately. The AO has defined following treatment principals with regards to the patient, his environment, the injury mechanism, and specific properties of the fracture [22]:

- fracture reduction and fixation to restore anatomical relationships;
- fracture fixation that provides absolute or relative stability in adaption to the "personality" of the fracture, the patient, and the injury;
- preservation of the blood supply to soft tissues and bone warranted by gentle reduction techniques and carful handling;
- early and safe mobilization and rehabilitation of the injured part and patient.

The main aim of osteosynthesis is the achievement of an instant and, if possible, unrestricted recovery of function of the injured extremity and the soonest remobilization of the patient. Restoration of the anatomy, stable fracture fixation with preservation of blood supply, and early mobilization of the patient are therefore designated as the substrate of a good internal fixation [22].

The influence on bone healing of diverse fracture stabilization techniques is mainly based on their mechanical function. In a non-treated fracture, semi-rigid stabilization of the fracture fragments will be provided naturally by muscle contraction and local swelling. A non-reduced fracture will however result in an unaligned shape of the bone, thus leading to severe functional impairments. Therefore, the conservative treatment begins with a reduction of the fracture fragments under traction to restore length, axis, and rotation. A correct position will be maintained by an external splinting. The mechanical efficiency may be diminished by a loose coupling of the fracture ends because of interjacent soft tissues [22].

Flexible stabilization is provided by the use of nails, external fixation or bridging plates (e.g. Küntscher-nails). There exists no clear definition about the elastic properties or amount of relative stabilization of the implants, which are required for appropriate fracture stabilization. All flexible stabilization techniques have in common that interfragmentary

micromovements occur, which can on the one hand induce a callus formation, but on the other hand also suppress a direct bony consolidation. This depends mainly on the interfragmentary ductility and local hydrostatic pressure, which influence the immigration of cells, as well as their functionality [22]. Flexible fixation allowing micromovements can thereby positively influence the formation of callus tissue [37, 38]. However, if the interfragmentary stability is too low (instability), a bony bridging will fail and lead to a pseudarthrosis, even when a hard callus formation was already achieved [39]. On the other hand, a more rigid fixation without interfragmentary movements can lead to stress shielding and inhibitation of callus formation [40].

Absolute rigid stability can only be achieved by compression of the fracture fragments. This can be performed by special designed lag screws or compression plates. The result would be an intramembranous direct bone healing without a preliminary stage of callus formation. Compression screws have to ensure an interfragmentary static pre-strain for the whole duration of fracture healing [22]. Rigid fixation systems are mainly applied in intraarticular or metaphyseal fractures, as well as in fractures with a distinct disturbance of the local blood supply [22]. Intraarticular fractures require an anatomical reposition and absolute stability to ensure the healing of the joint cartilage and early mobilization [22].

1.1.2.1 Specifics of paediatric fracture treatment

The paediatric skeleton differs significantly from adults' because of a continuous bone growth. By that, it undergoes anatomic changes, which are the reasons for specific fractures, which do not appear in adults. Paediatric bones possess the unique ability to correct certain fracture malalignments and dislocations such as axial deviations, rotation deformities and fracture shortening, spontaneously. Paediatric fractures do almost always heal, whereas pseudoarthroses are barely observed. The younger the child, the higher is the probability of a fast bone healing. However, a risk of growth disturbance has to be considered, and long-term morbidities have to be avoided. Thus, a successful trauma management requires a profound knowledge of bone physiology, child-specific patterns of fracture morphologies and therapeutic concepts including conservative castings and children- and age-specific osteosynthesis techniques [41]. For the treating physician it is important to evaluate each injured child towards its physical and psychological development to set an age-dependent fracture management. A common treatment goal is an achievement of early mobilization and reintegration into daily's life. This led to the current trend of early surgical fracture

management. Nevertheless, the treatment has always to be as atraumatic and painless as possible, wherefore conservative treatment should be favored whenever justifiable [42].

Conservative treatment

Conservative treatment should not require general anaesthesia and can be generally performed in all non-dislocated paediatric fractures. However, in dislocated diaphyseal and metaphyseal fractures the conservative treatment by casting after reduction is also an appropriate method. Due to the high spontaneous correction potential, minor axial deviations can be tolerated in children. The correction potential of a fracture mainly depends on the patient's biological age (greatest below age of 10), the fracture proximity to the growth plate and its growth potency (metaphyseal fractures correct better than diaphyseal fractures), and the functional load of the axial deviation itself (correction by remodelling or asymmetric physeal growth) [33, 42].

Operative treatment

The aim of an operative intervention is provide an efficient osteosynthesis that allows functional and/or static load stability and rapid mobilization of the patient. This requires, especially in paediatric fracture management, an experienced surgeon who is skilled in different osteosynthesis techniques, has an adequate knowledge of the available materials and is aware of the type of fracture, related age-specific spontaneous correction potential, and possible expected growth disturbances [42]. Further considerations should maintain that every surgical treatment go along with a certain risk of morbidities and can cause deeply held anxiety to the paediatric patient.

Open reduction and fracture fixation become more important in children with increasing age and body weight and are in general necessary in following indications:

- dislocation of intraarticular epiphyseal fractures with a visible step or fracture dehiscence of ≥ 2 mm,
- luxations with osseous and/or ligamentous injuries,
- fractures with associated nerve or vascular injuries,
- open fractures of 2^{nd} and 3^{rd} degree, and
- fractures irreducible in closed technique or remaining unstable after reduction, requiring exploration and surgical stabilization thereafter.

In children below the age of 12 years, most fractures that require surgical stabilization are treated by Kirschner-wire (K-wire), elastic stable intramedullary nails (ESIN) or external fixators, whereas above the age of 12, fractures are treated in correspondence to adult trauma management and need an osteosynthesis that serves a greater stability such as provided by plate osteosynthesis or reamed intramedullary nails [33, 41, 42].

1.1.3 Biomaterials for orthopaedic devices

Materials for osteosynthesis have to provide basic requirements of mechanical function, biocompatibility and applicability. When it comes to osteosynthesis, appropriate biomechanical and biological properties are important to stabilize a fracture until the bone healing has completed and the bone has regained its normal function. An osteosynthetic implant has thereby the function to reduce the interfragmentary strain of the fracture gap in a magnitude that physiologic callus formation can take place. Biomaterials like metals, ceramics, polymers, glasses, carbons and composite materials play a significant role in many aspects of contemporary orthopaedic treatments. Especially, various metallic biomaterials have been employed to substitute damaged structural components and to restore lost functions in the human body. Metals provide high stiffness, strength, ductility, fracture toughness, hardness, corrosion resistance and biocompatibility at the same time. For that reason, metals have been the material of choice for loadbearing roles like fracture fixation and total joint arthroplasty. For implant manufacturing Fe, Cr, Co, Ni, Ti, Ta, Mo and W are used [2], although the three principal metal alloys in orthopaedics are: (1) titanium-based alloys, (2) cobalt-based alloys, and (3) iron-(stainless steel) based alloys. They all have in common a high corrosion resistance, which has led to their widespread use as loadbearing implant materials [8]. The invention of commonly used stainless steel 316LV, CoCrMo-alloy ASTM F75/F76, CoNiCrMo ASTM F562, commercially pure titanium CPTi ASTM F67, and Ti-6Al-4V have provided immeasurable benefits to patients by maintaining, restoring or enhancing function and level of activity, thus positively contributing to the overall quality of life. Although in some cases, orthopaedic biometals have been associated with adverse local and remote tissue responses, mainly because of degradation products generated by wear and electrochemical corrosion [43]. The amount of material release, the location and quantity of material deposition, the chemical form of the released degradation products, and finally the pathophysiological interactions and consequences of these degradation products determine the clinical limitations of the current implants. These limitations can include the development

of inflammation arising from limited long-term bio- and haemo-compatibility, inadequate tissue integration, and time- dependent deterioration of the biomaterial properties [2, 44, 45].

Not always is the implant with the highest strength and stiffness the most appropriate. The choice of implant-material always depends on the circumstances. In dependence to the presented demands, a more stable and mechanically more tolerant material can be more appropriate than an electrochemically inert and biologically superior, but mechanically weaker material [22].

To define the most appropriate material, selection depends on biomechanical, as well as biofunctional properties. Mechanical properties of implant materials are usually defined in the following characteristics:

- **Stiffness**

Stiffness is the resistance of an implant against deformity. Stiffness is depending on the specific elastic modulus of a material but can also be influenced by implant design and dimension. It has been shown that materials with lower elastic modulus can reduce stress shielding (a reduction in bone density as a result of the removal of normal stress from the bone by an implant) [46].

- **Strength**

Strength is the ability of an implant to withstand an applied stress without failure. The ability to resist against cyclic loading and fatigue failure is however in implantology more important than the static strength [22]. The strength can also be influenced by size and dimension of an implant.

- **Ductility**

Ductility is the material's ability to deform under tensile or torsional stress. In practice maximal torques are usually limited with the use of torque handlers to prevent an implant failure [22].

- **Corrosion resistance**

Corrosion is the gradual destruction of materials by chemical reaction with their environment. Corrosion determines thereby the release of ions or molecules into the surrounding tissue. In conventional materials a high corrosion resistance and long durability

is envisaged, whereas by the application of degradable materials a controlled breakdown and corrosion after loss of functionality is supposed to occur (s. biodegradation).

- **Surface structure**

In implants like plates or screws, the force transmission occurs through friction between the implant and the bone. Special surface treatments can therefore improve the bone-implant-interface and increase the biofunctionality of the implant (s. biofunctionality) [22].

In addition to mechanical material characterizations, the biological properties and biological function of an osteosynthetic material are defined as:

- **Biocompatibility**

The definition of biocompatibility has been renewed and adapted for many times since the fast advancements of implantology. Williams definition of biocompatibility has been one of the latest and most widely accepted definitions: *"Biocompatibility refers to the ability of a biomaterial to perform its desired function with respect to a medical therapy, without eliciting any undesirable local or systemic effects in the recipient or beneficiary of that therapy, but generating the most appropriate beneficial cellular or tissue response in that specific situation, and optimising the clinically relevant performance of that therapy"* [47]. The adjective "biocompatible" subsumes thereby a variety of mechanisms of interaction between biomaterials and tissues or tissue components and can only be considered in the context of the characteristics of both the material and the biological host within which it is placed [48].

- **Bone-Implant-Interface properties**

The interface between implant and bone is one of the most crucial issues in implantology. In this area, local inflammatory reactions, biofilm formations, but also cell or bacterial adhesion, osteointegration and mechanical friction takes place. Frequently the result of a successful treatment occurs in this region. Bone-implant-interface properties include mechanical, electrochemical and also moleculobiological function of a material. But also implant design, implantation technique and the level of disturbance of the local blood supply have a particular influence of the quality of the bone-implant-interface [49].

- **Biofunctionality**

Several factors can affect the biological response to implanted materials. Improvements in implant design, surface preparation, osteoinductive or osteoconductive

coatings, or the implementation of additives like antibiotics or bone morphogenetic proteins are used to improve implant longevity and functionality. Implants are thereby no longer supposed to act simply inert to the host organism. Modern biofunctional materials try to enhanced fracture healing by evoking positive local tissue reactions.

- **Biodegradation**

Biodegradation describes a material breakdown in a biological environment. The degradation mechanism are various at different biomaterials and mainly depending on electrochemically respectively plasticizing reactions in an aggressive aqueous and ionic milieu like blood, biological reactions of adsorbed proteins, and on oxidizing agents and enzymes secreted by adhered cells (e.g. macrophages) [8]. The degradation products formed during this process are meant do be non-toxic and non-irritating to the surrounding environment and possess the same biocompatibility as the bulk material.

Recently, there has been an increasing demand for biofunctional materials that combine fundamental mechanical support with enhanced functional properties including advanced biocidal and antifouling surface properties, enhanced fracture healing and patient recovery, and/or increased biocompatibility [2]. Therefore, biomaterials and implants that minimise patient's morbidity and the length of hospital stay have been in the focus of biomaterial research. In the last years, there has been a considerable amount of attention in the development of fully absorbable/degradable implant devices. These devices are specifically designed to remain physico-chemical stable for a predefined length of time. Once their task is completed, the implantable device undergoes controlled degradation under the influence of the physiological environment [2, 50]. Under such biodegradable metals that can support tissue regeneration and healing, particularly where a load-bearing function is required, especially Magnesium (Mg) is considered as one of the most promising biomaterials [51].

1.1.4 Magnesium as biodegradable material for osteosynthesis

Magnesium was first discovered by Joseph Black in 1755 and named after Magnesia, a district of Eastern Thessaly in Greece, where it appeared in great quantities. Mg is the eighth most abundant element in the world, however it is rarely found in its pure form due to easily bonding with other elements. It was initially produced by Sir Humphrey Davy in 1808 and industrial production began in Germany 1886. Having a density of 1.7g/cm, Mg is the

lightest of all structural metals (33 percent lighter than aluminum and 75 percent lighter than steel). It also possesses excellent heat dissipation, damping, and electromagnetic shield. These made the material peculiar attractive for automotive and aerospace industry, but also for modern sport equipment and electronic devices.

Besides being a lightweight metal, Mg ions are the fourth most abundant metal ions within the human body, half of it stored within bone tissue. Mg^{2+} is present in every cell type, essential to human metabolism and therefore highly biocompatible and non-toxic [52-56]. This opened the door for many medical applications. In early days Mg was used for ligatures, plates, and screws, although most failed because of low purity levels or lacking knowledge about corrosion behavior [13, 57-60]. Starting in the early 2000s, advancement in Mg purity and better understanding of corrosion kinetics, have reenhanced the research of Mg as a biomaterial. One main research area of Mg is its application as resorbable intravascular stent for the treatment of arterial disease. The other one is osteosynthesis, as Mg offers high primary stability, high tensile strength and resistance to fracture, high damping capacity, ease of machinability, biocompatibility, and biofunctionality [2, 20]. However, what truly differentiates Mg from other metallic biomaterials is its ability to degrade in an organic environment [20].

Mg corrodes in a neutral aqueous environment due to the chemical reaction of

$$Mg(s) + 2H_2O(aq) = Mg(OH)_2(aq) + H_2(g),$$

generating one hydrogen gas molecule per one atom of Mg. This degradation has second-order effects. On the one hand, magnesiumhydroxide has been shown to promote bone regeneration [61] and possesses osteoconductive properties [62], but on the other hand, a too quick material degradation can result in toxicity, loss of mechanical strength, localized hydrogen gas accumulation and alkalisation [10]. In fact, a high susceptibility to corrosion of Mg limits it clinical application as biomaterial.

It has been shown, that alloying Mg with other elements is the most profound way to influence the corrosion behavior. Since that realization by Boyer in 1927 [63] and the pioneering fundamental work of Hanawalt in the 1940s [64, 65], many variations in Mg-alloys were designed with different physico-chemical properties. In fact, by adding certain ligands it has been reported that the corrosion rate can be altered over many magnitudes (ranging fromm 1-100 mm/y), which is unique for a metal system [66]. Boyer and Hanawalt outlined that two factors control the corrosion of Mg: (1) Alloy purity, as impurities like Fe,

Nu and Cu accelerates the corrosion rapidly [65], and (2) scavenging of impurities by the addition of other elements to create specific intermetallic phases [63]. Although, most alloys have been developed on the basis of physical properties, such as strength, ductility, creep resistance ore ease of production, because pure Mg is incapable of providing the mechanical properties required for many implant applications [20, 53, 67, 68]. The most frequent utilization of alloying elements in metallurgy for magnesium based implants are listed in **Table 1.1**. However, the addition of many alloying elements, especially rare earth elements, remains under discussion with regard to their potential toxicity. The evaluation of their definite applicability in a biodegradable context will be one of the major issues in coming years.

Table 1.1: Current alloying elements for Mg-based implants (modified from [20, 69])

Alloying Element	Influences on Mg corrosion
Aluminium	Al is more noble than Mg and the most common addition to Mg alloys [70]. Al increases mechanical properties and ease of castability. Al additions below the solubility limit can slightly decrease Mg corrosion by lowering the rate of anodic reaction [71]. Mg-Al alloys have the lowest corrosion rate of commercial available Mg alloys [70].
Calcium	Ca additions at levels below the solubility levels do not affect or slightly increase corrosion rates in Mg, although additions above the solubility limit (~1 wt%) lead to exceptionally high corrosion rates [66]. By the addition of Ca the ductility of the bulk material can be increased.
Iron	Fe is an unfortunately common impurity in Mg alloys. With a very low solubility limit in Mg (~0,001 wt%), already small amounts can increase the corrosion rate significantly. Typically, the Fe content must be less than 0.005 wt%) [70].
Manganese	Manganese is primarily added to magnesium alloys to improve the corrosion resistance [71]. This is achieved by reducing the harmful effects of impurities via incorporation of essentially insoluble metals into an intermetallic phase [63, 64].
Rare Earths (Cerium, Lanthanum, Neodymium)	The strength of the bulk material is increased linear with the total RE content. The influence of RE additions on corrosion rate depends upon the type of the RE elements. The increase in corrosion from Nd additions is less than that arising from Ce or La [72].
Yttrium	Yttrium can refine the microstructure, change the morphology of intermetallic phases, and decrease slightly the corrosion rate [73].
Zinc	The yield strength of magnesium alloys can be increase with its zinc content [74]. In MgZnCa alloys the formation of intermetallic phases with high Zn content lead to an increased degradation susceptibility [75, 76].
Copper	The addition of copper increase the strength of magnesium casts, but also accelerates magnesium alloy corrosion rate in a NaCl solution [77].
Zirconium	Excess Zr causes significant corrosion, however Zr at low levels in multielement alloys react innocuous [78].

1.2 Aim of the project and outline of the thesis

Because of the growing skeleton, bone implants are generally removed in children. Of about 170,000 children injured annually in Austria, 15-20% are subjected to osteosynthesis. This number has constantly increased in the recent past [79]. Due to a lack of knowledge and implementation of child-specific bone implants, paediatric surgeons are still forced to use permanent implants with their need for a second intervention for removal. The use of biodegradable implants instead of permanent ones would lead to several major benefits: An implant removal would be unnecessary, thus reducing physical and psychological stress and associated morbidity in pediatric patients. Costs would be saved by the avoidance of a second surgery and a reduction of hospitalization time. In addition, a significant benefit for children could be achieved, when fracture healing was encouraged by special properties of these implants. Furthermore, by the implementation of biodegradable implants, a lot of associated benefits could be transferred to adults' orthopaedic surgery and traumatology.

To improve fracture healing in infants and reduce invasive surgery, a clear-cut goal has been set: Development of a new implant material meeting the special requirements of children. This includes a bioabsorbable, specially designed implant that (1) takes into account the characteristics of growing patients such as different metabolism, growth rates, fracture healing time, and mechanical properties of immature bones, (2) provides an adequate biocompatibility that causes no chronic local or systemic inflammation and does not contain elements that can be harmful for children in a long-term relation, and (3) supports the healing process due to biofunctional and/or mechanical properties.

In a successful implant development process, the knowledge of scientists from different research fields, which encompass basic science (biology, chemistry, physics), engineering and medicine science, is required. In fact, most biomaterials, which are currently used, derive from applications from non-medical industries. The knowledge transfer from other scientific fields and engineering can facilitate the establishment of new methodologies, but can also lead to problems of understanding and miscommunication. In this aspect, educational cross-disciplinary communication is one of the key issues in the development process of new functional materials. To successfully translate biomaterial science to clinically important medical devices, the capability of the implant material and requirements of the host must be clearly defined, and the complex physical and chemical interactions between biological systems and implant material familiar to both, engineers and physicians. Important implant characteristics like mechanical properties, processability, reproducibility,

and scalability of the technology, which is used to produce the biomaterial and the final implant, must be geared to biological criteria like biodegradation, bone-implant interfaces biocompatibility, and biofunctionality.

Simplified, the realization of a novel functional implant depends on material engineering design, testing in vitro, in animals and in humans, clinical realities, and the involvement of industry permitting product development and commercialization [8]. **Figure 1.1** displays the interdisciplinary development workflow between medical science, materials science and industry involvements.

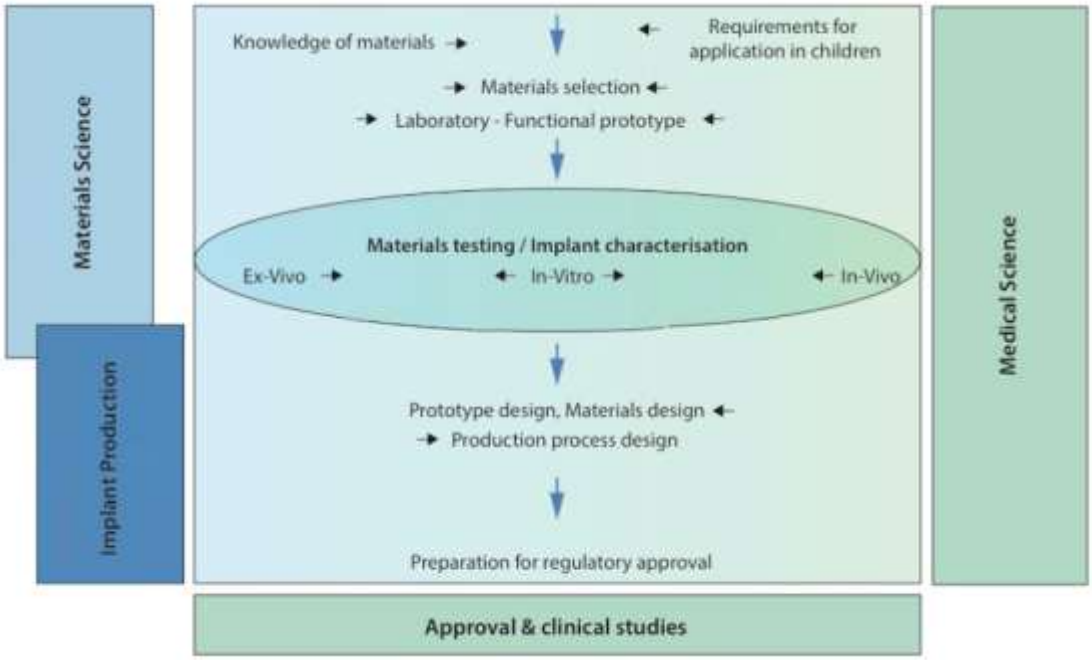

Figure 1.1: Interdisciplinary development process of a biofunctional material

Outline of the thesis

This thesis focuses on the biological characterization of novel Mg-based implants. The clinical applicability of a new implant as an osteosynthetic device requires sufficient mechanical properties on the one hand, and acceptable biodegradation, bone-implant-interface properties, biocompatibility and biofunctionality on the other hand. The former can be easily tested under laboratory investigations. Biological testing, however, requires standardized and reproducibly settings of a complex environment. As in vitro tests are not able to fully emulate every complexity of the human body, in vivo tests are still necessary for some basic science researchs questions. The following chapters exemplify the in vivo characterization of the major biological properties in the development process of a new biodegradable Mg-based alloy.

References

[1] Breasted JH. The Edwin Smith surgical papyrus. Chicago: University of Chicago Press; 1930.

[2] In: Ivanova EP, Bazaka K, Crawford RJ, editors. New Functional Biomaterials for Medicine and Healthcare: Woodhead Publishing; 2014.

[3] Greenhagen RM, Johnson AR, Joseph A. Internal Fixation: a Historical Review. Clinics in Podiatric Medicine and Surgery 2011;28:607-18.

[4] Konig F. Uber die Implantation von Elfenbein zum Ersatz von Knochen und Gelenken. Nach Experimentellen und klinischen Beobachtungen. Beitr Klin Chir 1913:91–114 [in German].

[5] Aufrecht E. Ueber Riesenzellen in Elfenbeinstiften, welche zur Heilung einer Pseudoarthrose eingekeilt waren. Centrallblat Med Wissensch 1877:465–7 [in German].

[6] Senn N. I. A New Method of Direct Fixation of the Fragments in Compound and Ununited Fractures. Annals of Surgery 1893;18:125-51.

[7] Bartonicek J. Early history of operative treatment of fractures. Archives of orthopaedic and trauma surgery 2010;130:1385-96.

[8] Ratner BD, Hoffman AS, Schoen FJ, Lemons JE. Biomaterials Science: An Introduction to Materials in Medicine: Elsevier Science; 2012.

[9] Bérenger-Féraud LJB. Traite de l'immobilisation directedes fragments osseux dans les fractures. Adrien Delahaye, Paris 1870.

[10] Witte F. The history of biodegradable magnesium implants: a review. Acta biomaterialia 2010;6:1680-92.

[11] Payr E. Beiträge zur Technik der Blutgefäß- und Nervennaht nebst Mittheilungen über die Verwendung eines resorbirbaren Metalles in der Chirurgie. Arch Klin Chir 1900;62:67-93.

[12] Payr E. Blutgefäß- und Nervennaht (nebst Mittheilung über die Verwendung eines resorbirbaren Metalles in der Chirurgie). Centralblatt für Chirurgie 1901;28:31-7.

[13] Lambotte A. L'utilisation du magnésium comme matériel perdu dans

l'ostéosynthèse. Bull Mém Soc Nat Cir 1932;28:1325–34.

[14] Lambotte A. Technique et indications de la prothèse perdue dans la traitement des fractures. Presse Med Belge 1909;17:321–3.

[15] Sherman WO. Vanadium steel bone plates ad screws. Surg Gyn Obst 1912:629–34.

[16] Venable CS, Stuck WG. The internal fixation of fractures. Oxford (UK): Blackwell Scientific Publications; 1947.

[17] Venable CS, Stuck WG, Beach A. The effects on bone of the presence of metals; based upon electrolysis: an experimental study. Ann Surg 1937;105:917-38.

[18] Leventhal GS. Titanium, a metal for surgery. The Journal of bone and joint surgery American volume 1951;33-A:473-4.

[19] Rostock P. Ist das Magnesium als Naht- und Schienungsmaterial für Knochenoperationen geeignet? Archives of orthopaedic and trauma surgery 1937;38:486–92.

[20] Kirkland NT, Birbilis N. Magnesium Biomaterials: Design, Testing, and Best Practice: Springer International Publishing; 2013.

[21] Johnson A, Houlton J. AO Principles of Fracture Management in the Dog and Cat: Thieme International; 2005.

[22] Rüedi TP, Buckley RE, Moran CG. AO Principles of Fracture Management: Principles: Thieme; 2007.

[23] Hulse D, Hyman B. Fracture biology and biomechanics. In: Slatter D, editor. Textbook of Small Animal Surgery. Philadephia WB Saunders; 1993. p. 1595–603.

[24] Kaderly RE. Primary bone healing. Seminars in veterinary medicine and surgery (small animal) 1991;6:21-5.

[25] Hunter J. Experiments and observations on the growth of bones. In: Palmer JR, editor. The Transactions of a Society for the Improvement of Medical and Chirurgical Knowledge. London: Longman, Rees, Orme, Brwon, Breen, & Longman; 1837.

[26] Richards RR, Schemitsch EH. Effect of muscle flap coverage on bone blood flow following devascularization of a segment of tibia: an experimental investigation in the dog. J Orthop Res 1989;7:550-8.

[27] Perren SM, Boitzy A. Cellular differentiation and bone biomechanics during the consolidation of a fracture. Anat Clin 1978;1.

[28] Binnington AG. Bone remodeling and transplantation. In: Wittick WG, editor. Canine Orthopedics 2nd ed Section III: Preparation, principles, and procedures for surgery. Philadelphia: Lea & Febiger; 1990. p. 166–89.

[29] Mann FA, Payne JT. Bone healing. Seminars in veterinary medicine and surgery (small animal) 1989;4:312-21.

[30] Rahn BA. Bone healing: histologic and physiologic concepts. In: Fackelman GE, editor. Bone in Clinical Orthopaedics. Stuttgart New York: Thieme; 2002. p. 287–326.

[31] Frost HM. The biology of fracture healing. An overview for clinicians. Part I. Clin Orthop Relat Res 1989:283-93.

[32] Remedios A. Bone and bone healing. The Veterinary clinics of North America Small animal practice 1999;29:1029-44, v.

[33] Van Laer L. Frakturen und Luxationen im Wachstumsalter. Stuttgart: Thieme Verlag; 2007.

[34] Peltier L. Fractures: A History and Iconography of Their Treatment. San Francisco, CA: Norman Publishing; 1990.

[35] Muller ME, Allgower JM, Schneider R, Willenegger H. Manual of Internal Fixation, 3rd. ed. Berlin: Springer-Verlag; 1992.

[36] Brunner CF, Weber BG. Special Techniques in Internal Fixation. Berlin: Springer-Verlag; 1982.

[37] Claes LE, Wilke HJ, Augat P, Rubenacker S, Margevicius KJ. Effect of dynamization on gap healing of diaphyseal fractures under external fixation. Clinical biomechanics (Bristol, Avon) 1995;10:227-34.

[38] Goodship AE, Kenwright J. The influence of induced micromovement upon the healing of experimental tibial fractures. J Bone Joint Surg Br 1985;67:650-5.

[39] Schenk RK, Müller J, Willenegger H. Experimentell — histologischer Beitrag zur Entstehung und Behandlung von Pseudarthrosen. Verhandlungen der Deutschen Gesellschaft für Unfallheilkunde Versicherungs-, Versorgungs- und Verkehrsmedizin E V: Springer Berlin Heidelberg; 1968. p. 15-24.

[40] Perren SM, Cordey J. The concept of interfragmentary strain. Berlin Heidelberg New York: Springer-Verlag; 1980.

[41] Slongo T. The choice of treatment according to the type and location of the fracture and the age of the child. Injury 2005;36:12–9.

[42] Weinberg A, Tscherne H, Henkel R. Tscherne Unfallchirurgie: Springer; 2006.

[43] Kamachimudali U, Sridhar TM, Raj B. Corrosion of bio implants. Sadhana 2003;28:601-37.

[44] Puleo DA, Huh WW. Acute toxicity of metal ions in cultures of osteogenic cells derived from bone marrow stromal cells. Journal of applied biomaterials : an official journal of the Society for Biomaterials 1995;6:109-16.

[45] Granchi D, Ciapetti G, Stea S, Savarino L, Filippini F, Sudanese A, et al. Cytokine release in mononuclear cells of patients with Co-Cr hip prosthesis. Biomaterials 1999;20:1079-86.

[46] Tonino AJ, Davidson CL, Klopper PJ, Linclau LA. Protection from stress in bone and its effects. Experiments with stainless steel and plastic plates in dogs. J Bone Joint Surg Br 1976;58:107-13.

[47] Williams DF. On the mechanisms of biocompatibility. Biomaterials 2008;29:2941-53.

[48] Williams DF. There is no such thing as a biocompatible material. Biomaterials 2014;35:10009-14.

[49] Gautier E, Cordey J, Mathys R. Porosity and Remodelling of Plated Bone after Internal Fixation: Result ofStress Shielding or Vascular Damage. In: Ducheyne P, Van der Perre G, Aubert AE, editors. Biomaterials and Biomechanics: Elsevier Science Publisher; 1984. p. 195-200.

[50] Hermawan H. Introduction to Metallic Biomaterials Biodegradable Metals. Berlin, Heidelberg: Springer; 2012.

[51] Shimizu Y, Yamamoto A, Mukai T, Shirai Y, Kano M, Kudo T, et al. Medical application of magnesium and its alloys as degradable biomaterials. In: Sasano T, Suzuki O, editors. Interface Oral Health Science 2009: Springer Japan; 2010. p. 318-20.

[52] Xin Y, Hu T, Chu PK. In vitro studies of biomedical magnesium alloys in a simulated physiological environment: a review. Acta biomaterialia 2011;7:1452-9.

[53] Staiger MP, Pietak AM, Huadmai J, Dias G. Magnesium and its alloys as orthopedic biomaterials: a review. Biomaterials 2006;27:1728-34.

[54] Saris NE, Mervaala E, Karppanen H, Khawaja JA, Lewenstam A. Magnesium. An update on physiological, clinical and analytical aspects. Clin Chim Acta 2000;294:1-26.

[55] Seiler HG, Sigel H. Handbook of toxicity of inorganic compounds. New York: Marcel Dekker Inc; 1988.

[56] Lusk JE, Williams RJ, Kennedy EP. Magnesium and the growth of Escherichia coli. The Journal of biological chemistry 1968;243:2618-24.

[57] Huse EC. A new ligature? Chicago Med J Examiner 1878;37:171-2.

[58] Verbrugge J. La tolérance du tissu osseux vis-à-vis du magnésium métallique. Presse Med Belge 1933;55:1112–4.

[59] Verbrugge J. L'utilisation du magnésium dans le traitement chirurgical des fractures. Bull Mém Soc Nat Cir 1937;59:813–23.

[60] Znamenskii MS. Metallic osteosynthesis by means of and apparatus made of resorbing metal. Khirurgiia 1945;12:60-3.

[61] Hofmann G, Claes L. Biodegradable implants in orthopedic surgery. Clinical materials 1992;10:1.

[62] Castellani C, Lindtner RA, Hausbrandt P, Tschegg E, Stanzl-Tschegg SE, Zanoni G, et al. Bone-implant interface strength and osseointegration: Biodegradable magnesium alloy versus standard titanium control. Acta biomaterialia 2011;7:432-40.

[63] Boyer JA. The corrosion of magnesium and of the magnesium aluminum alloys containing manganese American Magnesium Corporation 1927:Report No. 248.

[64] Hanawalt JD, Nelson CE. Corrosion studies of magnesium and its alloys. Trans AIME 1946 1942;147:273-99.

[65] McNulty RE, Hanawalt JD. Some corrosion characteristics of high purity magnesium alloys. J Electrochem Soc 1942;81:423.

[66] Kirkland NT, Lespagnol J, Birbilis N, Staiger MP. A survey of bio-corrosion rates of magnesium alloys. Corrosion Science 2010;52:287-91.

[67] Hort N, Huang Y, Fechner D, Stormer M, Blawert C, Witte F, et al. Magnesium alloys as implant materials--principles of property design for Mg-RE alloys. Acta biomaterialia 2010;6:1714-25.

[68] Vojtech D, Cizova H, Volenec K, vol. 44 (2006) n, pp. 211 - 223. Investigation of magnesium-based alloys for biomedical applications. Kovove Mater 2006;44:211-23.

[69] Persaud-Sharma D, McGoron A. Biodegradable Magnesium Alloys: A Review of Material Development and Applications. Journal of biomimetics, biomaterials, and tissue engineering 2012;12:25-39.

[70] Baker H, Committee ASMIH. ASM Specialty Handbook: Magnesium and Magnesium Alloys: ASM International; 1999.

[71] Makar GL, Kruger J. Corrosion of magnesium. Int Mater Rev 1993;38:138-53.

[72] Birbilis N, Easton MA, Sudholz AD, Zhu SM, Gibson MA. On the corrosion of binary magnesium-rare earth alloys. Corrosion Science 2009;51:683-9.

[73] Zhang J, Niu X. Effect of Yttrium-Rich Misch metal on the microstructures, mechanical properties and corrosion behavior of die cast AZ91 alloy. J Alloy Compd 2009;471:322-30.

[74] Bach FW, Schaper M, Jaschik C. Material Science Forum 2003;1037:419–22.

[75] Bakhsheshi-Rad HR, Abdul-Kadir MR, Idris MH, Farahany S. Relationship between the corrosion behavior and the thermal characteristics and microstructure of Mg–0.5Ca–xZn alloys. Corrosion Science 2012;64:184-97.

[76] Bakhsheshi-Rad HR, Idris A, Abdul Kadir MR, Farahany S, Yahya MY. Characterization and Corrosion Behavior of Biodegradable Mg-Ca and Mg-Ca-Zn Implant Alloys. Applied Mechanics and Materials 2012;121-126.

[77] Hillis JE, Murray RW. Finishing Alternatives for High Purity Magnesium Alloys. SDCE 14th International Die Casting Congress and Exposition. Toronto1987. p. Paper No. G- T87-003.

[78] Kirkland N, Staiger M, Nisbet D, Davies CJ, Birbilis N. Performance-driven design of Biocompatible Mg alloys. JOM 2011;63:28-34.

[79] AUVA Annual Report Statistics Austria. 2008.

2 Evaluation of the Biodegradation Behavior

Functional biomaterials are meant to degrade within its environment after loosening its functional relevance. In fracture healing the biodegradation is supposed to go along in equilibrium with the recovery of the bone. Implant and bone, both are determining the mechanical load capacity of the limb. Thus, stabilization and implant integrity has to be ensured especially in early stages of fracture healing. Further, the products of material degradation should not harm the surrounding tissues or accumulate elsewhere. Material interactions with the environment make the degradation process a complex mechanism that is hardly reproducible in in-vitro settings.

Magnesium Alloys for Temporary Implants in Osteosynthesis: In-vivo Studies of their Degradation and Interaction with Bone

Tanja Kraus, Stefan F. Fischerauer[*], *Anja C. Hänzi, Peter J. Uggowitzer, Jörg F. Löffler, Annelie M. Weinberg*

ACTA BIOMATER. 2012; 8(3): 1230-1238

This study investigates the bone and tissue response to degrading magnesium pin implants in the growing rat skeleton by continuous in vivo μCT monitoring over the entire pin degradation period with special focus on bone remodeling after implant dissolution. Moreover the influence on tissue performance of the gas release upon the degradation of magnesium is addressed. Two different magnesium alloys – one fast degrading (ZX50) and one slow degrading (WZ21) – were used for evaluating the bone response in 32 male Sprague Dawley rats. After femoral pin implantation μCTs were performed every 4 weeks over the 24 weeks study period. ZX50 pins exhibited early degradation and released large hydrogen gas volumes. Considerable callus formation occurred. However, bone function was not permanently harmed and the bone recovered unexpectedly fast after complete pin degradation. WZ21 pins kept their integrity for more than 4 weeks and showed good osteoconductive properties by enhancing bone accumulation at the pin surface. Despite excessive gas formation, the magnesium pins did not harm bone regeneration. At smaller degradation rates, gas evolution remained unproblematic and the magnesium implants proved good biocompatibility. Online μCT monitoring is shown to be suitable for evaluating materials degradation and bone response in vivo providing continuous information on the implant and tissue performance in the same living animal.

Keywords: Magnesium; biodegradation; growing rat skeleton; in vivo small animal imaging; microfocus computed tomography (lCT)

[*] Author's contribution to this study: study planing, surgery of animals and animal care, μCT performance and evaluations, statistical analysis, construction of figures, literature research, and writing the manuscript.

2.1 Introduction

In the recent years extensive research on magnesium and its alloys as potential biodegradable implant materials has been carried out [1-7]. Biodegradable magnesium alloys are more suitable for load-bearing implant applications than their polymeric counterparts due to their superior mechanical strength. Moreover, since their elastic properties resemble those of bone, they are considered ideal for hard tissue implants employed in fracture stabilization because stress shielding is avoided and bone regeneration is enhanced [1, 2]. Previous in vivo and in vitro studies have shown that magnesium alloys exhibit good biocompatibility with no systemic inflammatory reaction or affection of the cellular blood composition [3-6]. In addition, high mineral apposition rates and increased bone mass were found around degrading Mg implants in bone [7]. The beneficial influence of magnesium has been emphasized further in a study showing that the bone–implant interface strength and osseointegration is significantly greater for magnesium than for conventional titanium materials [8]. Using materials that degrade in physiological environments renders subsequent surgical intervention for implant removal after tissues healing [1, 3]. This is of great benefit because morbidity related to repeated surgery is reduced and additional health costs are avoided. It makes temporary implants also very attractive in pediatric cases – which are, as potential end application, in the focus of this study – where the growing bone is less interfered and its regeneration after fracture is supported.

Specific properties must be fulfilled in order to use biodegradable implants as material for osteosynthesis in a growing skeleton. The key issues include (i) an adequate stability during fracture healing, requiring sufficient strength to hold the replaced fracture; (ii) degradation and full regeneration of the bone structure within 12–15 months, requiring a moderate and homogeneous degradation performance in equilibrium with the bone healing process; and (iii) biocompatibility, requiring an adequate biological response. Magnesium is considered to meet many of these requirements. However, the fact that its degradation is accompanied by hydrogen gas formation ($Mg + 2H_2O \rightarrow Mg(OH)_2 + H_2$, [9]) has abated the optimistic predictions for its use in osteosynthesis, because its degradation generally results in considerable gas accumulations in the surrounding tissue [7]. Therefore, recent studies focused mainly on assessing the corrosion performance of various Mg alloys in vitro and in vivo and finding compositions that enable slow and homogeneous degradation [5, 10, 11]. It has remained unclear, however, to what extent gas accumulations are harmful and whether bone healing is negatively affected thereby. To our knowledge studies focusing on the bone

behavior at the end of the degradation process are also lacking as most studies were concluded before entire implant degradation was achieved. Thus, in this study we investigate the bone behavior during and after complete degradation of Mg pin implants by continuous μCT monitoring in the same living animal and by histological analysis.

Since its introduction by Feldcamp et al. [12], μCT has gained enormous significance in the quantitative assessment of cancellous bone [13]. In anthropology, this method of microarchitecture imaging finds widespread application, besides histological sectioning, planar radiography, and medical computed tomography [13]. The high-resolution imaging, with a resolution of tens of microns, is a pivotal advantage of μCT over previously used methods, since studies have indeed demonstrated that accurate assessment of trabecular architecture depends on image resolution [14]. Moreover, μCT based on quantitative bone morphometry is key for three-dimensional (3D) measurements of trabecular bone structure [15].

The animal model deployed in our study is the growing rat skeleton. This model was chosen for two reasons: (i) the anatomical size of the laboratory rat is considered appropriate for bone implant experiments in small animals, and (ii) feasibility of μCT examination is guaranteed within the entire growth process of the rat and even on full-grown animals. For gaining information on the influence of the degradation rate and thus the gas formation rate on bone healing, two different Mg alloys were evaluated: the alloy ZX50 and the alloy WZ21 (their compositions are listed in Table 1). Both alloys have similar mechanical performance and a chemical composition considered promising for temporary implant applications [5, 16, 17]; however, they considerably differ in their degradation performance. The alloy ZX50 degrades rather rapidly in vitro in physiological solutions and was deliberately chosen to achieve complete degradation in an appropriate time period. It represents also a material that evolves considerable amounts of hydrogen gas in short time periods. For Mg alloys to be used as viable implant materials, their degradation rates should not exceed the healing rate of the affected tissue, however. For adults they should maintain their mechanical integrity at least for 12–18 weeks [1, 7], while in pediatric trauma patients a shorter presence in the bone is tolerated. To study the effect of gas evolution besides the fast degrading ZX50 material the alloy WZ21 was used as reference material degrading slowly and thus exhibiting much smaller gas formation rates than ZX50 [5].

Based on this concept the present study aims at answering the following essential questions: (i) How fast do the selected alloys degrade in vivo and how long do they maintain

their integrity, respectively? (ii) To which extent does the hydrogen gas evolved upon degradation of the magnesium implants irritate the surrounding tissues? (iii) Is the living organism able to remodel the alterations caused by the degradation after complete absorption of the implant? And (iv), is μCT the appropriate method for evaluating the degradation performance of such temporary implants and studying the related tissue response?

2.2 Materials and methods

2.2.1 Implants

In the present study, machined cylindrical pins made of two different Mg–Zn alloys were used. All implants were 1.6 mm in diameter and 8 mm in length, and exhibited a smooth polished surface. The biodegradable magnesium alloys ZX50 and WZ21 were recently developed for the purpose of degradable implant applications [16, 17]. Their nominal compositions are shown in **Table 2.1**. The ZX50 alloy typically exhibits a yield stress of 210 MPa, an ultimate tensile strength of 295 MPa, a uniform elongation of 18%, and an elongation at fracture of 26%. The WZ21 alloy features a yield stress of 150 MPa, an ultimate tensile strength of 250 MPa, a uniform elongation of 20%, and an elongation at fracture of 28%. Thirty-two pins per alloy were implanted. The pins were carefully dry-machined with clean tools to avoid contamination and allow for good surface quality. After machining they were cleaned in a cascade of pure ethanol in an ultrasonic bath and dried in warm air.

Table 2.1: Nominal chemical composition in weight-% of the two magnesium alloys implanted. Alloy ZX50 degrades faster than alloy WZ21. The alloys were produced using direct chill casting and hot extrusion. Details on alloy fabrication process and the microstructures are given in [16, 17].

Alloy	Mg	Zn	Ca	Mn	Y
ZX50	Balance	5	0.25	0.15	-
WZ21	Balance	1	0.25	0.15	2

2.2.2 Experimental design

All animal experiments were conducted under animal ethical respect and were authorized by the Austrian Ministry of Science and Research (accreditation number BMWF-66.010/0113-II/10b/2009). Rats were housed in groups of four in clear plastic cages on standard bedding. Water and a standard pellet diet were given ad libidum.

Thirty-two male Sprague–Dawley rats with a body weight of 140–160 g and five weeks of age were used in this study. The rats were divided in two groups: sixteen rats belonged to the "continuous-μCT" group and sixteen to the "histological" group. Each rat in each group got two identical pins (either WZ21 or ZX50) implanted into its femoral bones. Accordingly eight rats with ZX50 and eight rats with WZ21 were assigned to the "continuous-μCT" group while eight rats per alloy belonged to the "histological" group. The rodents in the "continuous μCT" group underwent μCT evaluation at the 7th day after operation followed by further μCT examinations every four weeks up to the 24th week. Histological examinations were performed at week 4, 12, 24, and 36 post operationem in which two rats of each group (ZX50 and WZ21) were sacrificed.

2.2.3 Surgical procedure

Volatile isoflurane (Forane®, Abbot AG, Baar, Switzerland) was administered for general anesthesia proceeded by a subcutaneous combined sedation, administering a mixture of Fentanyl (20 μg kg^{-1} Fentanyl®, Janssen-Cilag GmbH, Neuss, Germany), Midazolam (400 μg kg^{-1} Midazolam Delta®, DeltaSelect GmbH, Dreieich, Germany) and Medetomidine (200 μg kg^{-1} Domitor®, Pfizer Corporation Austria GmbH, Vienna, Austria).

The mid-diaphyseal region of the femur was exposed through a lateral approach. A drill (1.5 mm) with ascending diameter (Synthes®, Paoli, PA, USA) was used to prepare the transcortical implantation bed with the longitudinal axis of the drill hole perpendicular to the longitudinal axis of the femoral diaphysis. Drilling was performed at low rotational speed of 200 rpm and profuse physiological saline irrigation was applied using a syringe in order to minimize frictional heat and thermal necrosis. The cylindrical implant was inserted by gentle tapping, resulting in a uniform press fit. After transcortical placement was ensured, the operating field was irrigated thoroughly with physiological saline solution and the wound was closed in layers. Thereafter the contra-lateral side was operated in the same way and by using the same type of implant. The general anesthesia was then antagonized by an intraperitoneal injection of a mixture of Naloxone (120 μg kg^{-1}; Narcanti®, Torrex Chiesi Pharma GmbH, Vienna, Austria), Flumazenil (50 μg kg^{-1}; Anexate®, Roche Austria GmbH, Vienna, Austria) and Atipamezole (250 μg kg^{-1}; Antisedan®, Pfizer Corporation, Vienna, Austria). Postoperatively all animals received 200 mg kg^{-1} Caprofen (Rimadyl®, Pfizer Corporation, Vienna, Austria), which was injected subcutaneously on the day of operation to ensure analgesia. During the first postoperative week (up to the 7th day) analgesia was

maintained by administration of 60 mg Piritramid (Dipidolor®; Janssen-Cilag GmbH, Neuss, Germany) in 40 ml 5% Glucose added to 500 ml drinking water. Postoperatively the rats were allowed to move freely in their cages without external support and unrestricted weight bearing. Daily clinical observation was performed throughout the study period.

2.2.4 Euthanasia

For euthanasia in the "histological group" volatile isoflurane (Forane®, Abbot AG, Baar, Switzerland) was used for general anaesthesia. Subsequently, 25 mg sodium thiopental (Thiopental® Sandoz, Sandoz GmbH, Kundl, Austria) was injected into the cardiac ventricle, leading to immediate cardiac arrest. Immediately after harvest of the femur, all soft tissues were carefully removed. The bone implant specimens of both alloys were subsequently fixed in neutral buffered 4% formalin solution and further processed for histological examination.

2.2.5 Microfocus computed tomography

Microfocus computed tomography (μCT) is an emerging technology that combines both noninvasive, tissue-preserving imaging and quantitative morphometry of bone structure in three dimensions [12] [18]. During the μCT-examinations the animals were generally anaesthetized by volatile isoflurane (Forane®, Abbot AG, Baar, Switzerland). The rats were scanned using a Siemens Inveon Acquisition Workplace 1.2.2.2. Scans were made at 70 kV voltage, 500 μA current, and 1000 ms exposure time. Rotation of 210 degrees by 180 rotation steps led to a resolution of the whole femoral bone with an effective pixel size of 35.55 μm. For reconstruction a down-sample factor of 1 was used. The system allowed the 3D reconstruction of a specimen from a set of 2D projections using the back projection of a filtered projection algorithm.

The scan data were converted into DICOM format and as such imported into the Medical Image Processing software Mimics® (Materialise NV, Leuven, Belgium), constructing a 3D model of the pin through image processing and 3D reconstruction technologies. Three-dimensional pin-bone surface models were also extracted from the μCT images, using the optimal parameter settings. The volume of interest was defined for each part using region-growing of determined Hounsfield units (HU) and manual drawing of bone-implant-contours at the cortical sites. The threshold for the pin was set at 226 to 3071 HU and for the gas volume at -1000 to -1024 HU. The volume of each part was measured by 3D morphometric analysis. Pin volume, pin surface, and gas volume were quantified using the

software program “Mimics“ (Version 14.0, Materialise, Leuven, Belgium), and histological evaluations were performed on each group after pin explantation.

For a reasonable statistical analysis of the μCT data six femoral rat bones were chosen for each alloy. The statistical evaluations were performed with SPSS 16.0 (SPSS Inc., Chicago, IL, USA), and the data displayed as medians and standard deviations.

2.2.6 Histological sample processing

Explanted bones were dissected from soft tissues and fixed in neutral buffered 4% formalin solution. The region of interest was excised using a high-precision saw (Exakt Apparatebau, Norderstedt, Germany). The samples were dehydrated in ascending grades of alcohol and embedded in light-curing resin (Technovit 7200 VLC, Kulzer & Co., Hanau, Germany). The blocks were processed with the Exakt Cutting and Grinding Equipment (Exakt Apparatebau, Norderstaedt, Germany) according to Donath [19]. Undecalcified thin ground sections were prepared through the central axis of the implant and parallel to the longitudinal axis of the femur shaft. In cases where nothing of the material was preserved, the orientation was approximated as precisely as possible to the original position of the implant. Sections were reduced to a thickness of approximately 30 μm and stained with Levai-Laczko dye. Digital virtual microscopic overview images at a 200x magnification were produced with the Olympus dotSlide Microscpic system (dotSlide - Virtual Slide System, Olympus, Japan).

2.3 Results

The Mg pins were implanted into 64 rat femura in 32 rats. One half of the femura (32 in 16 rats) belonged to the μCT group while the other half belonged to the histological group. In 16 femura of the μCT group WZ21 was implanted, in the other 16 femura ZX50 was implanted. One rat (2 femura) of the μCT –ZX50 group was lost intraoperatively due to anaesthetic complications. Furthermore one femur fractured in this group in consequence of drilling, and in 2 femura the pins displaced. In the WZ21 μCT group one femur fractured and 3 pins showed inadequate placement.

The histological group was also devided into two groups: in 16 femura WZ21 was implanted and in 16 femura ZX50 was implanted. In the WZ21 histo-group as well as in the

ZX50 histo-group two femura fractured in consequence of drilling. Two pins showed displacement in the WZ21 group while one showed displacement in the ZX50 group.

Animals with fractured femura and animals with displaced pins were ruled out of the study. At the end of the study period in the 24th week 12 femura of WZ21 and 11 femura of ZX50 in the µCT group were available. In the histological group 12 WZ21-pins and 11 ZX50-pins remained. For quantitative measurements by Mimics® only six implants per alloy (ZX50 and WZ21) were used. Note that the µCT sections, the 3D reconstructions, and the histological sections indicated in the figures are representative examples for the respective times in vivo.

2.3.1 Degradation performance

The volume and surface changes and the amount of hydrogen gas formation of the ZX50 and WZ21 pins were followed by in vivo µCT analysis throughout the entire study period of 24 weeks (see **Figs. 2.1 a-d**). As expected, the alloys ZX50 and WZ21 exhibited very different degradation rates, as indicated by the change in volume shown in **Fig. 2.1a**. The ZX50 pins did start to corrode immediately after implantation and exhibited surface pits already within the first week, as illustrated in the 3D reconstructions shown in **Fig. 2.1d**. In parallel, the measured pin surface initially slightly increased as a result of the degradation (**Fig. 2.1b**), which in turn accelerated further corrosion. As a consequence the surface area of the ZX50 pins decreased after 4 weeks along with a loss in implant volume. The overall volume decrease of ZX50 pins was about 1.2% per day, and 50% median degradation was reached after approximately 6.5 weeks. Simultaneously to pin degradation considerable release of hydrogen gas occurred within a short time period, as illustrated in **Fig. 2.1c**. According to the electrochemical reaction $Mg + 2H_2O \rightarrow Mg(OH)_2 + H_2$ [9] one molecule of hydrogen gas is formed per one atom of Mg, which is about 920 mm^3 H_2 generated by the degradation of 1 mg Mg [20] (Note: according to the pin weight of 27 mg complete degradation leads to the formation of 25 cm^3 hydrogen gas). Consequently, in average about 270 mm^3 H_2 per day was produced within the first 12 weeks of ZX50 pin degradation. After 4 months no pin material and also no hydrogen bubbles were detected by µCT as reflected in **Fig. 2.1a**, **Fig. 2.1c**, and **Fig. 2.1d/o**. It is worth noting that the determination of the hydrogen gas volume using Mimics® gives most likely only a rough estimation since the applicability of this method is proven only for measurement of solid structures [19] [20]. However, in our

case its reliability is assumed to be sufficient since similar values can be derived from the size of gas bubbles visible in histological thin sections.

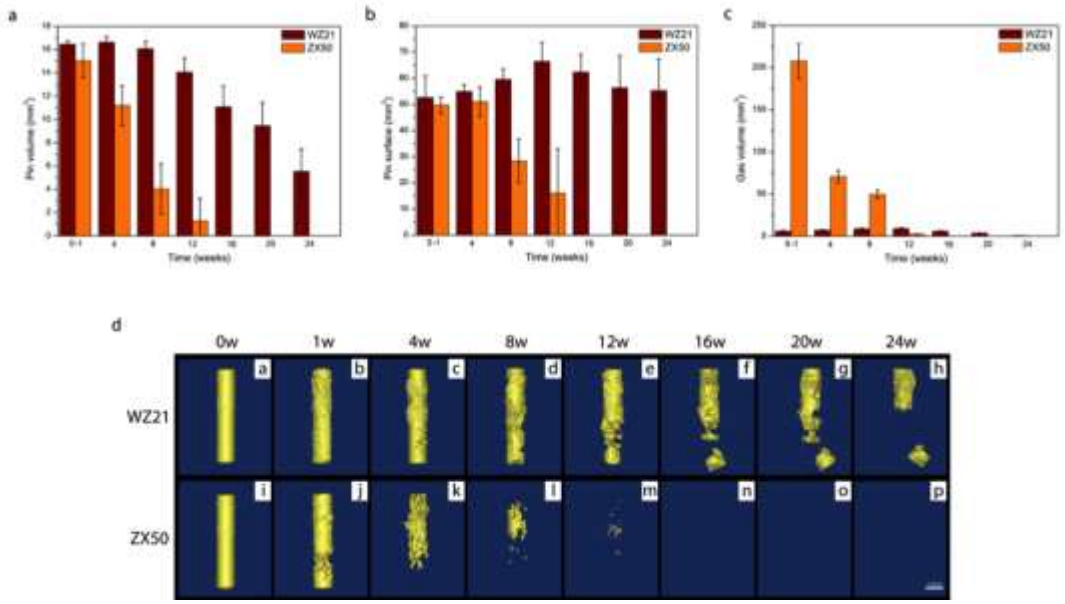

Figure 2.1: Degradation performance of implanted WZ21 and ZX50 alloys during the 24 weeks study period detected by µCT measurements. (a) loss of volume; (b) change of surface area; (c) volume of hydrogen gas bubbles; (d) 3D reconstruction of the pins. WZ21 alloy shows a moderate loss of pin volume and a degradation process in a rather linear manner after the 8th week (a, d). During degradation only few gas bubbles were visible. In ZX50 corrosion is rather fast and grooving is already detectable after the first week (d/j), and no more pin remnants are visible at week 16 (d/n). The rapid corrosion of ZX50 forms great amounts of gas within a short period.

In contrast, the volume of the WZ21 pins (**Fig. 2.1a**) decreased only moderately during the initial months after implantation. Merely 2.3% of the initial pin volume degraded within the first two months. A slight increase of pin volume was observed at week 4, which can be related to the formation of corrosion products on the magnesium pin. After week 8 the degradation proceeded in a rather linear manner with an average volume loss of around 0.5% per day. 50% pin degradation was reached after approximately 21.5 weeks. Since the degradation occurred markedly slower in WZ21 pins a large surface area was measured over the whole period of 24 weeks, with a maximum at 12 weeks, as indicated in **Fig. 2.1b**. For WZ21 implants it is worth mentioning that the type of the surrounding tissue significantly affects the degradation characteristics. Pin parts situated in the soft tissue degraded the fastest, starting corrosion after 4 weeks. Subsequently, after around 16 weeks, degradation in the intramedullary cavity followed (**Fig. 2.1d/e**). However pin material surrounded by cortical bone lasted occasionally more or less undissolved for a longer period than 24 weeks. The observed hydrogen gas volume during WZ21 corrosion was moderate and nearly constant for the whole period of observation (**Fig. 2.1c**), in average about 7 mm^3. As about

50% of the pin volume degraded from week 8 to week 21.5 in a more or less linear manner, a corresponding hydrogen gas evolution of about 130 mm^3 H_2 per day can be calculated. Since the observed gas volume around the implant did not change significantly and was always about 7 mm^3, the important conclusion can be drawn that the surrounding tissue is able to carry away a daily dosage of 130 mm^3 H_2.

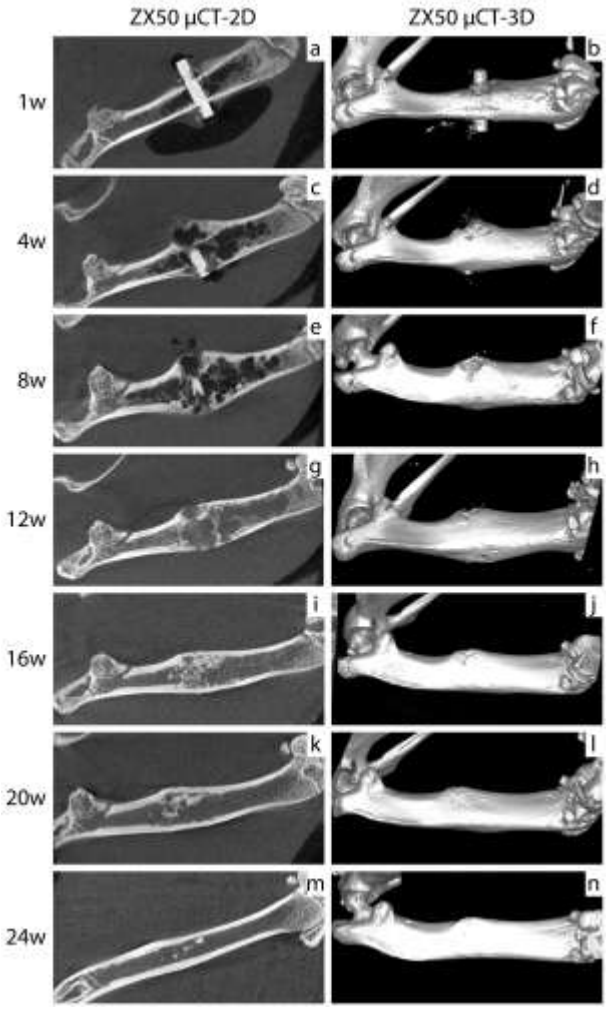

Figure 2.2: µCT reconstructions showing the degradation process of ZX50 pins and bone response in 2D slices (left pictures) and 3D displays (right pictures). (a) shows the pin situated bicortically in the femoral bone with adjacent gas bubbles (black colored). During corrosion gas bubbles also appear within the medullary cavity (c,e), while intense callus formation occurs around the implantation site (d). After the pin corroded entirely the bone exhibits rapid and entire recovery (week 16 to 24).

2.3.2 Biological response

Both implant materials were well tolerated by the rats. Clinically, all animals showed slight reddening of the wound, as well as mild wound swelling resulting from surgery. However, both incidences resolved completely after 3-5 days post operationem and no wound infections were observed. All animals also tolerated full weight bearing post operationem.

The biological response to the inserted and degrading implants is illustrated in **Figs. 2.2 to Fig. 2.4. Figures 2.2 and 2.3** show µCT reconstructions of the degradation process and bone response of the ZX50 and WZ21 implants, respectively, and **Fig. 2.4** displays the corresponding histological features.

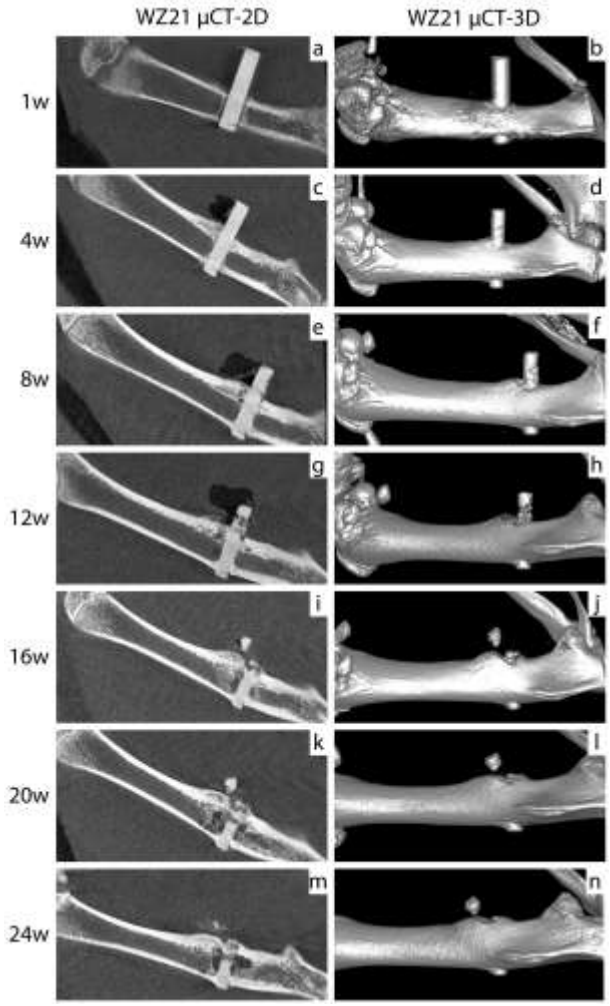

Figure 2.3: µCT reconstructions showing the degradation process of WZ21 pins and bone response in 2D slices (left pictures) and 3D displays (right pictures). Bicortically implanted WZ21 pin exhibit degradation primary in the surrounding soft-tissue (e) followed by corrosion in the intramedullary cavity (i) and slight degradation within the cortical bone (m). Gas bubbles (black) only occur in small amounts (c,e,g).

In terms of bone reaction to the inserted ZX50 implants, the fast Mg ion release during degradation led to an enhanced neo-formation of bone tissue around the implant, as can be seen in the µCT reconstructions of **Fig. 2.2c-f** and the histological preparation of **Fig. 2.4a**. In parallel, substantial gas formation appeared in the intramedullary cavity and extraosseal around the ZX50 pins, which is well visible in the µCT sections of **Fig. 2.2**. Thereby the gas pressure induced some mechanical disturbance of bone regeneration, which resulted in distinct callus formation, especially at the medial pin outlet, which can nicely be

seen in **Figs. 2.2c and 2.2e**. Both, new bone formation and bone resorption, occurred to a great extent at the same time. This was not accompanied by inflammation, however, as indicated by the histological thin ground section in **Fig. 2.4a**. At the time (week 12) when the major pin volume was degraded (**Fig. 2.1a and Fig. 2.1d/m**) and no further hydrogen formation took place (**Fig. 2.1c**), the gas bubbles were resorbed expeditiously and the bone remodeled in a fast way (**Fig. 2.2g-n**). At week 16 cortical bone defects were almost entirely healed (**Fig. 2.2i,j**). After 24 weeks the medullary cavity was regenerated to a nearly normal extent (**Fig. 2.2m and Fig. 2.4c**).

The WZ21 alloy resulted in enhanced bone formation around the pins from week 4 to 8, as displayed in **Figs. 2.3c-f**. Histological analysis did not reveal obvious adverse tissue reactions around this alloy (**Fig. 2.4**). Gas formation occurred in an amount that did not affect bone regeneration and was almost entirely resorbed by surrounding tissue (**Figs. 2.3 and 2.4**). New bone formation around the pin occurred in the medullary cavity and in an enhanced way at the medial corticalis (**Fig. 2.4e** and **2.4f**). Also, new bone formation showed close contact to the implant at the cortical and medullary cavity site within the first 12 weeks. Afterwards, when degradation started in the medullary cavity, both, bone resorption and formation occurred simultaneously (**Fig. 2.4g**). The junction between cortical bone and WZ21 implant surface remained tight. Here hardly any signs of corrosion were seen within the 36 weeks study period (**Fig. 2.4h**).

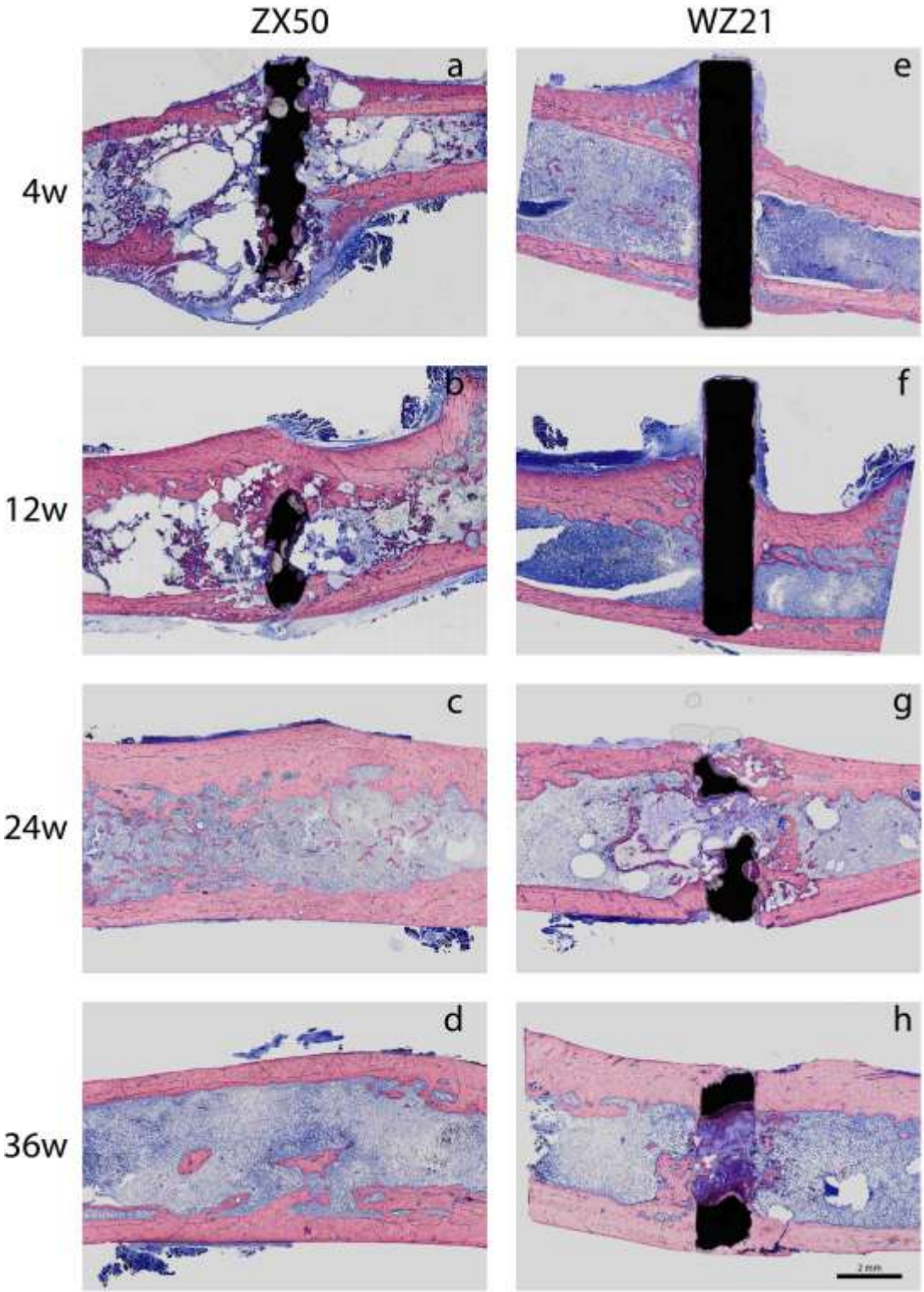

Figure 2.4: Histological thin slides of ZX50 (a-d) and WZ21 (e-h) pins in a Levai-Laczko staining. WZ21 represents the positive properties of Mg alloys by enhancing new bone formations around the implant. Even in case of massive callus formation and release of high amounts of gas (a) the bone shows no permanent harming but complete restitutio ad integrum.

2.4 Discussion

In osteosynthesis, biodegradable metallic implants are considered an attractive alternative to their permanent counterparts, particularly in pediatric cases where surgical interventions are intended to be minimized. In this context, numerous studies have been focusing on evaluating the degradation performance of the implant materials and its optimization, i.e. [3-7]. However, the impact of degradation products, gas formation and degradation rates on the remodeling potential of the bone after full implant degradation remained unclear. Based on a growing rat skeleton model we demonstrate that the bone is able to remodel entirely after complete degradation of magnesium pin implants despite high degradation rates and the release of considerable gas amounts. Moreover, online µCT monitoring is shown to be very suitable for studying the degradation performance of temporary Mg implants and the related bone remodeling in the same living animal. It complements the information gained by histological analysis and provides supplemental data essentially without requiring extra animals.

During the study period, pin implantation did not affect the moving ability of the rodents, nor was the daily behavior of the animals altered. Besides some initial redness and swelling of the surgical wound, no reaction to pin degradation such as macroscopically visible gas bubbles in the operation area were observed. However, histologically and µCT-morphologically, considerable bone tissue reactions occurred when large amounts of hydrogen gas evolved within a short time period, as observed in the case of the ZX50 alloy. Crystalline Mg–Zn–Ca alloys such as ZX50 tend to degrade rather rapidly in buffered physiological solutions [5] thereby releasing large amounts of Mg ions into the surrounding tissue. As a result magnesium hydroxide is formed [9], which promotes the accumulation of calcium phosphates and new bone formation around the implants [7, 21]. At the same time, however, substantial hydrogen gas accumulations occur as a result of the rapid corrosion of the magnesium alloy [22]. These gas bubbles impede a good connectivity of osteocytes with the ZX50 implant surface, as observed for the histological specimens (**Fig. 2.4a**).

In contrast, the gas evolution played a subordinate role in the in vivo degradation of the WZ21 pins. In fact the gas formation and absorption rates were rather equal and a daily amount of 130 mm^3 H_2 was calculated from the mass loss (see section 3.1), whereas for the ZX50 implants a daily formation of about 270 mm^3 H_2 was evaluated, with the consequence

of massive gas bubble formation (**see Figs. 2.2c-f**). Despite the fact that the average amount of 130 mm^3 H_2 per day is only a vague estimation (because it does not take into account the surface area, local differences in vascularization, and the effect of gas pressure in the bubbles), it gives for the first time an approximate number of how much hydrogen can be carried away by the surrounding tissue for typical implant geometries in well-vascularized locations. For WZ21, tissue healing appeared quite undisturbed and newly formed bone entered tight connection to the implant surface (**Fig. 2.4c and Fig. 2.5e,f**). A delayed degradation occurred within the first 4 weeks. This may be attributed to the formation of a fairly stable corrosion product layer on the implant surface, which protected the material against further degradation [7].

Besides disturbing the bone implant connectivity the hydrogen gas formation had another effect, which was particularly pronounced in the case of the ZX50 pins. The space-consuming gas pockets increased the inner mechanical pressure, which interfered with the initial cortical bone healing process, resulting in callus formation (**Fig. 2.3c, e and Fig. 2.5a**). As bone also reacts on mechanical instabilities, the callus formation was more pronounced on the medial than on the lateral side, and by the fact that gas moves towards the area of least resistance, cortical defects appeared mainly at the medial side (**Fig. 2.3f**). Simultaneously to the formation of new bone, bone tissues that did not exhibit mechanical function were detached again (**Fig. 2.5b**). This is in line with the definitions of Roux-Wolff `s law, postulating that bone formation is governed by mechanical forces and that bone furthermore has the capacity to form and adapt its architecture in accordance with the externally applied loads [23] [24] In a more recent study Huiskes proved and validates this statement by μCT and μFEA (finite element analysis) [25].

In that way excessive new bone formation and bone resorption occurred at the same time without inflammation reactions, as seen in the histological images. When implant degradation completed and gas evolution decreased, the positive influence of magnesium prevailed, resulting in rapid full regeneration of the cortical bone defects (**Fig. 2.3i-n**). Concurrently, resorption of the before formed futile bone proceeded in the medullary cavity and recovered restitution ad integrum (**Fig. 2.2m**). It is therefore assumed that the gas, which evolved during degradation of the Mg material, does not significantly affect the physiological functionality of the surrounding tissue. Even though such favorable situation occurred in our case where a small implant was chosen, the implant size would be significantly larger for the intended use as intramedullar nail in pediatric orthopedics and result in higher amounts of

evolved gas. However, on the condition of similar or ever higher aspect ratio of the implant the tissue structures available for gas resorption would proportionally increase and consequently their 'burden' might be on a similar level.

With respect to fracture stabilization the corrosion rate and also the homogeneity of degradation play a more fundamental role, however. Optimally, the mechanical strength of the material should be maintained for at least 4 weeks [26]. Although the bone tissue seems to be able to cope with fast degradation and gas evolution rates the implant strength may be significantly deteriorated. The present study indicates also that the type of environmental tissue plays an important role in the degradation process. The fastest degradation rate was seen in soft tissues (**Figs. 2.2e and 2.4g**) and may be caused by the superior vascularization and/or due to the avoidance of changes in local pH-value. (Note: Mg corrosion is generally accompanied by a pH increase, which in turn reduces the corrosion rate [27]). Accelerated degradation was also seen at the outer corticalis, which may have been induced by crevice effects. In general there could be seen a faster degradation of intramedullary compared to cortical areas (**Fig. 2.3m and 2.4g**). This is attributed to the enhanced vascularization of the bone marrow. Here pH neutralization and degradation product removal may occur more easily. When degradation occurred in the cortical area, bone was sometimes seen to dislocate into the bone marrow (**Fig. 2.2e**) due to loosening of the hard cortical bone structure. Although degradation took place faster in the intramedullary area than in cortical and newly grown bones, no inflammatory reactions were observed. In the case of WZ21 pins, the implant parts located in the cortical bone remained undissolved for more than 36 weeks, probably due to the tight junction of the implant and the cortex, which inhibits contact with aqueous fluids. However, for the use in pediatric trauma the degradation in the medullary cavity is of crucial importance as the functional parts of the osteosynthesis materials are located mainly intramedullary.

In contrast to the ZX50 material, the WZ21 alloy combines good mechanical properties and an appropriate degradation rate. Also with respect to the gas formation WZ21 is the more ideal material because its gas evolution is very moderate. Although this material may be well tolerated in adults, there are some concerns in using rare-earth containing alloys (e.g. the element Y) in degradable implant solutions for children. It is recommended that their influence is studied in detail, particularly since bone and bone marrow are known to exhibit very slow release rates of such substances [28, 29] and the tolerance limits in children are small.

Microfocus computed tomography (µCT) enables both, in vivo monitoring of implant degradation in small animals and observation of the bone tissue response and adaptation in the living animal. **Fig. 2.5** illustrates the remarkably good coherence between histological thin sections and µCT slices. As it can be seen in the µCT (middle picture) the cortical bone and the implant pin appear strongly hyperintense (bright) and the gas formations hypointense (black). Those structures are in good concordance with the rose (bone) and black (pin) structures within the histological stainings (left picture), and also fibrous tissue-like reactions and callus formation (blue in the histological staining) can be pursued by µCT. By using 3D-resonstructions of the µCT slices the extent of gas pockets can be represented visually (pink, right picture) and volume and surface area measurements can be accomplished. While histological examinations will keep their importance for immunological and histomorphological demands, our study shows that for the interpretation of degradation behavior and bone tissue recovery, µCT analysis is highly efficient in terms of reproducibility and added value with respect to information gained via 3D reconstruction. In addition, it has the great advantage that animals do not need to be euthanized for such investigations.

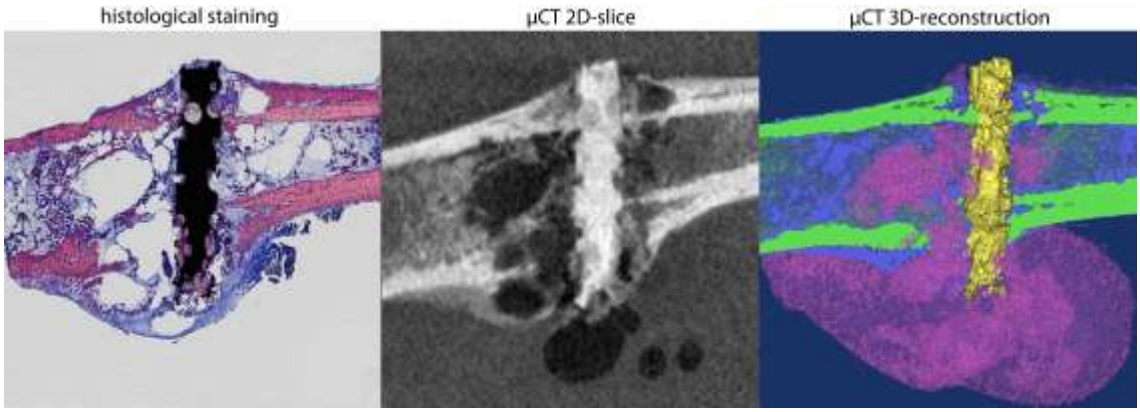

Figure 2.5: Alloy ZX50 after 4 weeks study period: comparison between histological stained thin slide (left), µCT 2D-slice (middle) and µCT Mimics® 3D-reconstruction (right).

2.5 Conclusions

The in vivo degradation performance of two different magnesium alloys and the corresponding bone response were investigated in a growing rat model by continuous in vivo µCT monitoring. A fast degrading magnesium alloy (ZX50) with corresponding massive gas formation within a short period of time and a slowly degrading alloy (WZ21) were tested. The results attest that:

(i) WZ21 implants maintain their integrity for 4 weeks and corrode subsequently with about 0.5% volume loss per day; ZX50 alloys commence the degradation process immediately after implantation and degrade with ≈ 1.2% daily volume loss.

(ii) WZ21 alloys generate enhanced bone neoformation around the implant and give evidence for good osteoconductivity and osteoinductivity of magnesium.

(iii) Bone recovers restitutio ad integrum after complete degradation of the magnesium implant, even in the case of massive gas formation (as for ZX50 degradation) and corresponding alterations of the bone.

These results are considered to be of substantial significance in view of Mg-implant application in pediatrics, where, besides material compatibility with the living organism, primarily two key factors are required: mechanical integrity for at least 4 weeks and complete recovery of the bone.

Acknowledgements

The authors appreciate support from the Laura Bassi Center of Expertise BRIC (Bioresorbable Implants for Children; FFG -Austria) and from the Staub/Kaiser Foundation, Switzerland. Furthermore authors would like to thank Mag. Stefan Tangl (Department of Oral Surgery, Medical University of Vienna, Austria) for the histological workup of the specimen.

References

[1] Staiger MP, Pietak AM, Huadmai J, Dias G. Magnesium and its alloys as orthopedic biomaterials: a review. Biomaterials. 2006;27:1728-34.

[2] Claes L. Mechanical Characterization of Biodegradable Implants. Clinical Materials. 1992;10:41-6.

[3] Witte F, Hort N, Vogt C, Cohen S, Kainer KU, R. W. Degradable biomaterials based on magnesium corrosion. Curr Opin Solid State Mater Sci. 2008;12:63-72

[4] Krause A, von der Höh N, Bormann D, Krause C, Bach F-W, Windhagen H, et al. Degradation behaviour and mechanical properties of magnesium implants in rabbit tibiae. J Mater Sci Mater Med. 2010;45:624-32.

[5] Hänzi AC, Gerber I, Schinhammer M, Loffler JF, Uggowitzer PJ. On the in vitro and in vivo degradation performance and biological response of new biodegradable Mg-Y-Zn alloys. Acta Biomater. 2010;6:1824-33.

[6] Huan ZG, Leeflang MA, Zhou J, Fratila-Apachitei LE, Duszczyk J. In vitro degradation behavior and cytocompatibility of Mg-Zn-Zr alloys. J Mater Sci Mater Med. 2010;21:2623-35.

[7] Witte F, Kaese V, Haferkamp H, Switzer E, Meyer-Lindenberg A, Wirth CJ, et al. In vivo corrosion of four magnesium alloys and the associated bone response. Biomaterials. 2005;26:3557-63.

[8] Castellani C, Lindtner RA, Hausbrandt P, Tschegg E, Stanzl-Tschegg SE, Zanoni G, et al. Bone-implant interface strength and osseointegration: Biodegradable magnesium alloy versus standard titanium control. Acta Biomater. 2011;7:432-40.

[9] Pourbaix M. Atlas of electrochemical eqilibria in aqueous solutions. Housten, Texas: National Association of Corrosion Engineers; 1974.

[10] Zberg B, Uggowitzer PJ, Loffler JF. MgZnCa glasses without clinically observable hydrogen evolution for biodegradable implants. Nat Mater. 2009;8:887-91.

[11] Gu X, Zheng Y, Cheng Y, Zhong S, Xi T. In vitro corrosion and biocompatibility of binary magnesium alloys. Biomaterials. 2009;30:484-98.

[12] Feldkamp LA, Goldstein SA, Parfitt AM, Jesion G, Kleerekoper M. The direct examination of three-dimensional bone architecture in vitro by computed tomography. J Bone Miner Res. 1989;4:3-11.

[13] Fajardo RJ, Muller R. Three-dimensional analysis of nonhuman primate trabecular architecture using micro-computed tomography. Am J Phys Anthropol. 2001;115:327-36.

[14] Kothari M, Keaveny TM, Lin JC, Newitt DC, Genant HK, Majumdar S. Impact of spatial resolution on the prediction of trabecular architecture parameters. Bone. 1998;22:437-43.

[15] Balto K, Muller R, Carrington DC, Dobeck J, Stashenko P. Quantification of periapical bone destruction in mice by micro-computed tomography. J Dent Res. 2000;79:35-40.

[16] Gunde P, Hänzi A, Sologubenko A, Uggowitzer P. High-strength magnesium alloys for degradable implant applications. Materials Science and Engineering A. 2011;A:1047-54.

[17] Hänzi AC, Sologubenko AS, Uggowitzer PJ. Design strategy for new biodegradable Mg–Y–Zn alloys for medical applications. Int J Mat Res. 2009;100:1127-36.

[18] Kinney JH, Lane NE, Haupt DL. In vivo, three-dimensional microscopy of trabecular bone. J Bone Miner Res. 1995;10:264-70.

[19] Nalcaci R, Ozturk F, Sokucu O. A comparison of two-dimensional radiography and three-dimensional computed tomography in angular cephalometric measurements. Dentomaxillofac Radiol. 2010;39:100-6.

[20] Bowers M, Trinh N, Tung G, Crisco J, Kimia B, Fleming B. Research confirms accuracy of Mimics' segmentation tools. The Warren Alpert Medical School of Brown University, USA2011.

[21] Xu L, Zhang E, Yin D, Zeng S, Yang K. In vitro corrosion behaviour of Mg alloys in a phosphate buffered solution for bone implant application. J Mater Sci Mater Med. 2008;19:1017-25.

[22] Song G, Sing S. A Possible Biodegradable Magnesium Implant Material. Advanced Engineering Materials. 2007;9:298-302.

[23] Wolff J. Das Gesetz der Transformation der Knochen. Berlin: Springer; 1986.

[24] Roux W. Der Kampf der Teile im Organismus. Leipzig:1881

[25] Huiskes R. If bone is the answer, then what is the question? J Anat. 2000;197 (Pt 2):145-56.

[26] Wilkins KE. Principles of fracture remodeling in children. Injury. 2005;36 Suppl 1:A3-11.

[27] Song G, Atrens S. Understanding Magnesium Corrosion—A Framework for Improved Alloy Performance. Advanced engeneering Materials. 2003;5:837-58.

[28] Wells W, VW. The Lanthanides, Rare Earth Metals. Metals and Compounds, Compunds of inorganic Nitrogen, Carbon, Oxygen and Halogens. New York Eula Bingham: Bingham, E; 1984. p. 423-58.

[29] Hirano S, Suzuki K. Exposure, metabolism and toxicity of rare earths and related compunds. . Environmental health perspectives. 1996;104:85-95.

3 Determination of the Bone-Implant-Interface

The bone-implant-interface is the crucial area of biological interactions. Transfer of mechanical loads due to friction, but also bone cell adherence, inflammatory reactions or agglomeration with gametes occurs herein. Therefore a quick and tight connection of bone with the material is of particular importance.

PHB, crystalline and amorphous magnesium alloys: promising candidates for bioresorbable osteosynthesis implants?

Anna Celarek, Tanja Kraus, Elmar K. Tschegg, Stefan F. Fischerauer[*]*, Stefanie Stanzl-Tschegg, Peter J. Uggowitzer, Annelie M. Weinberg*

MATER SCI ENG C. 2012; 32(6): 1503-1510

In this study various biodegradable materials were tested for their suitability for use in osteosynthesis implants, in particular as elastically stable intramedullary nails for fracture treatment in paediatric orthopaedics. The materials investigated comprise polyhydroxybutyrate (PHB), which belongs to the polyester family and is produced by microorganisms, with additions of ZrO_2 and a bone graft substitute; two crystalline magnesium alloys with significantly different degradation rates ZX50 (MgZnCa, fast) and WZ21 (MgYZnCa, slow); and MgZnCa bulk metallic glasses (BMG). Push-out tests were conducted after various implantation times in rat femur meta-diaphysis to evaluate the shear forces between the implant material and the bone. The most promising materials are WZ21 and BMG, which exhibit high shear forces and push-out energies. The degradation rate of ZX50 is too fast and thus the alloy does not maintain its mechanical stability long enough during the fracture-healing period. PHB exhibits insufficient mechanical properties: it degrades very slowly and the respective low shear forces and push-out energy levels are unsatisfactory.

Keywords: Polyhydroxybutyric acid; PHB; magnesium; biodegradation; shear; bone healing

[*] Author's contribution to this study: study planing, surgery of animals and animal care, literature research, and revision of the manuscript.

3.1 Introduction

Interest in biodegradable materials for use as temporary implant material in osteosynthesis has increased continuously over the past few years [1-7]. Using biodegradable implants may circumvent the disadvantages of (e.g.) permanent titanium or stainless steel devices , such as prolonged physical irritation or chronic inflammation [8,9]. In addition, using biodegradable materials renders subsequent surgical intervention for implant removal unnecessary and morbidity-related repeated surgery can be reduced. This creates new opportunities for trauma treatment, not least for the benefit of the paediatric population.

In recent years magnesium alloys have been considered promising candidates for applications in osteosynthesis and have already been tested *in vivo* [1,2,10,11]. Their elastic properties resemble those of bone [7,12] and they are considered ideal for hard tissue implants employed in fracture stabilization because stress shielding is avoided and bone regeneration is enhanced. Magnesium alloys also exhibit good biocompatibility with no systemic inflammatory reaction or effect on cellular blood composition [4,10,12,13].

In this study both crystalline and amorphous magnesium alloys were investigated as potential candidates for implant applications. Their glassy structure leads to higher strength and elasticity and allows much higher fractions of alloying elements than crystalline Mg, where the solubility of elements like Zn or Ca is limited to a few percent. This makes possible better control over the degradation rate and thus hydrogen evolution, which is an important issue when crystalline Mg alloys are deployed [14,15].

Another new biodegradable implant material which is not yet popular is PHB (Poly-D-(-)-3-hydroxybutyrate). PHB is a polymer produced by numerous different microorganisms as their carbon and energy storage. It is highly crystalline and degrades in water or aqueous solutions to D-(-)-3hydroxybutyric acid, which is also naturally found in human blood. One of its decisive advantages is its less severe environmental pH change during degradation [3,16,17].

For use as osteosynthesis implant material, in particular as elastic stable intramedullary nailing (ESIN) in paediatric fracture treatment, biodegradable materials must fulfil several criteria. Ideally, an implant is meant to stabilize a fracture until the bone is restored enough to carry loads. This may take 3-6 weeks, depending on the age of the child [18]. After this time the implant should gradually lose its mechanical stability and dissolve into non-harmful components which are carried away by body fluids or even integrated into

the newly formed bone [19]. The mechanical, chemical and biological requirements for implant materials are manifold. Most crucially, they must (i) possess adequate stiffness, ideally similar to that of bone; (ii) show moderate ductility, to allow simple surgical insertion of the implant; (iii) cause no inflammatory reactions; (iv) activate enhanced bone growth; (v) demonstrate a balanced degradation rate, optimized in such a way that the implant starts to lose volume and mechanical strength towards the end of the healing process by decomposing completely within at most one year; (vi) possess non-toxic corrosion products, which do not accumulate in body organs; and (vii) show minimal relative bone-implant movement [3,20].

With regard to the latter quality in particular, the aim of this study was to determine and compare the quality of the bone-implant interface by means of implant push-out tests. A rat model was deployed, plus a mechanical push-out protocol which was mainly established during previous research [21-23]. This protocol was used both as a guideline and a means of comparison with current commercial materials (Ti alloy, PLGA and Mg WE43). Valuations were made at different intervals *post operationem* (p.o.), with respect to (i) shear strength; (ii) energy absorption; and (iii) stiffness of the implant-bone system.

3.2 Materials and Methods

3.2.1 Materials

Three types of PHB, two crystalline Mg alloys, and 3 modifications of bulk amorphous Mg were used in this study. **Table 3.1** provides an overview of their chemistry and properties. PHB was synthesized at the Institute for Chemistry and Technology of Materials at Graz University of Technology [16], the Mg alloys were produced at the Laboratory for Metal Physics and Technology at ETH Zurich [12,14,15]. The implants comprised cylindrical pins of 1.6 mm in diameter and 8 mm in length. They were carefully dry-machined with clean tools to avoid contamination and allow good surface quality. After machining they were cleaned in a cascade of pure ethanol in an ultrasonic bath and dried in warm air.

3.2.2 Animals

Male Sprague–Dawley rats five weeks of age with body weights of 140–160 g were used in this study. Each rat received two identical pins (**Tab. 3.1**) implanted meta-diaphyseally in each distal femur. All animal experiments were conducted according to the

rules of ethical respect for animals and were authorized by the Austrian Ministry of Science and Research (accreditation number BMWF-66.010/0113-II/10b/2009).

3.2.3 Surgical Procedure

Volatile isoflurane (Forane, Abbot AG, Baar, Switzerland) for general anaesthesia proceeded by sedation was administered to the rats. The meta-diaphyseal region of the distal femur was exposed through a lateral approach. A drill (1.5 mm) with ascending diameter (Synthes®, Paoli, PA, USA) was used to prepare the transcortical implantation bed with the longitudinal axis of the drill hole perpendicular to the longitudinal axis of the femoral diaphysis. Drilling was performed at a low rotational speed of 200 rpm. Profuse physiological saline irrigation was applied using a syringe in order to minimize frictional heat and thermal necrosis. The cylindrical implant was inserted by gentle tapping, resulting in a uniform press fit. After transcortical placement was ensured, the operating field was irrigated thoroughly with physiological saline solution and the wound was closed in layers. The contra-lateral side was then treated identically and using the same type of implant. The general anaesthesia was then antagonized and analgesia was ensured postoperatively and during the first postoperative week (up to the 7th day). Postoperatively the rats were allowed to move freely in their cages without external support and with unrestricted weight bearing. Regular clinical observations were performed throughout the study period.

Table 3.1: Designation, chemical composition and properties of the biodegradable materials investigated.

Designation	Chemistry	Description	Properties *
PHB	Poly-D-(-)-3-hydroxybutyrate	Bulk polymer	R_m = 37.6 MPa
			E = 3.0 GPa.
			M = $8*10^4$ g mol^{-1}
P3Z10H **	PHB + 3% ZrO_2 + 10% Herafill®** [wt-%]	Polymer composite with ZrO_2 and bone graft substitute.	R_m = 31.0MPa
			E = 2.9 GPa.
P3Z30H **	PHB+ 3% ZrO_2 + 30% Herafill®**[wt-%]		R_m = 25.3 MPa
			E = 2.8 GPa
Mg ZX50	5 % Zn, 0.25 % Ca,	Crystalline Mg; grain size 4 µm	R_m = 295 MPa
	0.15 % Mn. [wt-%]		E = 45 GPa
Mg WZ21	2 % Y, 1.0 % Zn, 0.25 % Ca, 0.15 % Mn [wt-%]	Crystalline Mg; grain size 7 µm	R_m = 250 MPa
			E = 45 GPa
Mg Am29	29 % Zn; 5 % Ca [at-%]	Amorphous Mg bulk metallic glass (BMG)	$R_m \approx$ 820 MPa
Mg Am32	32 % Zn; 5 % Ca [at-%]		E = 55 GPa
Mg Am35	35 % Zn; 5 % Ca [at-%]		

* R_m … Tensile strength; E … Young's modulus
** Addition of ZrO_2 to make it visible for X-rays in radiography and µCT against the background of soft tissue; Herafill® bone graft substitute (calcium carbonate, calcium sulphate, antibiotics gentamicin, glycerol tripalmitate) buffers the pH value to physiological levels, counteracting the acid-generating degradation of PHB; osteoinductive and osteoconductive properties; the antibiotic decreases the danger of an infection.

3.2.4 Specimens

Generally 8 pins per material were used. For the BMG alloy, however, only 4 implants per BMG type were applied. Biomechanical examinations were performed at predetermined times: 1, 3 and 6 months *post operationem*. Since Mg WZ21 was valued as most promising material additional measurements were performed after 2 months. Immediately after the harvest of the femur, all soft tissues were carefully removed. The bone implant specimens were subsequently moistened in physiological saline and kept frozen (-20°C) until further mechanical testing took place. The specimens were thawed at least one hour and at most 5 hours before testing. The influence of freezing on the mechanical properties was assumed to be negligible [24]. For the mechanical testing only 'qualified'

pin/femur samples were used. Improper samples with incorrect pin placement, with bones overgrowth on one or both ends of the pins, or with fractured bone or pin were excluded from the test.

3.2.5 Optical Assessment

Prior to mechanical testing, all samples were inspected by optical microscopy (SZH-ILLD, Olympus, Japan) and photographed for subjective visual assessment of the state of the implant and bone. The degradation and position of the outermost parts of the pin were documented, as well as the state of the peripheral cortex. Pins were excluded from push-out testing if they did not intersect the cortex on both sides of the diaphysis or were overgrown by a thick layer of new bone.

3.2.6 Histology

Specimens for histology were fixed in neutral buffered 4% formalin solution, dehydrated in ascending grades of alcohol, embedded in light-curing resin (Technovit 7200 VLC and 9100, Heraeus Kulzer, Hanau, Germany) and cut with a high-precision saw (Exakt Apparatebau, Norderstedt, Germany) [25]. Undecalcified thin ground sections were cut through the central axis of the implant, in plane with the longitudinal axis of the bone. Sections were reduced to a thickness of approximately 30 µm. The Mg samples were stained with Laczko-Levai dye, which dyes bone pink-red, collagen fibres blue-violet, and elastic fibres red. The PHB samples were stained with Toluidine Blue O which dyes cells and soft tissue blue [26,27]. Both procedures, Laczko-Levai and Toluidine Blue O, are known to be applicable for this kind of samples [25, 26, 28].

Microscopic overview images were typically taken at 200x magnification (dotSlide - Virtual Slide System, Olympus, Japan).

3.2.7 Mechanical Testing

The push-out displacement of the pin was achieved by pressing a cylindrical steel rod of 1mm diameter (63% of the pin diameter) vertically against the lateral end of the pin at a constant rate of 1mm min^{-1}. A system of custom-engineered clamps ensured the vertical position of the pin during measurement (see **Fig. 3.1a**).

The acting force was applied by a testing machine (QTS 10, QuickTest), gauged (transducer type S9 2kN, HBM, Germany), amplified (KWS 3072, HBM, Germany), digitalized (U6, LabJack, USA) and recorded on a computer. The displacements were measured with a self-engineered video extensometer with a spatial resolution of about 3 µm (0.03 mm/pixel, enhanced by sub-pixel edge detection) using a camera (uEye UI-1225LE, IDS, Germany) with a 25mm lens (1:1.6 Tamron, Japan) and a 10 mm distance ring. Markers for the displacement tracking were glued to the rod and the bone. Force and position data were acquired every 100ms and a documental bitmap of the current frame was saved to the data disc every 2s. The pin displacement was calculated from the vertical distance of the marker positions.

A similar setup was used by Castellani et al. [21], Lindtner [22] and Tschegg et al. [23], who point out the advantages of a contact-free displacement measurement which minimizes errors introduced by the compliance of the setup. In our setup we used a more stable mounting system and a thinner press plunger to avoid contact with the clamps.

3.2.8 Data Analysis

The force was plotted versus the pin displacement (**Fig. 3.1b**). Shear strength, fracture energy and stiffness were determined from the plot as follows:

The ***shear strength***, R_s, was calculated by dividing the first local force maximum (point of failure: see **Fig. 3.1b**) by the area of the pin-bone-interface, which was determined as πDL (D: pin diameter 1.6mm; L: average pin length inside the bone, determined from 4 calliper gauge measurements, proximal, distal, anterior and posterior of the pin). If no distinct force maximum occurred (as is frequent with PHB), the point of failure was defined as the first sharp kink in the curve (see **Fig. 3.1c**). The shear strength is a commonly used parameter to evaluate push-out or pull-out tests [29-31]; however caution is needed when comparing results from different test conditions [32].

The ***energy absorption***, G_f, was defined as the integral of the force over the displacement from 0 to 0.5mm (hatched area in **Fig. 3.1b, Fig. 3.1c**). This is an arbitrarily chosen distance which assumes that an implant that has moved by 0.5 mm in clinical conditions can be considered a failure. Castellani et al. [21] calculated the energy absorption as the integral from 0 to failure displacement, defining failure displacement at maximum force. However, in PHB implants in particular the maximum is often not reached until after 1

or 2 mm. This may be explained as an effect of bulging and wedging of the elastic implant rather than interface failure [23]. Measuring the energy absorption between 0 and 0.5 mm is independent of the point of failure and thus might be a more reliable value than the shear strength of elastic materials without distinct force maximum. In addition, setting the integration area to 0.5mm also allows comparison with earlier results [23].

The ***interface stiffness, C_i***, was determined as the first linear slope in the F-dx plot between zero force and the shear strength (**Fig. 3.1b, Fig. 3.1c**). It gives a rough estimate of the implant-bone interface compliance.

Statistics: An average number of 20 specimens per materials group (up to 7 per time point) were investigated, with the exception of the amorphous Mg, where only a very limited number of 1-3 per group was available. Due to the statistically entirely inadequate situation the test results for amorphous Mg should be considered only as preliminary information.

For each material and inspection time, the median value,, 1st and 3rd quartile were calculated for shear strength, energy absorption and stiffness. If the pin could be pushed out gently with a finger, or if the shear strength was below 0.1 Nmm^{-2} and the fracture energy below 0.5mJ, the pin was classified as 'loosened' and quoted separately as a zero result.

A Shapiro-Wilk test showed that several groups were not normally distributed at 0.1 level. One-way ANOVA using Bonferroni means comparison was used to compare normally distributed groups with each other. The non-parametric Kruskal-Wallis analysis was performed on all groups with at least 3 samples. Significance level 0.1 was used for both ANOVA and Kruskal-Wallis.

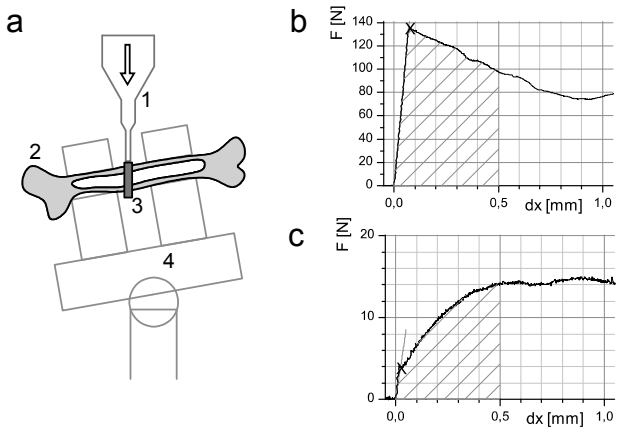

Figure 3.1: (a) Setup for push-out testing: (1) press plunger; (2) bone; (3) implant pin; (4) tiltable clamps; push-out force versus pin displacement: (b) the maximal force specifies the shear strength in Mg WZ21 3m sample; (c) the first sharp kink specifies the shear strength in P3Z10H 3m sample.

3.3 Results

In this section we first summarize the specific features that we observed by optical assessment and histological inspection. A visualisation by means of optical images, however, cannot reflect the situation properly. Thus, we concentrate on narrative description of the visible degradation and the implant-bone arrangement. For each material type the particularly noticeable peculiarities are quoted. Afterwards, the mechanical properties measured by means of the push-out test are listed for each material type and compared to each other.

3.3.1 Optical Assessment and Histology

PHB: The arrangement of the explanted implant-bone system six months p.o. is shown as an example in **Fig. 3.2a**. No material degradation is visible; the pin surface stayed smooth and intact even after such a long period. In most cases good bone apposition is visible. In some cases, however, the bone degenerates near the pin, leading to different grades of interface detach. Some specimens exhibit both effects (bone growing on one side of the pin and degenerating on the other), as shown in **Fig. 3.2a** (black arrows).

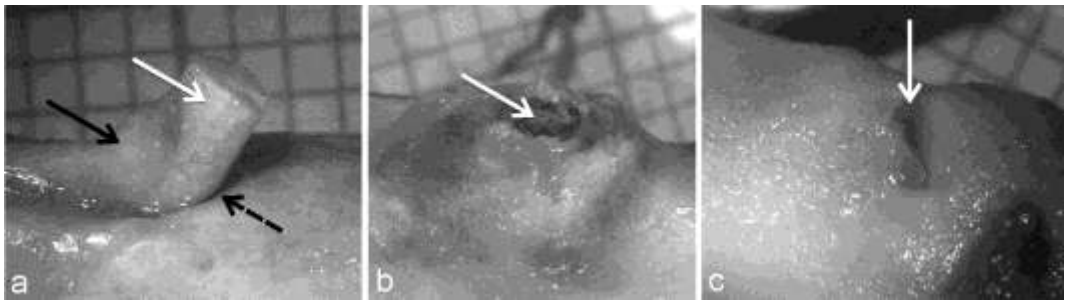

Figure 2.2: Photographs of typical implant-bone arrangement (Background grid 1mm). White arrow: implant; (a) P3Z30H, 6 months: bone degeneration proximal (dashed black arrow), bone apposition distal (solid black arrow); (b) Mg ZX50, 1 month, medial: volcano-shaped bone growth around the pin. (c) Mg ZX50, 1 month: pin almost completely overgrown by bone.

The histology displayed the formation of a thin bone layer (ca. 0.1mm) around the pin in the medullary cavity as early as 1 month p.o. (solid arrows in **Fig. 3.3a**). On the outer pin ends, in most cases massive bone growth could be observed (specifically, medial more than lateral and distal more than proximal: see solid arrow in **Fig. 3.3b**). However, it could be observed that some parts of the pin were not in direct contact with bone (dashed arrows in **Fig. 3.3a, Fig. 3.3b**). Generally, the bone apposition increased with implantation time.

No substantial differences could be seen between pure PHB and PHB with ZnO_2 and bone graft substitute additions after 3 months and later; the differences between individual bones were more pronounced.

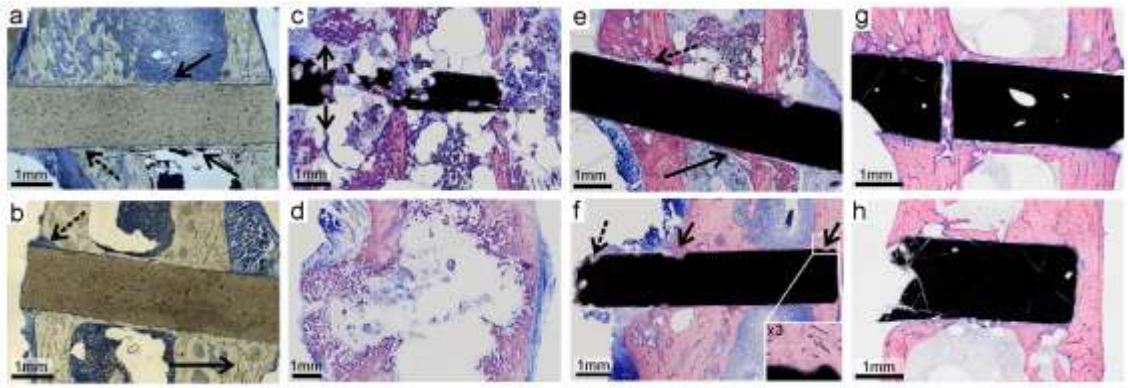

Figure 3.3: Optical images of stained slices of histological specimens (implant + bone), extracted after 1 month (a, c, e) and 3 months (b, d, f, g, h) post operationem; P3Z30H (a, b), Mg ZX50 (c, d) Mg WZ21 (e, f), Mg Am26 (g), Mg Am32 (h). Dashed arrows in (a,b,e): non-contact; solid arrow in (b): new bone; solid arrows in (a, e): bone layer forms on implant; solid arrows in (c): volcano shaped formation; solid arrows in (f): corrosion pits with ingrowing bone; dashed arrow in (f): degradation pits in contact with soft tissue. Soft tissue is blue in all images, bone is pink in c to h.

Mg ZX50: During the 1st month severe corrosion started. In some cases the pin diameter was reduced by almost half. Strong bone degeneration and loosening took place in one case. In most samples volcano-shaped bone growth with a hole around the pin was visible (**Fig. 3.2b**, solid arrows in **Fig. 3.3c**). In samples where the pin end was close to the original bone surface a bone layer did grow over the pin (**Fig. 3.2c**). These specimens were excluded from mechanical testing. In histology gas bubbles were discernible (**Fig. 3.3c**), most probably caused by the release of high amounts of hydrogen gas ($Mg + 2H_2O \rightarrow Mg(OH)_2 + H_2$) which cannot be carried away by the body if the degradation rate is too fast [2,12,14]). After 3 months, all implants were almost completely degraded. Only sporadically small fragments were visible in the medullary cavity (**Fig. 3.3d**). In most samples a shallow hollow was visible from the medial and lateral sides, and in one case a narrow tunnel occurred through the entire diaphysis, separated from the marrow by osseous walls. After 4-5 months no traces of the pin remained.

Mg WZ21: After 1 month superficial corrosion was visible on some pins, without substantially reducing the pin diameter. Bone did grow well on the pin, in most cases with direct contact (**Fig. 3.3e**). In only a few cases a narrow gap between implant and bone was observed (dashed arrow in **Fig. 3.3e**). In the medullary cavity a thin bone layer often formed on the implant (solid arrow in **Fig. 3.3e**). After 2 and 3 months severe corrosion pits

developed, especially in contact with soft tissue (dashed arrow in **Fig. 3.3f**), taking up to 10-20% of the pin diameter. The bone mostly grew well on the Mg alloy. After 3 months, direct bone contact was visible in all cases and bone also grew into the corrosion pits (solid arrows in **Fig. 3.3f**). After 6 months substantial degradation reduced the pin diameter significantly, several specimens had to be excluded from mechanical measurements for this reason.

Mg BMG: After 3 months excellent bone growth around and on the pins was visible. A relatively thick bone layer was formed around the pins, also in the medullary cavity. However, distinct crack formation occurred; the pins more or less disintegrated into smaller pieces (**Fig. 3.3g, Fig. 3.3h**). **Fig. 3.3g** illustrates that new bone grew into one of the cracks.

Table 3.2: Results of the mechanical push-out tests: median of shear strength (RS), energy absorption (Gf) and stiffness (Ci); 1st and 3rd quartile in parantheses; number of pushed out and evaluated samples (NE); number of loosened samples with zero result (NL).

Type	**time**	**R_S**	**G_f**	**Ci**	**N_E**	**N_L**
	[mo]	**[MPa]**	**[mJ]**	**[Nmm-1]**		
pure PHB	1	0,07	1,2	140	1	7
	3	0.20 (0.16-0.55)	2.51 (2.44-2.58)	275 (250-300)	2	-
	6	0.34 (0.16-0.55)	4.83 (3.06-6.65)	200 (150-280)	6	-
P3Z10H	1	0.11 (0.09-0.22)	1.43 (1.08-2.52)	45 (30-88)	7	-
	3	0.24 (0.16-0.61)	4.99 (2.91-6.5)	185 (115-190)	7	1
	6	0.22 (0.14-0.51)	5.14 (3.88-7.05)	210 (192-333)	4	1
P3Z30H	1	0.21 (0.19-0.65)	3.17 (2.96-5.39)	86.5 (63-96)	4	4
	3	0.17 (0.16-0.89)	2.2 (1.49-7.17)	118 (47-170)	3	1
	6	0.32 (0.29-0.62)	6.73 (4.42-7.28)	237.5 (220-250)	6	-
Mg ZX50	1	1.61 (0.7-2.35)	11.37 (5.09-17.39)	775 (460-1370)	6	1
	3	-	-	-	4	-
Mg WZ21	1	1.20 (0.44-1.37)	9.15 (5.35-20.04)	1400 (480-1670)	7	-
	2	3.87 (1.79-5.93)	33.97 (14.79-58.23)	885 (720-1200)	6	1
	3	6.05 (3.1-7.2)	59.08 (28.13-68.35)	2000 (983-8275)	4	-
	6	6.16 (2.13-8.93)	54.7 (11.63-80.78)	950 (680-2200)	3	-
Mg Am29	3	7,25	47,28	700	1	-
Mg Am32	3	5.02 (3.93-6.48)	35.4 (29.22-54.65)	(465-995)	4	-
Mg Am35	3	4,5	25,02	425	1	-

3.3.2 Mechanical properties

Table 3.2 lists the median shear strength, R_S; energy absorption, G_f; and stiffness, C_i, measured by means of the push-out experiment, including quartiles and sample numbers. **Fig. 3.4** gives an overview of the shear strength values. Two typical force-displacement curves are illustrated in **Fig. 3.1a** and **Fig. 3.1b**.

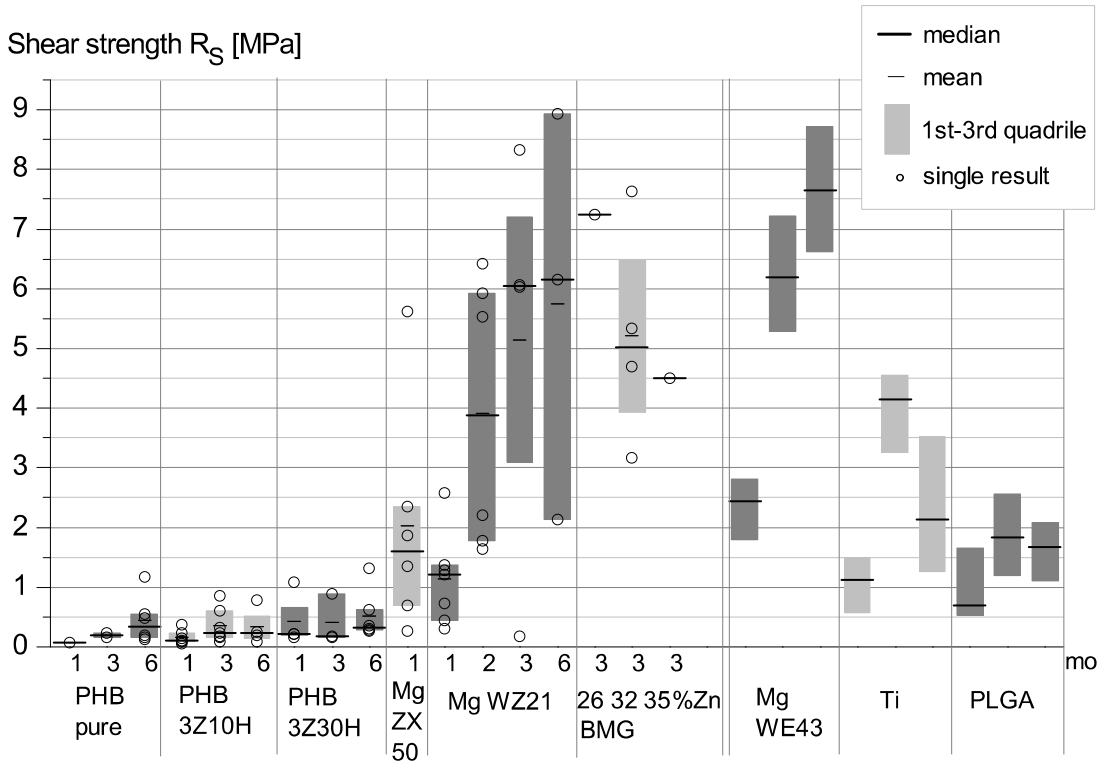

Figure 3.4: Shear strength of pure PHB, P3Z10H, P3Z30H, Mg ZX50, Mg WZ21 and BMG. The numbers below the x-axis indicate the implantation time in months. Grey boxes represent the interquartile range. Median and mean are represented by long and short horizontal lines. Circles are single results. For comparison reasons shear strength data for commercial Mg WE43, Ti alloy and PLGA are given on the right side of the diagram [21-23]; for these data no single results or mean values were available.

PHB shows the lowest mechanical values for all materials. After 1 month, shear strength and energy absorption are significantly below Mg in most cases. 4 out of the 8 P3Z30H samples revealed zero results, and pure PHB loosened in 7 out of 8 cases. P3Z10H exhibits low mechanical values, but no zero results. P3Z30H has a higher energy absorption than P3Z10H, but the shear strength does not differ significantly. After 3 and 6 months energy absorption increases significantly in some PHB types, but in all cases shear and energy absorption values are significantly lower than in Mg WZ21 and Mg Am32. Differences among the PHB groups are not significant.

The fast and irregular degradation of ***Mg ZX50*** after 1 month leads to significantly higher shear strength values than those for PHB. The shear strength is slightly higher than of Mg WZ21 after the same period, but with higher data scatter and no statistical significance. One implant loosened and yielded a zero result. Mechanical data could not be recorded after more than 1 month because there was not enough implant material left to push out.

The shear strength and energy absorption values of ***Mg WZ21*** at any time are higher than those of PHB. Generally, compared to PHB and its derivates R_S and G_f are roughly one order of magnitude higher in Mg WZ21 and increase monotonically with implantation time. Relatively high data scatter confirms the large differences between individual bones already observed in the optical evaluation. Only one Mg WZ21 implant loosened (after 2 months). The stiffness is the highest of all materials and stayed fairly constant over time.

Among the ***Mg BMG*** alloys there is a tendency to decreasing mechanical values with increasing Zn fraction. The energy and shear strength of Mg Am32, the only group with sufficient samples, does not differ significantly from Mg WZ21 after 3 months. However, the data may be biased not only due to the low number of samples, but also to crack formation and crumbling, which is discussed in section 4.

Table 3.3: Statistical analysis of shear (RS) and energy (Gf). ANOVA analysis with Bonferroni means comparison (AB) was used for groups distributed normally at 0.1 level according to a Shapiro-Wilk test. Kruskal-Wallis (KW) analysis was used for all groups with at least 3 samples. Significant results (level 0.1) are bold. ΔRS and ΔGf are the differences between the medians of shear strength and energy absorption. P is given for ANOVA and P>χ2 for Kruskal-Wallis.

Compared groups:			**ΔRS (1st-2nd)**	**P / P>χ2**	**RS stat. method**	**ΔGf (1st-2nd)**
all PHB	all PHB	all	* ≈0	** 0.221	KW	
P3Z10H	P3Z30H	1m	-0,1	**	KW	-1,74
P3Z10H	Mg ZX50	1m	-1,5	0,003	KW	-9,94
P3Z10H	Mg WZ21	1m	-1,09	0,004	KW	-7,73
P3Z30H	Mg ZX50	1m	-1,4	0,033	KW	-8,2
P3Z30H	Mg WZ21	1m	-0,99	0,038	KW	-5,98
Mg ZX50	Mg WZ21	1m	0,41	1 / 0.475	AB/KW	2,22
all PHB	all PHB	3m	*	**	KW	≈0
P3Z10H	Mg WZ21	3m	-5,81	0.002 / 0.089	AB/KW	-54,09
P3Z10H	Mg Am32	3m	-4,78	0.002 / 0.008	AB/KW	-30,41
P3Z30H	Mg WZ21	3m	-5,88	0,077	KW	-56,88
P3Z30H	Mg Am32	3m	-4,7	0,034	KW	-33,2
Mg WZ21	Mg Am32	3m	1,03	1 / 0.564	AB/KW	23,68
all PHB	all PHB	6m	*	**	KW	≈0
pPHB	Mg WZ21	6m	-5,82	0.003 / 0.020	AB/KW	-49,87
P3Z10H	Mg WZ21	6m	-5,94	0.005 / 0.034	AB/KW	-49,56
P3Z30H	Mg WZ21	6m	-5,84	0,02	KW	-47,97
pPHB	3m	6m	*	**	KW	-2,32
P3Z10H	1m	3m	*	**	KW	-3,56

3.4 Discussion

In this study several different Mg alloys and PHB were tested with regard to their biomechanical properties. The selected biodegradable materials were developed for elastic stable intramedullary nailing (ESIN) as used for osteosynthesis in paediatric fracture treatment. The rat model with transcortically inserted implants is assumed to provide a useful example of the bone-implant interface, which in humans corresponds to the junction of the ESIN with cortical bone at the insertion site. The progress of healing, the development of mechanical interfacial strength, possible tissue irritation and bone remodelling can be systematically and easily studied. The rate and characteristics of the degradation provides indications about the time period over which a specific ESIN material could fulfil the load carrying function.

To qualify and compare the performance of the bone-implant interface, we determined (i) the shear strength, (ii) the energy absorption, and (iii) the stiffness of novel biodegradable materials (PHB, crystalline and amorphous Mg).

3.4.1 Shear strength and processes occurring at the implant-bone interface

The shear strength provides an indication of the interface quality. Generally, biomechanical parameters are influenced by several factors. Obviously, the chemical composition will affect osseointegration, i.e. the ability of bone cells to attach and grow on the material's surface. The surface roughness also has to be taken into account. A series of studies indicate that an increasing of the surface roughness improves implant-bone integration [33,34]. In the case of degradable materials the surface roughness already increases in the early stages of implantation and thus better bone attachment can be assumed. Mechanical interlocking is also a very important factor if degradable materials are used. Due to fluctuations in the chemical composition caused by microstructural features and thus the presence of micro-galvanic sites, the alloys often exhibit localized corrosion attack. This causes the formation of pits and cavities into which bone can grow easily (**Fig. 3.3f**). This mechanical interlocking is pronounced for materials with fast and irregular corrosion, optimally leading to a situation when bone or material failure is required for implant displacement rather than pure interface failure. For the same rat model as presented here, Kraus et al. [2] and Wessels et al. [14] showed by means of micro-focus computed tomography (μCT) that the pin's surface area of crystalline and amorphous Mg alloys increases during the first period of implantation. This can be seen as an indication of

localized corrosion attack. Because it is more pronounced for ZX50 than for Mg WZ21, the slightly higher shear strength value of ZX50 after 1 month seems plausible. Even the increase in shear strength with time on the part of WZ21 may be partly related to mechanical interlocking, but also to a general increase in bone-implant contact, i.e. better bone apposition, as mentioned in the results section. Concerning the amorphous Mg alloys, it is important to note that Mg Am29 exhibits a slightly higher degradation rate than Mg Am32 and Mg Am35 [15]. Accordingly, the higher shear strength and energy absorption of Mg Am29 can be explained by the above-mentioned mechanical interlocking concept. On the other hand, PHB and its derivate exhibit very low degradation rates and thus their surface morphologies remain smooth and even during the whole implantation period. Not least because of this, the shear strength and the energy absorption stay at a low level.

3.4.2 Gas formation

The formation of hydrogen gas during Mg degradation is another effect that must be seriously considered [12,14]. As mentioned by Kraus et al. [2], only a limited amount of hydrogen gas can be carried away by the surrounding tissue. If the corrosion rate is too rapid, as it is for ZX50, gas bubbles form around the implant which impede good connectivity of osteocytes with the ZX50 implant surface, as observed in the histological specimens.

3.4.3 Energy absorption

Once the interface has failed, the implant still offers some resistance to displacement. This is quantified, at least in part, by the energy absorption. In the case of Mg alloys the resistance to displacement is mostly caused by friction, which is influenced by the surface roughness. Because in each case the roughness of Mg alloys increases over time the time-dependent values of G_f (**Table 3.2**) are quite comprehensible. In the case of PHB, bulging and wedging have a strong effect. Because of both the very low Young's modulus and the low yield and tensile strength, mechanical compression may cause distinct bulging of the implant and thus falsify the experimental result [23]. As clearly seen in **Fig. 3.1c**, the shear stress increases further after failure initiation (labelled with x), which illustrates the partial inadequacy of the push-out test for soft implant materials such as PHB.

3.4.4 Stiffness

Stiffness, C_i, describes the compliance of the system prior to failure. It not only indicates the quality of the interface, i.e. the implant's surface fraction covered by bone, but is also affected by the Young's modulus of the material. Since the bone apposition for PHB and its derivates was fairly good, their low C_i-values can therefore be explained by the low modulus. While for the PHB group the stiffness tends to increase with time, for Mg WZ21 the stiffness remains roughly constant while R_S and G_f increase with time. We attribute this divergent behavior to the surface roughness of the samples. For PHB with the constantly smooth surface all mechanical parameters increase due to increased bone apposition, while for Mg ZX50 the increase in R_S and G_f is predominantly caused by enhanced interlocking, which affects stiffness less.

3.4.5 Comparison with other materials

Today titanium and titanium alloys as well as stainless steels are very common, widely used materials for osteosynthesis. Also PLA, PGA and their copolymers are already used for smaller non-load bearing implants. **Fig. 3.4** shows the shear strengths of the tested materials in comparison to the Ti alloy TiAl6Nb7, the biodegradable co-polymer PLGA and the commercial Mg alloy WE43 [21-23], which has a slightly lower corrosion rate than Mg WZ21 [1]. The interface strength of the Ti alloy is not only weaker than that of the Mg alloys, but also decreases after 3 months, while the strength of Mg alloys increases continuously, probably due to the interlocking of bone growing into the expanding corrosion cavities. PLGA shows higher shear strength values than the PHB material. Because its surface also remained smooth even after 6 months [22], enhanced mechanical interlocking may not serve to explain this effect. Swelling, which was observed in PLGA but not in PHB, may be a reason. If the volume of an implant increases, it fastens itself more and more into place. Witt et al. [35] and Lee et al. [36] report a volume swelling of 15% for PLGA after two days, while in a first rough attempt in this study only 0.4% was measured for PHB after the same period.

3.4.6 Bone growth

For all implant types we observed that bone tends to grow medially rather than laterally. This is probably an effect of the asymmetric load distribution exerted by muscles and weight via the implant on the bone, resulting in different remodelling processes on each

side. It was also found that degradation is irregular along the length of the implant, probably due to the variation in vascularisation of the cortical bone, marrow channel and outside muscles. Zhang et al. [11] described the degradation of a Mg-Mn-Zn alloy in more detail, using cross-sections and histological slices. They observed faster corrosion in the marrow channel than in the cortical bone, and also noted new bone formation around the implant. Similar observations were made by Kraus et al. [2], who analysed the shape and the volume change of Mg implants *in vivo* by means of μCT .

3.4.7 PHB and derivates

PHB, including the ZrO_2 and bone graft substitute compounds in their current state, are not suitable for the osteosynthesis treatment of children, mainly because of their poor mechanical performance and very slow degradation rate. However, further material development is feasible, and chemical alterations are currently being investigated. As mentioned above, the main reason for the low shear strength of PHB is the very slow degradation and the resulting lack of mechanical interlocking. Keeping in mind the good apposition of cells on PHB even on smooth surfaces, roughening might improve attachment and thus push-out strength. Surface roughening has been investigated for titanium alloys [37,38]; this may be a starting point for the development of beneficial methods of roughening the PHB surface. The Young's moduli and the ultimate tensile strength values of PHB and its derivates are low. For any chemical alteration it is imperative to not only increase the degradation rate but also to increase mechanical performance before using the material in stabilizing implant applications. We assumed that the addition of a resorbable bone graft substitute would enhance bone attachment and thus the interphase strength, and that it would increase the degradation rate by reducing the total PHB content and by increasing the surface area of the remaining PHB. However, these expectations have not been met.

3.4.8 Magnesium alloy Mg ZX50

The degradation of ***Mg ZX50*** is too rapid, and the implant does not maintain its shape and strength long enough during the fracture healing period. However, it seems to have no long-term negative influence on the healing process itself, as after 4 to 6 months the bone recovers *restitutio ad integrum* [2]. Its mechanical properties are similar to those of Mg WZ21. The authors of the present study are currently testing an appropriate surface treatment in order to delay the onset of degradation. Ongoing research into Mg ZX50 is giving rise to

hopes that the degradation rate may be reduced by using ultra-pure grades with extremely low trace element content. The big advantage of Mg ZX50 is that it contains no yttrium or other rare earth metals, in contrast to Mg WZ21 and commercial Mg WE43.

3.4.9 Magnesium alloy Mg WZ21

Among the tested materials, ***Mg WZ21*** is the most suitable for application in osteosynthesis and would not require substantial alterations. The degradation rate is slow enough to ensure sufficient stability during the healing phase. There is some room for further increase of the degradation rate, however: given a healing time of 3-6 weeks for child bone, full implant strength is not required after 6 months. The Young's modulus of Mg WZ21 (45 GPa [39]) is higher than that of bone (trabecular: 10.4-14.8 GPa; cortical: 18.6-20.7 GPa [40,41]) but still much closer to bone than that of Ti alloys used in biomedical applications, most of which have Young's moduli between 74-114 GPa [42]. The yield stress of Mg WZ21 in compression is 145MPa, the ultimate tensile strength 250MPa and the elongation to fracture 28% [1]. These properties justify expectations of convenient surgical handling of the implant and of sufficient bone support during healing. Yttrium content may be a critical issue, especially for use in children.

3.4.10 Bulk metallic glass Mg BMG

For ***Mg BMG*** not enough statistically significant data exists at the moment due to the low number of samples, but the trends are obvious. All samples were explanted after 3 months. The bone growth on all of them was excellent, the shear force and energy absorption was high and none of the implants had loosened. These observations agree with those of Wessels et al. [14]. However, further material development is mandatory to circumvent premature crack formation. Magnesium-based bulk metallic glasses are known to exhibit structural relaxation, accompanied by embrittlement, at body temperature [14,43]. Novel grades are currently being developed in the laboratory of one of the authors (PJU). The new alloys should exhibit a delayed start of the tough-to-brittle transition at body temperature. Clinically, if crack formation started towards the end of the healing period, this would present the advantage of increasing the degradation surface and avoiding stress shielding.

3.5 Conclusions

For medical implants such as those for fracture fixation in paediatrics it would be very desirable to replace Ti alloys with bioresorbable materials in order to solve the problems of second surgical explantation intervention and stress shielding. Among the materials investigated in this study, the magnesium alloy WZ21 is the most promising with regard to degradation performance and mechanical properties and can be seen as an important competitor for Ti. The alloy Mg ZX50 has the decisive advantage of lacking rare-earth elements, but under current conditions it degrades too rapidly. PHB degrades very slowly and exhibits insufficient mechanical properties. Like Mg ZX50, it requires significant structural and/or electrochemical improvements before it can be recommended for use in medicine. Mg BMG seems very promising, but in its current state it lacks structural and therefore mechanical stability.

Acknowledgements

The authors very much appreciate the funding support received from the FFG (Austrian Research Promotion Agency) in the context of the BRIC (Bioresorbable Implants for Children) research project, Laura Bassi Centres of Expertise program. We also thank the Applied Physiology research group at the Institute of Biotechnology and Biochemical Engineering and the Institute for Chemistry and Technology of Materials at Graz University of Technology for providing the polymeric materials. We thank the Karl Donath Laboratory for Hard Tissue and Biomaterial Research at Bernhard Gottlieb Universitätszahnklinik and the Department of Oral and Maxillofacial Surgery, Medical University of Innsbruck, for the histological slices. The provision of Herafill® bone graft substitute by Heraeus Holding GmbH is also gratefully acknowledged.

References

[1] Hanzi AC, Gunde P, Schinhammer M, Uggowitzer PJ. On the biodegradation performance of an Mg-Y-RE alloy with various surface conditions in simulated body fluid. Acta biomaterialia. 2009;5(1):162-71.

[2] Kraus T, Fischerauer SF, Hanzi AC, Uggowitzer PJ, Loffler JF, Weinberg AM. Magnesium alloys for temporary implants in osteosynthesis: in vivo studies of their degradation and interaction with bone. Acta biomaterialia. 2012;8(3):1230-8.

[3] Nair L, Laurencin C. Biodegradable polymers as biomaterials. Prog Polym Sci 2007;32(8-9):762–98.

[4] Virtanen S. Biodegradable Mg and Mg alloys: Corrosion and biocompatibility. Materials Science and Engineering: B. 2011;176(20):1600-8.

[5] Sastri V. In: Sastri VR, editor. Plastics in Medical Devices: Properties, Requirements and Applications. Boston: William Andrew Publishing; 2010.

[6] Shadanbaz S, Dias GJ. Calcium phosphate coatings on magnesium alloys for biomedical applications: a review. Acta biomaterialia. 2012;8(1):20-30.

[7] Staiger MP, Pietak AM, Huadmai J, Dias G. Magnesium and its alloys as orthopedic biomaterials: a review. Biomaterials. 2006;27(9):1728-34.

[8] Witte F, Kaese V, Haferkamp H, Switzer E, Meyer-Lindenberg A, Wirth CJ, et al. In vivo corrosion of four magnesium alloys and the associated bone response. Biomaterials. 2005;26(17):3557-63.

[9] Witte F, Fischer J, Nellesen J, Crostack HA, Kaese V, Pisch A, et al. In vitro and in vivo corrosion measurements of magnesium alloys. Biomaterials. 2006;27(7):1013-8.

[10] Krause A, von der Höh N, Bormann D, Krause C, Bach F-W, Windhagen H, et al. Degradation behaviour and mechanical properties of magnesium implants in rabbit tibiae. J Mater Sci Mater Med. 2010;45:624-32.

[11] Zhang E, Xu L, Yu G, Pan F, Yang K. In vivo evaluation of biodegradable magnesium alloy bone implant in the first 6 months implantation. Journal of Biomedical Materials Research Part A. 2009;90A(3):882-93.

[12] Hanzi AC, Gerber I, Schinhammer M, Loffler JF, Uggowitzer PJ. On the in vitro and in vivo degradation performance and biological response of new biodegradable Mg-Y-Zn alloys. Acta biomaterialia. 2010;6(5):1824-33.

[13] Huan ZG, Leeflang MA, Zhou J, Fratila-Apachitei LE, Duszczyk J. In vitro degradation behavior and cytocompatibility of Mg-Zn-Zr alloys. J Mater Sci Mater Med. 2010;21(9):2623-35.

[14] Wessels V, Le Mené G, Fischerauer SF, Kraus T, Weinberg A-M, Uggowitzer PJ, et al. In Vivo Performance and Structural Relaxation of Biodegradable Bone Implants Made from Mg-Zn-Ca Bulk Metallic Glasses. Advanced Engineering Materials. 2012;14(6):B357-B64.

[15] Zberg B, Uggowitzer PJ, Loffler JF. MgZnCa glasses without clinically observable hydrogen evolution for biodegradable implants. Nat Mater. 2009;8(11):887-91.

[16] Koller M, Salerno A, Dias M, Reiterer A, Braunegg G. Modern biotechnological polymer synthesis: a review. Food Technol Biotechnol 2010;48(3):255-69.

[17] Reddy CS, Ghai R, Rashmi, Kalia VC. Polyhydroxyalkanoates: an overview. Bioresource technology. 2003;87(2):137-46.

[18] Slongo T. The choice of treatment according to the type and location of the fracture and the age of the child. Injury 2005;36(Suppl 1):12–9.

[19] Pietrzak WS, Sarver D, Verstynen M. Bioresorbable implants--practical considerations. Bone. 1996;19(Suppl 1):109-19.

[20] Bohner M. Resorbable biomaterials as bone graft substitutes. Materials Today. 2010;13(1–2):24-30.

[21] Castellani C, Lindtner RA, Hausbrandt P, Tschegg E, Stanzl-Tschegg SE, Zanoni G, et al. Bone-implant interface strength and osseointegration: Biodegradable magnesium alloy versus standard titanium control. Acta biomaterialia. 2011;7(1):432-40.

[22] Lindtner R. Biomechanical and radiological evaluation of the bone-implant interface of new biodegradable implants in comparison to conventional titanium pins - findings in a transcortical rat model: Medical University of Graz; 2009.

[23] Tschegg EK, Lindtner RA, Doblhoff-Dier V, Stanzl-Tschegg SE, Holzlechner G, Castellani C, et al. Characterization methods of bone-implant-interfaces of bioresorbable and titanium implants by fracture mechanical means. Journal of the mechanical behavior of biomedical materials. 2011;4(5):766-75.

[24] Nazarian A, Hermannsson BJ, Muller J, Zurakowski D, Snyder BD. Effects of tissue preservation on murine bone mechanical properties. J Biomech. 2009;42(1):82-6.

[25] Donath K. Die Trenn-Dünnschliff-Technik zur Herstellung histologischer Präparate von nicht schneidbaren Geweben und Materialien. Deutsche Zeitschrift für Mund-Kiefer Gesichtschirurgie. 1988(34):197-206.

[26] Regauer M. Knochenneubildung und Knochendefektheilung durch den rekombinanten humanen Wachstumsfaktor Osteogenic Protein-1 (BMP-7): Medizinische Fakultät der Universität zu München; 2009.

[27] Strobl S. Knochen- und Knorpelzellenwachstum im dreidimensionalen Ko-Kultursystem: Medizinische Fakultät, Ludwig-Maximilians-Universität zu München; 2007.

[28] Fritsch H. Staining of different tissues in thick epoxy resin-impregnated sections of human fetuses. Stain technology. 1989;64(2):75-9.

[29] Branemark R, Ohrnell LO, Nilsson P, Thomsen P. Biomechanical characterization of osseointegration during healing: an experimental in vivo study in the rat. Biomaterials. 1997;18(14):969-78.

[30] Giavaresi G, Fini M, Cigada A, Chiesa R, Rondelli G, Rimondini L, et al. Mechanical and histomorphometric evaluations of titanium implants with different surface treatments inserted in sheep cortical bone. Biomaterials. 2003;24(9):1583-94.

[31] Muller M, Hennig FF, Hothorn T, Stangl R. Bone-implant interface shear modulus and ultimate stress in a transcortical rabbit model of open-pore Ti6Al4V implants. J Biomech. 2006;39(11):2123-32.

[32] Berzins A, Sumner D. Implant Pushout and Pullout Tests. An Y, Draughn R, editors. Boca Raton: CRC Press; 2000.

[33] Shalabi MM, Gortemaker A, Van't Hof MA, Jansen JA, Creugers NH. Implant surface roughness and bone healing: a systematic review. J Dent Res. 2006;85(6):496-500.

[34] Wong M, Eulenberger J, Schenk R, Hunziker E. Effect of surface topology on the osseointegration of implant materials in trabecular bone. J Biomed Mater Res. 1995;29(12):1567-75.

[35] Witt C, Mader K, Kissel T. The degradation, swelling and erosion properties of biodegradable implants prepared by extrusion or compression moulding of poly(lactide-co-glycolide) and ABA triblock copolymers. Biomaterials. 2000;21(9):931-8.

[36] Lee L, Wang C, Smith K. Micro-porous paclitaxel-loaded PLGA foams - a new implant material for controlled release of chemotherapeutic agents. Chemical and Pharmaceutical Engineering (CPE). 2007(01).

[37] Bagno A, Di Bello C. Surface treatments and roughness properties of Ti-based biomaterials. J Mater Sci Mater Med. 2004;15(9):935-49.

[38] Kapanen A, Danilov A, Lehenkari P, Ryhanen J, Jamsa T, Tuukkanen J. Effect of metal alloy surface stresses on the viability of ROS-17/2.8 osteoblastic cells. Biomaterials. 2002;23(17):3733-40.

[39] Avedesian M, Baker H. Magnesium and magnesium alloys. ASM Int. 1999.

[40] Poumarat G, Squire P. Comparison of mechanical properties of human, bovine bone and a new processed bone xenograft. Biomaterials. 1993;14(5):337-40.

[41] Rho JY, Kuhn-Spearing L, Zioupos P. Mechanical properties and the hierarchical structure of bone. Medical engineering & physics. 1998;20(2):92-102.

[42] Niinomi M. Mechanical biocompatibilities of titanium alloys for biomedical applications. Journal of the mechanical behavior of biomedical materials. 2008;1(1):30-42.

[43] Castellero A, Uhlenhaut DI, Moser B, Löffler JF. Critical Poisson ratio for room-temperature embrittlement of amorphous Mg85Cu5Y10. Philosophical Magazine Letters. 2007;87(6):383-92.

4 Investigation of Biocompatibility Qualities

Absolute biocompatibility of a biomaterial is more vital than its mechanical properties, as dealing with potential consecutive symptoms requires long-lasting effortful treatments. Local but also systemic reactions of the host need to be investigated intensively before a clinical application in humans can be permitted.

Immunological response to biodegradable magnesium implants

Karin Pichler, Stefan Fischerauer[*]*, Peter Ferlic, Elisabeth Martinelli, Hans-Peter Brezinsek, Peter J. Uggowitzer, Jörg F. Löffler, Annelie-Martina Weinberg*

JOM. 2014; 66(4): 573-579

The use of biodegradable magnesium implants in pediatric trauma surgery would render surgical interventions for implant removal after tissue healing unnecessary, thereby preventing stress to the children and reducing therapy costs. In this study, we report on the immunological response to biodegradable magnesium implants - as an important aspect in evaluating biocompatibility - tested in a growing rat model. The focus of this study was to investigate the response of the innate immune system to either fast or slow degrading magnesium pins, which were implanted into the femoral bones of 5-week-old rats. The main alloying element of the fast-degrading alloy (ZX50) was Zn, while it was Y in the slow-degrading implant (WZ21). Our results demonstrate that degrading magnesium implants beneficially influence the immune system, especially in the first postoperative weeks but also during tissue healing and early bone remodeling. However, rodents with WZ21 pins showed a slightly decreased phagocytic ability during bone remodeling when the degradation rate reached its maximum. This may be due to the high release rate of the rare earth-element yttrium, which is potentially toxic. From our results we conclude that magnesium implants have a beneficial effect on the innate immune system but that there are some concerns regarding the use of yttrium-alloyed magnesium implants, especially in pediatric patients.

Keywords: Immunology; biodegradable implant material; magnesium; pediatric traumatology

[*] Author's contribution to this study: study planing, surgery of animals and animal care, taking of blood samples, µCT performance and evaluations, statistical analysis, construction of figures, literature research, and revision of the manuscript.

4.1 Introduction

Pediatric fractures are very common. Today's treatment strategy includes operative treatment with ESINs (elastic stable intramedullary nails) and early postoperative load bearing. Early postoperative load bearing is very important in children as immobilization is not tolerated well. However, when the fracture has healed appropriately, ESINs need to be removed, which implies a second surgical intervention for the child. Surgical intervention is accompanied by the risk of morbidity and damage to the collateral tissues, and it is associated with a high complication rate [1,2]. Together with the associated hospital stays, it represents a major stress for the pediatric patient and is very cost-intensive from a socioeconomic point of view [3].

In recent years, research has focused on the development of biodegradable implants. These may represent a suitable tool for pediatric trauma surgery as their self-degrading properties would render surgical intervention for implant removal after tissue healing unnecessary, thereby preventing patient stress and reducing therapy costs. Magnesium alloys are promising candidate materials for such implants. Their mechanical strength is appropriate for load-bearing implant application, and their elastic properties resemble those of bone [4,5]. A drawback may be severe hydrogen gas bubble formation during degradation ($Mg + 2H_2O \rightarrow Mg(OH)_2 + H_2$ [6], but this problem can be overcome by the appropriate selection of slow-degrading Mgalloys [7,8]. Magnesium exhibits good biocompatibility in vivo and in vitro with no systemic inflammatory reaction or effect on cellular blood composition [9-12]. It has also been shown that mineral apposition rates around degrading magnesium implantsin bone are high and that bone mass increases [13].

However, it is also known that the products of metal implant degradation can induce several types of immune response. These include immune response mediated by type IV delayed hypersensitivity [14-16], immune suppression via apoptosis of responsible cells [17-19], and foreign-body reaction [20].

Perfect biocompatibility is a mandatory prerequisite for biodegradable implants designed for the use in pediatric patients, as the tolerance limits of potentially harmful substances are especially low in young individuals.

So far no studies have investigated how a growing body, such as that of a pediatric patient, reacts to degradation products of magnesium-based implants. In this study we aim to investigate the impact of such biodegradable magnesium implants on the innate immune

system of growing rats in vivo, i.e., the phagocytic ability of rat neutrophile granulocytes. The innate immune system represents a rapid first line of defense against any kind of microbial and infectious ‘‘nonself’’ and at the same time initiates the process leading to an eventual development of an adaptive immune response and establishment of an immunological memory. The phagocyte system is an essential component of innate immunity, where specialized phagocytes (macrophages, monocytes, and neutrophils) perform various host defense functions that rely on the phagocytic uptake of pathogens. For efficient function, adequate numbers of monocytes and neutrophils need to be present in the peripheral blood, and they must be able to respond to signals from the site of inflammation, migrate to this site, and ingest and kill the invading microorganisms.

On this basis we evaluated the effect of two different biodegradable magnesium alloys in a growing rat model: ZX50 and WZ21 (their compositions are listed in **Table 4.1**). We selected these alloys because of their substantially different degradation rate in physiological media; ZX50 degrades rather rapidly, whereas the degradation rate of WZ21 is significantly lower [21]. The two selected alloys differ in their type of main alloying element, i.e., Zn in the fast-degrading alloy (ZX50) and the rare-earth element Y in the slowdegrading implant (WZ21). This selection implies the intention to deliberately vary the element release rate and thus to apply a different ‘‘burden’’ on the innate immune system. Both alloys show good mechanical properties, acceptable for temporary implant application [9, 22].

Table 4.1: Nominal chemical composition in wt.% of the two magnesium alloys used.

Alloy	Mg	Zn	Ca	Mn	Y
ZX50	Balance	5	0.25	0.15	-
WZ21	Balance	1	0.25	0.15	2

4.2 Material and methods

4.2.1 Magnesium alloys

The implants used were machined cylindrical pins made of two different magnesium alloys. They were 1.6 mm in diameter and 8 mm in length, and they exhibited a smooth polished surface. The faster degrading alloy ZX50 typically exhibits a yield stress of 210 MPa, an ultimate tensile strength of 295 MPa, a uniform elongation of 18%, and an elongation at fracture of 26%. The slower degrading alloy WZ21 features a yield stress of 150 MPa, an ultimate tensile strength of 250 MPa, a uniform elongation of 20%, and an

elongation at fracture of 28%. The pins were carefully dry-machined with clean tools to avoid contamination and allow for good surface quality. During machining the surface temperature of the pins was kept significantly below 200" C to avoid microstructural changes. The pins were finally cleaned in a cascade of pure ethanol in an ultrasonic bath and dried in warm air.

4.2.2 Experimental design

All animal experiments were conducted according to the rules of animal ethical respect and were authorized by the Austrian Ministry of Science and Research (accreditation number BMWF-66.010/0070-II/3b/2011). Rats were housed in groups of three in clear plastic cages on standard bedding. Water and a standard pellet diet were given ad libidum.

Eighteen male 5-week-old Sprague–Dawley rats with body weights of 140–160 g were used in this study. They were divided into three groups of six rats each: the "no-implant" group underwent surgery and drilling but no pin was implanted into the femoral bone, whereas both the ZX50 and the WZ21 group had identical pins implanted in their two femoral bones (12 pins per group, made either of ZX50 or WZ21).

4.2.3 Surgical procedure

The rats were fully anaesthetized by administration of volatile isoflurane (Forane®, Abbot AG, Baar, Switzerland), preceded by a subcutaneous combined sedation via Fentanyl (20 µg/kg, Fentanyl®, Janssen-Cilag GmbH, Neuss, Germany), Midazolam (400 µg/kg Midazolam Delta®, DeltaSelect GmbH, Dreieich, Germany), and Medetomidine (200 µg/kg Domitor®, Pfizer Corporation Austria GmbH, Vienna, Austria).

For pin implantation, the regio intercondylaris of the femur was exposed through an incision medial to the patellary ligament and a lateral translation of the patella. Then a drill hole was created using a 1.5-mm drill with ascending diameter (Synthes®, Paoli, PA) in the longitudinal axis of the femoral diaphysis. This hole served as a transphyseal implantation bed for the implant. To minimize frictional heat, we drilled at a low rotational speed of 200 rpm under continuous physiological saline irrigation. The cylindrical implant was then entirely inserted into the drill hole by gentle tapping. The operating field was then irrigated again with a physiological saline solution. Finally the wound was closed in layers. After the pins were implanted, general anesthesia was antagonized by intraperitoneal injection of a mixture of Naloxone (120 µg/kg, Narcanti®, Torrex Chiesi PharmaGmbH, Vienna, Austria), Flumazenil (50 µg/kg, Anexate®, Roche Austria GmbH, Vienna, Austria), and Atipamezole

(250 µg/kg, Antisedan, Pfizer Corporation, Vienna, Austria). For analgesia, all animals received a subcutaneous injection of 200 mg/kg Caprofen (Rimadyl® , Pfizer Corporation,Vienna, Austria) on the day of the operation. During the first postoperative week, analgesia was maintained by administration of 8.34-mg Piritramid/ml drinking water (Dipidolor®, Janssen-Cilag GmbH, Neuss, Germany). The rats were allowed to move freely in their cages without external support and unrestricted weight bearing. They were clinically observed daily throughout the study period.

4.2.4 Microfocused computer tomography (µCT)

Scans were performed with a Siemens Inveon Acquisition Workplace 1.2.2.2 at 70 kV voltage, 500 µA current, and 1000 ms exposure time. Effective pixel size was 35.55 µm at a total rotation of 210° and by 180 rotation steps. Image reconstruction was performed without using a downsample algorithm. The image processing software Mimics® (Version 15.01, Materialise NV, Leuven, Belgium) was deployed to construct 3D models of pins and bubbles of emitted gas. The upper and lower thresholds for the pin were set at 480 and 1480 Hounsfield units (HU), for hydrogen gas at -1000 and -1024 HU, respectively. A detailed analysis protocol was published by Kraus et al. [21]. Pin volume and gas volume were quantified every week during the first 4 weeks and then at four-week intervals until week 24. The amount of element release of the implant during degradation was calculated as the ratio to the quantified implant volume loss, and respective to a total pin weight of 27 mg.

Micro-CT was further used for continuously monitoring of the bone remodelling up to 24 weeks. Two-dimensional µCT slices in sagittal plane of the femur were displayed by the use of a Siemens Inveon Research Workplace (Siemens AG, Erlangen, Germany).

4.2.5 Blood sample collection

For blood sample collection the rats were anesthetized by administering of volatile isoflurane (Forane®). Then the tongue vein was punctured with a hollow needle and 1.2 ml of blood was drawn into lithium herparin-coated tubes. To avoid blood coagulation 250 IE heparin was additionally added to each sample. Blood was drawn immediately before pin implantation, weekly in the first four postoperative weeks and then every 4 weeks up to the 24^{th} postoperative week.

4.2.6 Phagocytic assay

Immediately after blood sample collection the phagocytic activity of neutrophils was determined using the Phagotest kit (Opregen Pharma, Heidelberg, Germany). This test is based on the principle that phagocytes ingest FITC-labeled *E. Coli* thereby generating a green fluorescence signal which can be quantified by flow cytometry [23]. The test was performed according to the manufacturer's instructions. Briefly, 100 µl heparinized whole blood was incubated with FITC-labeled E. Coli (2 x 107 per 20 µl) at 37°C for 10 min. In parallel a negatve control sample was kept on ice. After the incubation time, the phagocytosis was stopped by placing the experimental sample on ice. To eliminate the fluorescence of non-phagocyted bacteria, 100 µl of quenching solution was added. The cells were washed twice with 3 ml washing solution (5 min, 250 × g, 4°C). Cells were then re-suspended and incubated for 20 min in 2 ml lysis solution in order to lyse erythrocytes and fix the leukocytes. This was followed by a final washing step (3 ml washing solution, 5 min 250 × g, 4°C). Then the cells were re-suspended in 200 µl of DNA staining solution to exclude aggregation artifacts of bacteria or cells, and analyzed by flow cytometry as described below.

4.2.7 Flow cytometric analysis

Analysis was perfomed using a FACSCanto II® flow cytometer (BD Biosciences, Heidelberg, Germany) and the data were processed with the FACSDiva 6.1.3® software (BD Bioscience). To exclude extracellular bacteria, a gate was set in the red fluorescence histogram on those events, which had the same DNA content as a rat diploid cell. Dead cells were excluded in the forward scatter (FCS) vs side scatter (SSC) diagram. The phagocytic ability was evaluated in neutrophil granulocytes. Live populations were gated by the software program in the scatter diagram (FCS vs SSC) and their green fluorescnece histogram (FL1) was analyzed. The phagocytic ability was expressed as the percentage of fluorescent cells in the total population studied and calculated by subtracting the percentage of the negative control sample (<1%) from the positive sample.

4.2.8 Statistical analysis

For statistical analysis SPSS® 19.0 software (SPSS Inc., Chicago, IL, USA) was used. Possible statistical significant differences between the groups at each selected time point were analyzed via the Kruskal Wallis test. To determine significant differences in the preoperative phagocytic activity within each experimental group the Wilcoxon test was

applied. Values were expressed as median with minimum and maximum. A p-value <0.05 was considered significant.

4.3 Results

Magnesium pins were succsessfully implanted in 24 femoral bones in 12 rats. Similar holes were drilled without insertion of pins in 12 femoral bones of 6 rats and served as controls. No rats were lost during the study period, and no bone was fractured. In the following, the results of implant degradation, bone remodeling, and phagocytic ability will be presented for the alloys ZX50 and WZ21 and compared with the "no implant" control group.

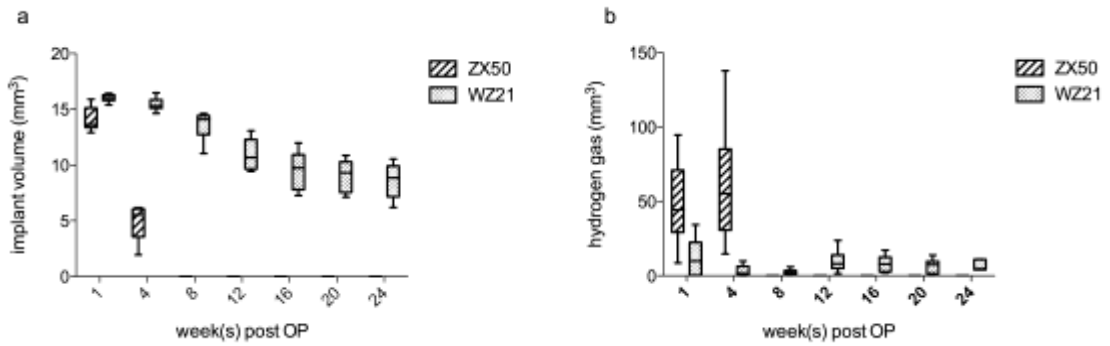

Figure 4.1: Continuous (a) implant volume loss and (b) hydrogen gas evolution during postoperative implant degradation.

4.3.1 Implant degradation and element release

Figure 4.1a displays the continuous volume loss of the ZX50 and WZ21 implants and **Fig. 4.1b** the appearance of gas formation at specific time points for the ZX50 and WZ21 implants. (Note that the detected gas volume is the difference of the accumulated gas volume formed by Mg-dissolution minus the gas amount resorbed by the organism [21]. Both implants started to degrade immediately after implantation, although their degradation rates differed significantly. As expected, ZX50 degraded rather fast, and after 4 weeks, about 70% of the implant material was already degraded (**Fig. 4.1a**). During this time, large gas bubbles were detected by µCT, predominantly inside the medullar cavity.

Figure 4.2 illustrates the amount of elements (Mg, Zn, Ca, Mn, Y) released during the degradation process of ZX50 (**a**) and WZ21 (**b**). The highest releasing rates of ZX50 were recorded between weeks one and four (avarage ion release per week; calculated from avarage volume loss per week and density of 1.8 mg/mm^3: Mg = 4.75 mg; Zn = 0.25 mg; Ca = 0.013 mg; Mn = 0.008mg). WZ21 degraded at a much slower rate. After four weeks 6% and after

24 weeks around 50% of the implant bulk material had degraded (**Fig. 4.1a**). The observed gas volume during WZ21 corrosion was moderate for the whole period of observation (**Fig. 4.1b**), on average around 7 mm^3. The element releasing rate achieved its maximum between weeks 9 and 12 according to an increased pin volume loss during this time period (average ion release per week: Mg = 1.05 mg; Zn = 0.01 mg; Ca = 0.003 mg; Mn = 0.002mg; Y = 0.02mg) (Fig. 2b).

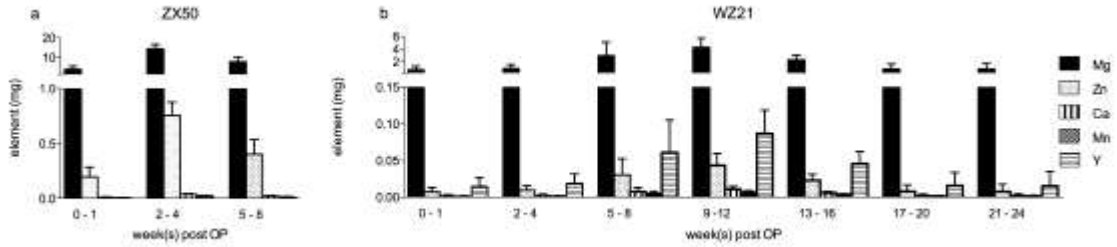

Figure 3.2: Element release from the investigated implants for (a) ZX50 and (b) WZ21 over time.

4.3.2 Bone remodelling

Figure 4.3 shows the bone remodelling of the three groups (no implant, ZX50, WZ21) are displayed over an observation time of 24 weeks. One week after surgery, gas formations were detected by µCT in both experimental groups (ZX50, WZ21). While for the WZ21 group further gas releasing decreased and the gas formations in the medullary cavity were resorbed, gas distribution remained high in the ZX50 group. For this group, the gas bubbles almost entirely filled up the medullary cavity up to 8 weeks post-operation. At the same time, the compact bone appeared to thicken at some diaphyseal sections as well as to reduce its mass at others. This is also indirectly seen by the appearance of gas formation in the surrounding soft tissue. After complete ZX50 pin degradation, an irregular bone shape occurred (weeks 8 and 12), which was successively adjusted to normal shape by bone remodeling in the following weeks. In fact, the bone recovered completely after the entire degradation of the ZX50 pins 24 weeks after operation. In general a good implant tolerance of the bone is observed, and the WZ21 group even showed unaltered bone remodeling in comparison with the control group.

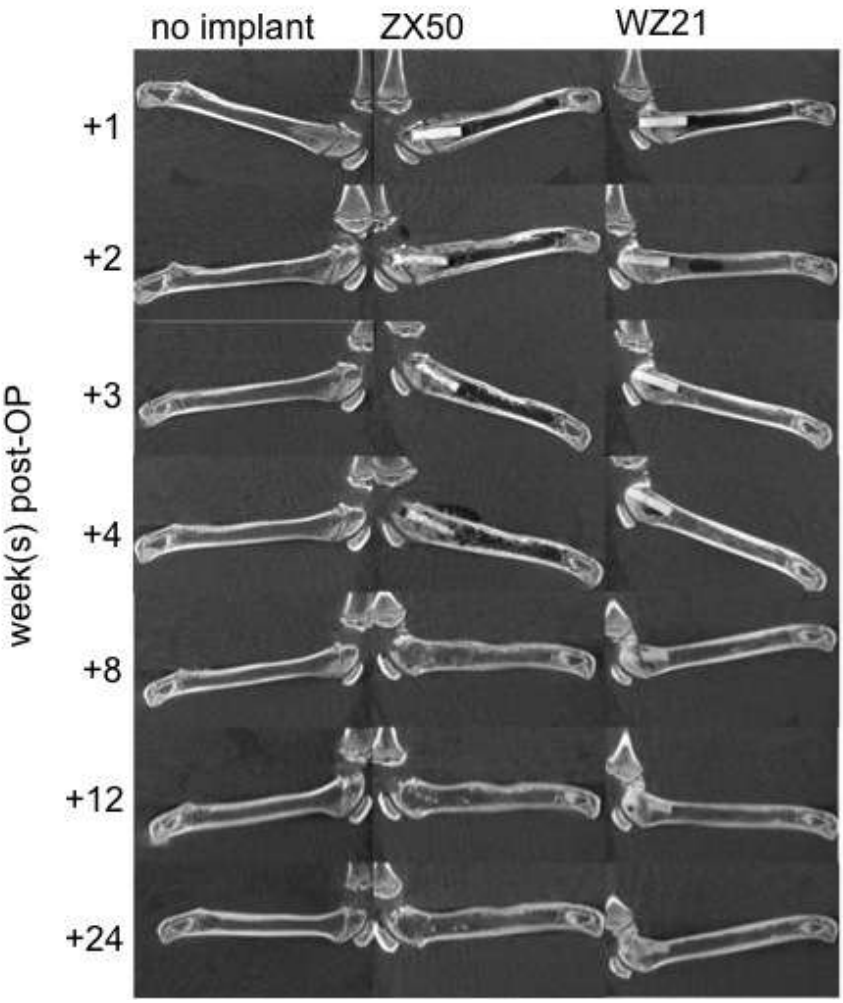

Figure 4.3: Bone remodeling of the three groups (no implant, ZX50, and WZ21) over an observation period of 24 weeks. Large amounts of gas bubbles can be observed in the medullary cavities of the ZX50-containing bones up to 8 weeks post-operation. Nevertheless, upon complete pin degradation, these bones achieve full remodeling similar to the control bones (see images 24 weeks after operation). The WZ21 pins are also well tolerated by the bones, and gas bubble formation during degradation is significantly lower than for the ZX50 pins.

4.3.3 Phagocytic ability

One week prior to the operation the phagocytic ability of neutrophil granulocytes was similar in all groups studied. **Figure 4.4** illustrates the phagocytic ability of the three investigated rodent groups "no-implant", ZX50 and WZ21. At first glance all data remained at more or less high values over the whole test period, indicating no severe irritation of the phagocytic ability. When comparing the groups with each other at selected time points a significantly decreased phagocytic ability in the no-implant group compared to both the ZX50 ($p=0.002$) and the WZ21 ($p=0.045$) groups can be noticed immediately after the operation. Similarly, the phagocytic ability of the granulocytes in in the no-implant group also decreased significantly at weeks 4 and 8 post-operation when compared to the ZX50

group (p=0.006/0.007). However, 12 weeks after the operation we detected significantly decreased phagocytic activity in the WZ21 group compared to both the no-implant (p=0.033) and the ZX50 groups (p=0.024). No significant differences between the groups were observed at the late time points investigated, i.e. 16, 20 and 24 weeks post-operation.

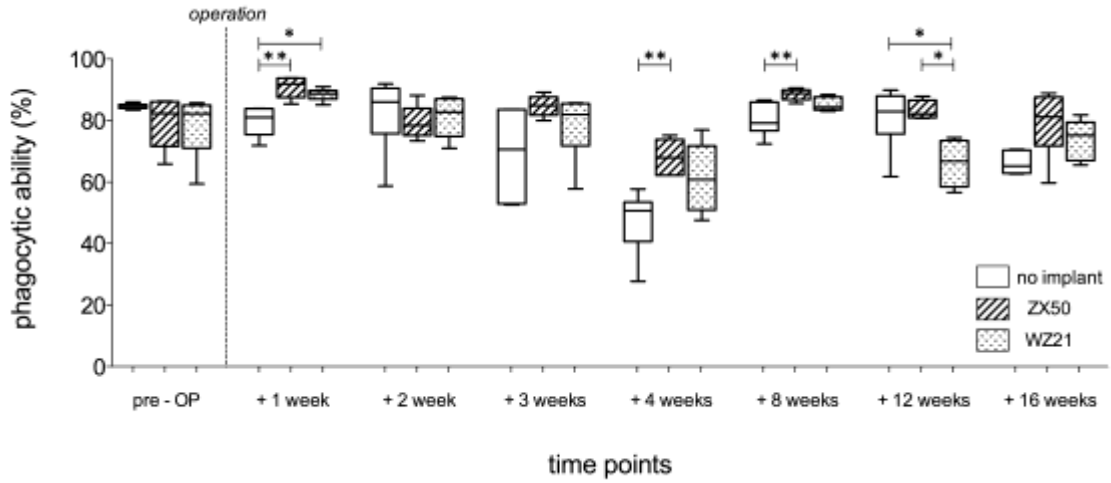

Figure 4.4: Phagocytic ability of neutrophile granulocytes at selected time points. The experimental groups are compared with each other at each time point: Statistically significant differences are labeled with one asterisk when $p < 0.05$ or two asterisks when $p < 0.01$.

4.4 Discussion

In the present study we focus on the response of the innate immune system to biodegradable Mg alloys, i.e. to the ions released from the implants during degradation. The innate immune system is responsible for defending the body against any kind of microbial or infectious “non-self”. An excessive immune response cannot be accepted when using biodegradable implants in children, as their bodies are particularly sensitive to any potentially harmful substance. In this article, we therefore concentrate mainly on this specific aspect and focus less on implant-tissue-reactions or the response of bone to the degrading alloys. For the latter, we refer to previous investigations; see Refs. [21] and [24].

According to our expectations from alloy design, the degradation rate of the ZX50 implants was significantly higher than that of the WZ21 implants. We attribute this to the high Zn content in ZX50, which causes the formation of the intermetallic phase $Mg_6Zn_3Ca_2$ [21,25]. This phase is nobler than the matrix and thus acts electrochemically as a cathode. This generates galvanic coupling with the α-Mg and thus results in fast dissolution of the Mg-

matrix [26]. For the WZ21 alloy, the amounts of yttrium were well balanced with respect to its solubility limit in order to prevent the formation of the $Mg_{24}Y_5$ phase [27]. Without the formation of this phase, the degradation resistance of Mg-Y alloys is very high [28].

The data for volume loss and gas formation displayed in **Fig. 4.1** correspond well to the values reported by Kraus et al. [21] despite that we used a transphyseal model instead of a transcortical one in the in vivo implantation. Correspondingly, the maximum element release rate of magnesium was much higher for ZX50 than for WZ21. In addition, the highest release rate, and thus the expected "burden" on the living organism, was observed earlier for ZX50 (weeks 2–4) than for WZ21 (weeks 9–12). Despite these circumstances and the fact that different ions were released from the implants (besides Mg-ions predominantly Zn-ions from ZX50 and Y-ions from WZ21), this study shows that biodegradable magnesium implants have no adverse effect on the immune system of a growing body. In fact, the phagocytic ability of neutrophile granulocytes was even increased in the experimental groups where biodegradable magnesium pins were implanted into the femoral bones compared with preoperative levels in the first 3 weeks and 8 weeks after the operation. In addition, the phagocytic ability was always comparable or significantly higher (weeks 1, 4, and 8) compared with the group that underwent surgery but had no pins implanted, with one important exception in the case of WZ21 after 12 weeks, where the Y-release was high. The reason for this exception will be discussed in detail below.

Our results therefore imply that magnesium implants not only have a positive effect on the immune system but also they can even overcome the negative immunological effects of anesthesia [29-31] and surgery [32,33]. The high phagocytic ability is crucially important for appropriate bone healing [34], which was indeed fully achieved in the fastdegrading ZX50 alloy group (as can be seen from **Fig. 4.3**), despite the initial large amount of hydrogen gas formation. The same complete bone healing is also expected to occur for the WZ21 group after the implant has fully degraded.

Our observations of the positive effects of Mg-alloys generally agree with the results of other groups. Witte et al. [35] showed, for example, in an animal model that magnesium ions released from biodegradable implants have no skin-sensitizing potential. Bondarenko et al. [36] compared morphological changes in efferent lymph nodes after implantation of resorbable and nonresorbable implants in rabbits and observed superior performance of magnesium alloys. Similar studies have also been conducted using classic nondegradable implant materials, such as titanium-, nickel-, or cobalt-chromium alloys. Here it was found,

however, that in cases of corrosion, i.e., ion release, the immunogenic potential for these alloys was high. Even in nontoxic concentrations, they can induce allergic reactions [37-40] and negatively influence human osteoblasts via induction of IL-1β, IL-6, and TNFα [41]. They may even stimulate osteoclast maturation, thereby leading to bone resorption [42] and, importantly, generate decreased phagocytic ability [43,44].

The superior immunological performance of magnesium alloys compared with that of classic nondegradable implant materials is not fully understood. Hypotheses include the local alkaline pH during degradation, as well as the fact that magnesium ions are necessary for many physiological processes. Thus, higher concentrations may be well tolerated. In contrast, nickel- or cobalt-chromium alloy corrosion products are nonphysiological or are present in the body only as micronutrients, and therefore even slightly increased concentrations induce cellular damage and pro-inflammatory cytokine production. What is left to discuss is the significant decrease in phagocytic ability of the WZ21 alloy group 12 weeks after the operation compared with that of the other groups (**Fig. 4.4**). In humans the phagocytic ability decreases with age [45,46]. Thus we may relate the phagocytic decrease 12 weeks post-operation to aging, but such an effect is much less clear in rats [47]. More important is indeed the fact that WZ21 is an yttrium-containing Mg-alloy. The element yttrium (which belongs to the family of rare-earth elements) can influence cellular processes in terms of apoptosis and expression of inflammatory markers [48,49] and preferentially deposits in tissues with phagocytic activity such as bone [50]. Since the results of the μCT measurements show (**Fig. 4.2b**) that between 9 weeks and 12 weeks after operation the highest amounts of yttrium are released from the degrading WZ21 implant (20 μg/week), we need to conclude that the decrease in phagocytic ability results from the enhanced yttrium release from the implant. As a consequence, Mg-alloys with rare-earth element additions may generate concerns in some biodegradable implant applications.

4.5 Conclusion

This study shows that biodegradable magnesium implants have a beneficial effect on the immune system in a growing rat model. As in a previous study [21], these results confirm that magnesium alloys are promising candidate materials for use in biodegradable implant application in pediatric trauma patients. However, some concerns exist regarding the use of rare-earth-containing alloys such as WZ21 in pediatrics, in particular because bone and bone

marrow are known to exhibit very slow release rates for such substances [51,52] and the tolerance limits for them in children are low.

Acknowledgements

The authors acknowledge support from the Laura Bassi Center of Expertise BRIC (Bioresorbable Implants for Children; FFG – Austria). The authors would also like to thank Ms. Katharina Angerpointer (Department of Pediatric Surgery, Medical University of Graz, Austria) and Ms. Verena Krischnan for their help with collection and workup of the blood specimens.

References

[1] Simanovsky N, Tair MA, Simanovsky N, Porat S. Removal of flexible titanium nails in children. Journal of pediatric orthopedics. 2006;26(2):188-92.

[2] Raney EM, Freccero DM, Dolan LA, Lighter DE, Fillman RR, Chambers HG. Evidence-based analysis of removal of orthopaedic implants in the pediatric population. Journal of pediatric orthopedics. 2008;28(7):701-4.

[3] Newton PO, Mubarak SJ. Financial aspects of femoral shaft fracture treatment in children and adolescents. Journal of pediatric orthopedics. 1994;14(4):508-12.

[4] Claes L. Mechanical Characterization of Biodegradable Implants. Clinical Materials. 1992;10:41-6.

[5] Staiger MP, Pietak AM, Huadmai J, Dias G. Magnesium and its alloys as orthopedic biomaterials: a review. Biomaterials. 2006;27(9):1728-34.

[6] Persaud-Sharma D, McGoron A. Biodegradable Magnesium Alloys: A Review of Material Development and Applications. Journal of biomimetics, biomaterials, and tissue engineering. 2012;12:25-39.

[7] Zberg B, Uggowitzer PJ, Loffler JF. MgZnCa glasses without clinically observable hydrogen evolution for biodegradable implants. Nat Mater. 2009;8(11):887-91.

[8] Aghion E, Levy G, Ovadia S. In vivo behavior of biodegradable Mg-Nd-Y-Zr-Ca alloy. J Mater Sci Mater Med. 2012;23(3):805-12.

[9] Hanzi AC, Gerber I, Schinhammer M, Loffler JF, Uggowitzer PJ. On the in vitro and in vivo degradation performance and biological response of new biodegradable Mg-Y-Zn alloys. Acta biomaterialia. 2010;6(5):1824-33.

[10] Huan ZG, Leeflang MA, Zhou J, Fratila-Apachitei LE, Duszczyk J. In vitro degradation behavior and cytocompatibility of Mg-Zn-Zr alloys. J Mater Sci Mater Med. 2010;21(9):2623-35.

[11] Krause A, von der Höh N, Bormann D, Krause C, Bach F-W, Windhagen H, et al. Degradation behaviour and mechanical properties of magnesium implants in rabbit tibiae. J Mater Sci Mater Med. 2010;45:624-32.

[12] Witte F, Hort N, Vogt C, Cohen S, Kainer KU, R. W, et al. Degradable biomaterials based on magnesium corrosion. Curr Opin Solid State Mater Sci. 2008;12:63-72.

[13] Witte F, Kaese V, Haferkamp H, Switzer E, Meyer-Lindenberg A, Wirth CJ, et al. In vivo corrosion of four magnesium alloys and the associated bone response. Biomaterials. 2005;26(17):3557-63.

[14] Lalor PA, Revell PA, Gray AB, Wright S, Railton GT, Freeman MA. Sensitivity to titanium. A cause of implant failure? J Bone Joint Surg Br. 1991;73(1):25-8.

[15] Merritt K, Rodrigo JJ. Immune response to synthetic materials. Sensitization of patients receiving orthopaedic implants. Clin Orthop Relat Res. 1996(326):71-9.

[16] Hallab N, Jacobs JJ, Black J. Hypersensitivity to metallic biomaterials: a review of leukocyte migration inhibition assays. Biomaterials. 2000;21(13):1301-14.

[17] Lam KH, Schakenraad JM, Esselbrugge H, Feijen J, Nieuwenhuis P. The effect of phagocytosis of poly(L-lactic acid) fragments on cellular morphology and viability. J Biomed Mater Res. 1993;27(12):1569-77.

[18] Rahman Q, Lohani M, Dopp E, Pemsel H, Jonas L, Weiss DG, et al. Evidence that ultrafine titanium dioxide induces micronuclei and apoptosis in Syrian hamster embryo fibroblasts. Environ Health Perspect. 2002;110(8):797-800.

[19] Wang L, Mao J, Zhang GH, Tu MJ. Nano-cerium-element-doped titanium dioxide induces apoptosis of Bel 7402 human hepatoma cells in the presence of visible light. World journal of gastroenterology : WJG. 2007;13(29):4011-4.

[20] Witte F, Ulrich H, Rudert M, Willbold E. Biodegradable magnesium scaffolds: Part 1: appropriate inflammatory response. J Biomed Mater Res A. 2007;81(3):748-56.

[21] Kraus T, Fischerauer SF, Hanzi AC, Uggowitzer PJ, Loffler JF, Weinberg AM. Magnesium alloys for temporary implants in osteosynthesis: in vivo studies of their degradation and interaction with bone. Acta biomaterialia. 2012;8(3):1230-8.

[22] Gunde P, Hänzi A, Sologubenko A, Uggowitzer P. High-strength magnesium alloys for degradable implant applications. Materials Science and Engineering A. 2011;A(528):1047-54.

[23] Hirt W, Nebe T, Birr C. [Phagotest and Bursttest (Phagoburst), test kits for study of phagocyte functions]. Wien Klin Wochenschr. 1994;106(8):250-2.

[24] Fischerauer SF, Kraus T, Wu X, Tangl S, Sorantin E, Hanzi AC, et al. In vivo degradation performance of micro-arc-oxidized magnesium implants: a micro-CT study in rats. Acta biomaterialia. 2013;9(2):5411-20.

[25] Hänzi AC, Sologubenko AS, Gunde P, Schinhammer M, Uggowitzer PJ. Design considerations for achieving simultaneously high-strength and highly ductile magnesium alloys. Philosophical Magazine Letters. 2012;92(9):417-27.

[26] Bakhsheshi-Rad H, Abdul-Kadir M, Idris M, Farahany S. Relationship between the corrosion behavior and the thermal characteristics and microstructure of Mg-0.5Ca-xZn alloys. Corrosion Science Conference Proceedings. 2012.

[27] Hanzi AC, Sologubenko AS, Uggowitzer PJ. Design strategy for new biodegradable Mg–Y–Zn alloys for medical applications. Int J Mat Res. 2009;100(8):1127-36.

[28] Yamasaki M, Nyu K, Kawamura Y. Corrosion Behavior of Rapidly Solidified Mg-Zn-Y Alloy Ribbons. Materials Science Forum Conference Proceedings. 2003.

[29] Frohlich D, Rothe G, Schwall B, Schmid P, Schmitz G, Taeger K, et al. Effects of volatile anaesthetics on human neutrophil oxidative response to the bacterial peptide FMLP. British journal of anaesthesia. 1997;78(6):718-23.

[30] Nakagawara M, Takeshige K, Takamatsu J, Takahashi S, Yoshitake J, Minakami S. Inhibition of superoxide production and Ca2+ mobilization in human neutrophils by halothane, enflurane, and isoflurane. Anesthesiology. 1986;64(1):4-12.

[31] Kurosawa S, Kato M. Anesthetics, immune cells, and immune responses. Journal of anesthesia. 2008;22(3):263-77.

[32] Menger MD, Vollmar B. Surgical trauma: hyperinflammation versus immunosuppression? Langenbeck's archives of surgery / Deutsche Gesellschaft fur Chirurgie. 2004;389(6):475-84.

[33] Hogan BV, Peter MB, Shenoy HG, Horgan K, Hughes TA. Surgery induced immunosuppression. The surgeon : journal of the Royal Colleges of Surgeons of Edinburgh and Ireland. 2011;9(1):38-43.

[34] Bolander ME. Regulation of fracture repair by growth factors. Proceedings of the Society for Experimental Biology and Medicine Society for Experimental Biology and Medicine (New York, NY). 1992;200(2):165-70.

[35] Witte F, Abeln I, Switzer E, Kaese V, Meyer-Lindenberg A, Windhagen H. Evaluation of the skin sensitizing potential of biodegradable magnesium alloys. J Biomed Mater Res A. 2008;86(4):1041-7.

[36] Bondarenko A, Hewicker-Trautwein M, Erdmann N, Angrisani N, Reifenrath J, Meyer-Lindenberg A. Comparison of morphological changes in efferent lymph nodes after implantation of resorbable and non-resorbable implants in rabbits. Biomedical engineering online. 2011;10:32.

[37] Thomsen M, Rozak M, Thomas P. Pain in a chromium-allergic patient with total knee arthroplasty: disappearance of symptoms after revision with a special surface-coated TKA -— a case report. Acta Orthopaedica. 2011;82(3):386-8.

[38] Summer B, Paul C, Mazoochian F, Rau C, Thomsen M, Banke I, et al. Nickel (Ni) allergic patients with complications to Ni containing joint replacement show preferential IL-17 type reactivity to Ni. Contact dermatitis. 2010;63(1):15-22.

[39] Thomas P, Bandl WD, Maier S, Summer B, Przybilla B. Hypersensitivity to titanium osteosynthesis with impaired fracture healing, eczema, and T-cell hyperresponsiveness in vitro: case report and review of the literature. Contact dermatitis. 2006;55(4):199-202.

[40] Thomas P, Schuh A, Eben R, Thomsen M. Allergie auf Knochenzementbestandteile. Orthopäde. 2008;37(2):117-20.

[41] Wang JY, Wicklund BH, Gustilo RB, Tsukayama DT. Prosthetic metals interfere with the functions of human osteoblast cells in vitro. Clin Orthop Relat Res. 1997(339):216-26.

[42] Haynes DR, Crotti TN, Zreiqat H. Regulation of osteoclast activity in peri-implant tissues. Biomaterials. 2004;25(20):4877-85.

[43] Rae T. A study on the effects of particulate metals of orthopaedic interest on murine macrophages in vitro. J Bone Joint Surg Br. 1975;57(4):444-50.

[44] Garrett R, Wilksch J, Vernon-Roberts B. Effects of cobalt-chrome alloy wear particles on the morphology, viability and phagocytic activity of murine macrophages in vitro. The Australian journal of experimental biology and medical science. 1983;61 (Pt 3):355-69.

[45] Butcher SK, Chahal H, Nayak L, Sinclair A, Henriquez NV, Sapey E, et al. Senescence in innate immune responses: reduced neutrophil phagocytic capacity and CD16 expression in elderly humans. Journal of leukocyte biology. 2001;70(6):881-6.

[46] Filias A, Theodorou GL, Mouzopoulou S, Varvarigou AA, Mantagos S, Karakantza M. Phagocytic ability of neutrophils and monocytes in neonates. BMC pediatrics. 2011;11:29.

[47] Cantrell W, Elko EE. Effect of age on phagocytosis of carbon in the rat. Experimental parasitology. 1973;34(3):337-43.

[48] Drynda A, Deinet N, Braun N, Peuster M. Rare earth metals used in biodegradable magnesium-based stents do not interfere with proliferation of smooth muscle cells but do induce the upregulation of inflammatory genes. J Biomed Mater Res A. 2009;91(2):360-9.

[49] Feyerabend F, Fischer J, Holtz J, Witte F, Willumeit R, Drucker H, et al. Evaluation of short-term effects of rare earth and other elements used in magnesium alloys on primary cells and cell lines. Acta biomaterialia. 2010;6(5):1834-42.

[50] Horovitz CT. Biochemistry of Scandium and Yttrium, Part 2: Biochemistry and Applications. New York: Springer US; 2000. 83-136 and 208-10 p.

[51] Hirano S, Suzuki KT. Exposure, metabolism, and toxicity of rare earths and related compounds. Environmental health perspectives. 1996;104(Suppl 1):85-95.

[52] Wells Jr WH, Wells VL. The Lanthanides, Rare Earth Metals. Patty's Toxicology: John Wiley &Sons, Inc.; 2001.

5 Exploration of Biofunctionality Features

A modern biofunctional implant for osteosynthesis is supposed to promote the bone healing. Actively involvements into the healing process by increased osteoconductivity or osteoinductivity, or anti-infectious contribution are nowadays favourable towards a conventional inert material behaviour. Biofunctionality features have its importance especially in early stages of healing process as tissue fragility is high and irritations or infections can occur easily.

In vivo degradation performance of micro-arc oxidized magnesium implants: A micro-CT study in rats

Stefan F. Fischerauer[*]*, Tanja Kraus, Xujun Wu, Stefan Tangl, Erich Sorantin, Anja C. Hänzi, Jörg F. Löffler, Peter J. Uggowitzer, Annelie M. Weinberg*

ACTA BIOMATER. 2013; 9(2):5411-5420

Biodegradable Mg alloys are of great interest for osteosynthetic applications because they do not require surgical removal after they have served their purpose. In this study, fast-degrading ZX50 Mg-based implants were surface-treated by micro-arc oxidation (MAO) to alter the initial degradation, and implanted along with untreated ZX50 controls in the femoral legs of 20 male Sprague-Dawley rats. Their degradation was monitored by microfocus computed tomography (□CT) over a total observation period of 24 weeks, and histological analysis was performed after 4, 12, and 24 weeks. While the MAO-treated samples showed almost no corrosion in the first week, they revealed an accelerated degradation rate after the third week, even faster than that of the untreated ZX50 implants. This increase in degradation rate can be explained by an increase in the surface-area to volume ratio of MAO-treated implants, which degrade inhomogeneously via localized corrosion attacks. The histological analyses show that the initially improved corrosion resistance of the MAO-implants has a positive effect on bone and tissue response: The reduced hydrogen evolution (due to reduced corrosion) makes possible increased osteoblast apposition from the very beginning and thus generate a stable bone-implant interface. As such, MAO-treatment appears to be very interesting for osteosynthetic implant applications, as it delays implant degradation immediately after implantation, enhances fracture stabilization, minimizes the burden on the post-operatively irritated surrounding tissue and generates good bone-implant connections, followed by accelerated degradation in the later stage of bone healing.

Keywords: Magnesium; biodegradation; micro-arc oxidation; *in vivo* animal imaging; micro-computed tomography

[*] Author's contribution to this study: study planing, surgery of animals and animal care, μCT performance and evaluations, statistical analysis, construction of figures, literature research, and writing the manuscript.

5.1 Introduction

Biodegradable osteosynthetic devices may revolutionize surgical fracture stabilization because they make redundant surgical follow-up intervention for implant removal. Thereby morbidity rates may be reduced, and health care systems can profit from cost savings. From a clinical point of view, biodegradable materials suitable for osteosynthetic applications must exhibit several fundamental properties: (i) biocompatibility with the living organism; (ii) sufficient mechanical flexural rigidity to ensure fracture stabilization during the inflammatory and reparative phases of fracture healing (4-16 weeks) [1]; and (iii) degradation performance in balance with fracture consolidation.

Among currently known biodegradable materials, magnesium-based alloys are promising candidates for osteosynthesis because:

1. Magnesium (Mg) is an essential element in the human organism and is naturally found in bone tissue [2, 3]. It is well tolerated by the human body and does not induce systemic inflammatory reactions or negatively affect the cellular blood composition [4-6].
2. Mg, as a biodegradable light metal, possesses mechanical properties that are beneficial for load-bearing fracture stabilization – not least because its Young's modulus is close to that of natural bone, thereby preventing stress shielding during fracture consolidation [7, 8].
3. Mg degrades in aqueous solutions, and is therefore also prone to degradation in body fluids. The degradation process generates tissue-compatible magnesium hydroxide, and hydrogen gas as a by-product [8].

Unalloyed Mg exhibits low mechanical strength and was found to corrode rather fast in aqueous solution, this accompanied by the release of considerable amounts of hydrogen gas [9, 10]. As a result the mechanical bond between bone and implant may be weakened and fracture healing insufficiently supported [11-13]. To overcome these limitations various efforts were undertaken to develop novel Mg alloys which offer improved mechanical properties and enhanced corrosion resistance [14-17]. By increasing their capability to resist corrosion, Mg alloys demonstrated that they possess good osteoconductive properties leading to appositional bone growth around the implant as well as to the formation of a highly stable bone-implant interface [8, 18-24]. Clinical demands concerning the rate of corrosion are ambivalent. On one hand slower implant degradation is desirable. On the other hand, they should not remain in the living organism for an unnecessary long period of time. Optimal

implants should feature increased corrosion resistance at the initial stages of implantation and a rather fast degradation after fracture consolidation. In this context protective surface coatings are considered interesting solutions, because they may reduce a material's specific susceptibility to corrosion and related phenomena such as stress corrosion cracking and may also prevent a delay in the onset of bulk degradation [25-29]. The degradation rates of bulk and surface (coating) may thus differ considerably, rendering the overall degradation performance potentially designable.

An elegant way of altering the surface and its degradation properties without adding a coating material, and thus inducing other (potentially irritating) materials, is micro-arc oxidation. This is a method of surface modification, based on the principle of plasma-electrolytic oxidation, which produces an increased oxide layer at the surface. Micro-arc-treated magnesium surfaces exhibit an improved corrosion resistance in various environments [27, 30]. In vitro test in simulated body fluid repeatedly confirmed the favorable behavior of surface-treated Mg alloys regarding reduced dissolution and enhanced biocompatibility [31-34]. However, only little information is available about the effects of micro-arc surface treatment on the *in vivo* degradation performance.

The aim of this study is to investigate the influence of micro-arc oxidation on fast degrading magnesium-based implants (ZX50) in a living rat model. In a previous study using the same animal model [19] we showed that ZX50 implants exhibit signs of severe and rapid corrosion immediately after implantation and degrade initially very fast while creating massive amounts of gas. By applying micro-arc surface treatment, our intention was thus to decrease the degradation rate of Mg implants in the initial post-implantation period, in order to reduce the impact of degradation products on the post-operatively irritated surrounding tissues. Yet later on, fast dissolution of the material takes place, once the implant's function has become redundant. The degradation performance of micro-arc-modified ZX50 pins and untreated ZX50 control implants in rat femurs and their influence on living tissue is assessed in this study by means of micro-CT measurements and histological analysis.

5.2 Materials and methods

5.2.1 Implants

Machined cylindrical pins ($n = 40$; diameter: 1.6 mm; length: 8 mm) made of ZX50 material were used. The ZX50 Mg alloy is known to be fast-degrading magnesium, alloyed with 5% Zn, 0.25% Ca and 0.15% Mn (in wt.%) [19, 35]. It exhibits a fine-grained microstructure (grain size ≈ 4 μm) with excellent mechanical properties: yield stress of 210 MPa, ultimate tensile strength of 295 MPa, uniform elongation of 18%, and elongation at fracture of 26% [14, 36]. The pins were dry-machined with clean tools. After machining they were cleaned in a cascade of pure ethanol in an ultrasonic bath and dried in warm air. Forty pins were produced and assigned either to a "surface treated" or an "untreated" group, containing 20 pins each.

5.2.2 Micro-arc oxidation treatment

Twenty pins were surface-treated by micro-arc oxidation, performed at AHC Oberflächentechnik using the MAGOXID-COAT® process [37]. The MAGOXID-unit was operated in saline solution electrolyte using a direct current supply, with a stainless steel container acting as cathode. The current density was kept at 14 $mAcm^{-2}$. The samples were oxidized until an oxide layer thickness of approximately 10 μm was formed. Electrical contact was placed on one end face of the pin, which therefore remained uncoated.

5.2.3 Experimental design

All animal experiments were conducted according to established guidelines of animal care and were authorized by the Austrian Ministry of Science and Research (accreditation number BMWF-66.010/0091-II/3b/2010).

Twenty five-week-old male Sprague–Dawley rats with a body weight of 140–160 g were used in this study. The rats were randomly divided into two groups of 10 each, designated 'ZX50' (untreated) and 'MAO' (micro-arc oxidized ZX50). In each rat an identical pin was implanted into each of its femoral bones. Four rats, i.e 8 pins, per group underwent micro-focus computer tomography (μCT) evaluation at pre-arranged times (weeks 1, 2, 3, 4, 8, 12, 16) over a total observation period of 24 weeks and were subsequently sacrificed at week 24 and subjected to histological analysis using undecalcified ground thin

sections. The remaining 6 animals per group were randomly chosen for histological analysis at weeks 4 and 12.

5.2.4 Surgical procedure

Under general anesthesia, the devices were implanted in the femoral mid-diaphyseal region of the rats as reported by Kraus et al. [19]. Perioperative pain-treatment was also identical [19]. After surgery the rats were allowed to move freely in their cages without external support and with their weight bearing unrestricted. Clinical observation was performed daily throughout the whole study period.

For euthanasia volatile isoflurane (Forane®, Abbot AG, Baar, Switzerland) was deployed for sedative anesthesia of the animals. Subsequently 25 mg sodium thiopental (Thiopental® Sandoz, Sandoz GmbH, Kundl, Austria) was injected into the cardiac ventricle, leading to immediate cardiac arrest.

5.2.5 Microfocus computed tomography

Since its introduction by Feldcamp et al. [38], µCT has gained enormous significance in the quantitative assessment of cancellous bone. Its high-resolution imaging, with a resolution of tens of microns, is a pivotal advantage of µCT over previously used methods [39]. In addition, µCT based on quantitative bone morphometry enables three-dimensional (3D) measurements of trabecular bone structure [40]. Online µCT monitoring is therefore highly suitable for studying the degradation performance of temporary Mg implants without harming the animal [19, 20, 41].

Scans were performed with a Siemens Inveon Acquisition Workplace 1.2.2.2 at 70 kV voltage, 500 µA current, and 1000 ms exposure time. Effective pixel size was 35.55 µm. Image reconstruction was performed without the use of a downsample-algorithm. The image processing software Mimics® (Version 14.12, Materialise NV, Leuven, Belgium) was deployed to construct 3D models of pins and bubbles of emitted hydrogen gas. The upper and lower thresholds for the pin were set at 226 and 3071 Hounsfield units (HU), for hydrogen gas at -1000 and -1024HU. A detailed analysis protocol was published by Kraus et al [19]. Pin volume, pin surface, and gas volume were quantified every week during the first 4 weeks and then at four-week intervals until week 24.

5.2.6 Data analysis

Micro-CT data for eight pins per group were evaluated for the statistical analysis, which was performed using IBM® SPSS® Statistics 20.0.0 (IBM Corporation, Armonk, NY, USA). Pin volume (V, mm^3), pin surface (S, mm^2), pin degradation rate (DR, mm per year), and the surface to volume ratio S/V were evaluated for each sample at weeks 1, 2, 3, 4, 8, 12 and 16. The degradation rate was calculated from the µ-CT data according to

$$DR_i = \frac{\Delta x_i}{\Delta t} \text{ with } \Delta x_i = \frac{\Delta V_i}{S_i}$$

where i designates the moment of observation, ΔV_i is the volume change during the time interval Δt (i.e. between the observation moment i-1 and i) S_i is the surface area at the moment i, and Δx_i is the corresponding degradation width. The Mann-Whitney-U-Test was used to compare the degradation performance of the implant groups. The statistical significance was set at p values < 0.05.

5.2.7 Histological preparation

For histological evaluation tissue blocks containing the implants were fixed in neutral buffered 4% formalin solution, dehydrated in ascending grades of alcohol, embedded in light-curing resin Technovit 7200 VLC® (Heraeus Kulzer, Hanau, Germany) for ZX50 implants and Technovit 9100 New® (Heraeus Kulzer, Hanau, Germany) for MAO implants. The implants were further processed with a high-precision equipment (Exakt Apparatebau, Norderstedt, Germany) according to the method of Donath [42]. Plastic embedded specimens were cut through the central axis of the implant, as well as parallel to the longitudinal axis of the femur shaft. Ground sections produced from this plane were reduced to a thickness of approximately 30 µm and stained with Levai-Laczko dye for ZX50 samples and with Toluidine Blue O for the MAO implants. Microscopic overview images were taken at 200x magnification (dotSlide- Virtual Slide System, Olympus, Japan). Both Levai-Laczko dye as well as Technovit 9100 New® with Toluidine Blue O dye are well established in bone research and are equally efficient to unequivocally recognize bone cells, bone tissue types (woven bone, lamellar bone) and different degrees of mineralization.

5.3 Results

5.3.1 MAO sample surface prior to implantation

The surface of an implant influences its ultimate ability to integrate into the surrounding tissue [43]**. Figure 5.1** shows the surface of the micro-arc-treated alloy (**Fig. 5.1a**) and the cross-section of the oxide layer (prepared using focused-ion beam milling (FIB) at a surface crater position). The surface of the micro-arc layer is characterized by the presence of numerous holes and calderas, as well as some surface cracks (**Fig. 5.1a**). The thickness of the oxide layer was on average about 10 µm (**Fig. 5.1b**). However, at the position of holes and calderas, it was significantly reduced to less than 2 µm. In general, the oxide layer contains a high density of pores, which is typical of micro-arc coatings [26, 31, 44-47]. As mentioned above, no oxide layer was present on one end of the pin, at the location of electrical contact during the MAO process.

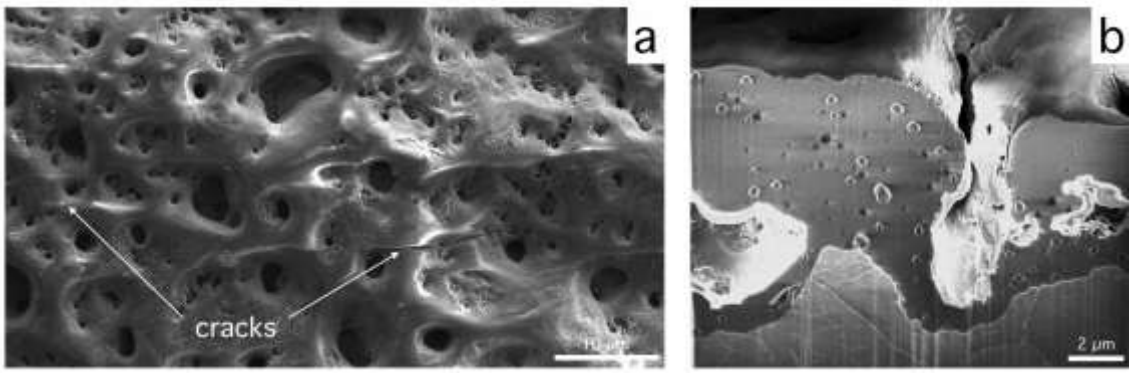

Figure 5.1: Focused-ion beam (FIB) images of MAO-modified Mg samples. (a) Typical surface characteristics; the oxide layer features numerous holes and calderas as well as a few cracks. (b) The average thickness of the modified surface is about 10 µm; at the position of calderas the thickness is reduced to < 2 µm [67].

5.3.2 Degradation performance

The µCT images in **Figure 5.2** provide examples of the degradation process of a ZX50 and MAO implant. Almost no corrosion of micro-arc-treated implants was observed within the first week, while the untreated ZX50 implants already exhibited several surface pits. The surface area of MAO preserved its integrity during the first week and the average degradation was significantly decreased (p=0.002). In consequence higher volumes of MAO pins were measured within the first few weeks (**Fig. 5.3a**). **Fig. 5.2 and Fig. 5.3c** reveal that the degradation process for MAO implants accelerated between weeks 3-4 (p=0.005) and 4-8 (p=0.046), and became significantly faster than in the ZX50 group. Because of the

accelerated degradation rate between weeks 3 and 8, MAO pins ultimately dissolved sooner than the untreated pins. While at week 12 the MAO implants completely vanished, there was still some pin debris visible from ZX50. It is important to note that acceleration of the degradation rate of the MAO sample went hand in hand with considerable macroscopic fragmentation of the pins (see for example **Figs. 5.2m, n**).

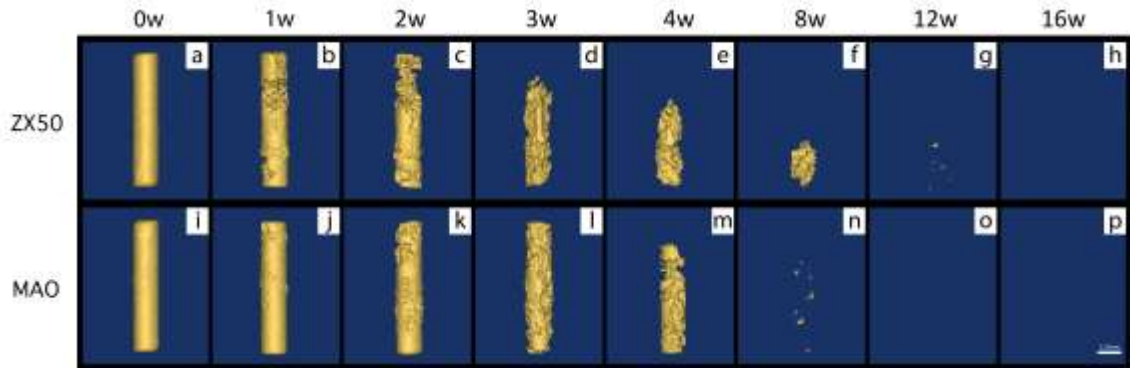

Figure 5.2: µCT images (3-D reconstruction) of implanted ZX50 (a-h) and MAO (i-p) pins. The pins degrade over time and vanish completely after 12 to 16 weeks.

Figs. 5.3 a-c show the sequence of the degradation process of ZX50 and MAO implants in more detail. **Fig. 5.3a** visualizes the volume reduction due to biodegradation as a function of the implantation time. As deduced from **Fig. 5.2** the corrosion resistance of the MAO pins was higher than that of the uncoated samples only during the first 3 weeks after implantation (**Fig. 5.3a**). Between weeks 3 to 4 an increase in volume loss for MAO pins occurred, which corresponds to an increase in degradation rate from week 3 until complete degradation (**Fig. 5.3c**). The surface areas of both implant types increased during the first period of implantation (**Fig. 5.3b**; note that the surface data at t = 0 are identical for ZX50 and MAO, despite the fact that the MAO surface is porous; this is caused by small pore size below the µCT-pixel size). However, for the MAO implants the increase was retarded by 1 to 2 weeks. The simultaneous increase in surface area and decrease in volume suggests the occurrence of severe localized corrosion, as is for example visible in **Fig. 5.2b** (ZX50 after 1 week). From week 3 to 4 onwards, the surface area of the pins decreased. This decrease obviously took place in parallel with the decrease in the pin volume. At week 4, where the volume of the ZX50 and MAO pins was comparable, the surface area of MAO implants was significantly greater ($p=0.015$).

Figure 5.3c shows that for the uncoated implants the degradation rate stayed at a constant level of DR ≈ 1.7 mm a^{-1} for 3-4 weeks and then gradually increased to a level of close to 4 mm a^{-1}. In contrast, the degradation rate of the MAO implants was close to zero

during the first week (DR ≈ 0.25 mm a^{-1}), increased to a level of DR ≈ 1.7 mm a^{-1} between weeks 2 to 3, and then increased substantially to about 6 mm a^{-1} at the final stage of the degradation process. However, in particular at the end of the implant's life high scatter was seen for the volume and surface data, and thus for the degradation rate (eq. 1).

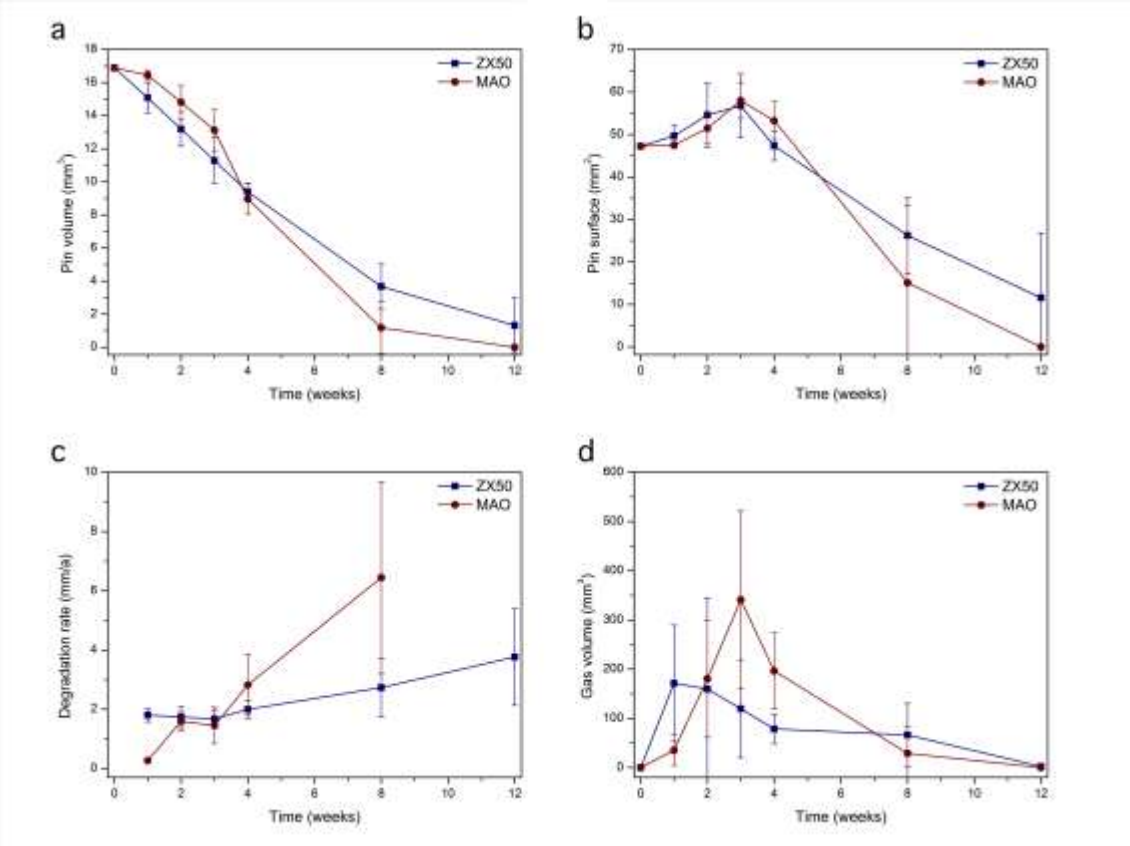

Figure 5.3: *In vivo* degradation performance of implanted ZX50 and MAO pins during the study period, assessed via µ-CT measurements. (a) Loss of pin volume; (b) change of pin surface area; (c) pin degradation rate; (d) detected hydrogen gas volume.

According to the electrochemical reaction $Mg + 2H_2O \rightarrow Mg(OH)_2 + H_2$[48] pin degradation results in considerable release of hydrogen gas, as illustrated in **Fig. 5.3d and Fig. 5.4**. One molecule of hydrogen gas is formed per one atom of Mg, which results in about 25 cm^3 H_2 generated by the degradation of the whole implant (pin weight of 27 mg). Because of the rapid degradation rate severe gas formation was observed for both implant types. While the ZX50 exhibited the highest gas formation at the beginning – seen both in the soft tissue and the intramedullary cavity – followed by monotonic decrease over the implantation time, little gas formation was observed around MAO implants within the first week ($p=0.002$); small gas bubbles formed solely at the uncoated face end of the pin. The acceleration of degradation between weeks 3 and 4 was accompanied by a pronounced increase in gas bubble volume. Note that the detected gas volume reflects the accumulated

H_2-volume, which is the net volume of the gas released by Mg-dissolution minus the gas evacuated by the organism. It does not necessarily correspond to the Mg-mass loss or degradation rate. After 12 weeks hydrogen bubbles were no longer detected by µCT. During the whole course of degradation, gas bubbles were in general observed in the soft tissue on both ends of the pins as well as in the intramedullary cavity.

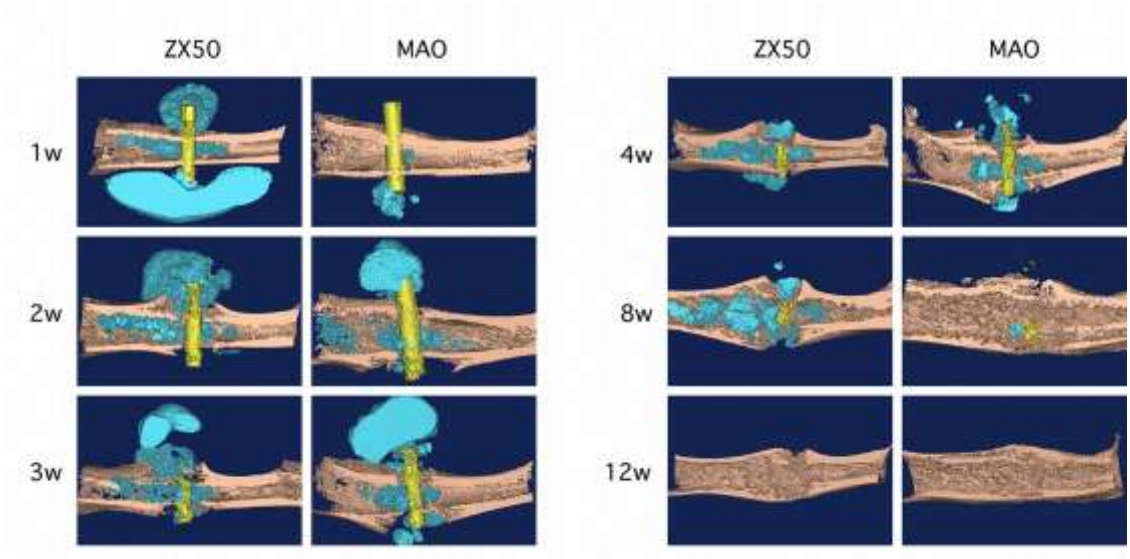

Figure 5.4: µCT Mimics® 3-D reconstructions of the implant site for ZX50 and MAO implants; gas bubbles are visible in light blue.

5.3.3 Biological response

In this section the bone and tissue response is evaluated based on results from the µCT investigations and the histological examination. All animals tolerated the operation well and regained full weight-bearing capability. Clinically, all rats showed slight reddening of the wound and mild wound swelling resulting from surgery. However, both symptoms disappeared completely after 3 to 5 days *post operationem* and no wound infections were observed.

The biological response to the inserted and degrading implants is illustrated in **Fig. 5.5** (µCT images) and **Fig. 5.6** (histological ground sections). **Fig. 5.5** shows the 2-D µCT reconstructions of the degradation process of the ZX50 and MAO implants and the bone response within the first 4 weeks, reflecting the time where micro-arc oxidation leads to a delayed degradation process. Untreated ZX50 alloys initially evolved large amounts of gas after implantation. The gas inhibited physiological bone reaction and generated distinct callus formation (**Figs. 5.5 a-d**). Bone around the implant was present in only small quantities due

to gas formation, but there was also a massive cortico-periostal reaction due to fast release of Mg (**Fig. 5.5d**). In MAO, decreased formation of gas within the first two weeks minimized callus formation in the cortical bone and allowed apposition of new bone along the MAO surface, clearly seen as hyperdense bone layers around the implant inside the bone marrow (**Figs. 5.5e and f**). This bone contact to the implant was still partly observable at week 4, when the first histological analysis was performed. **Figs. 5.6c and 6d** show the interface between mineralized bone tissue and the implant surface in the cortical bone (**Fig. 5.6c**) as well as in the bone marrow (**Fig. 5.6d**), where osteoblasts and new bone formation were present even inside of corrosion pits. In contrast, on the ZX50 corrosion layer, mesenchymal, fibrous tissue containing fibroblasts was observed (**Figs. 5.6a and b**). More peripherally to the ZX50 implant, a considerable number of activated osteoblasts formed woven bone. In between and in more peripheral areas of the medullar cavity, a multitude of myeloid cells at different hematopoietic stages were observed in both groups. No foreign-body reaction in terms of an increased number of inflammatory cells, such as plasma cells or lymphocytes, was visible in the histological slices of either the MAO or the ZX50 group.

Figs. 5.6 e-h illustrate the biological response of the cortical bone and the bone marrow at the timepoint when the implants had only just corroded fully and none of the original material was left unaltered (week 12). Small corrosion particles, remnants of originating in the ZX50 degradation process remained in the drill hole (**Fig. 5.6e**). These particles were surrounded by capsule-like layers of bone. MAO findings at this point in time showed a more progressive bone restoration at the original drill hole site (**Fig. 5.6g**). In the medullar cavity the enormous amount of gas formation during the degradation process generated a displacement of the original myeloid cells. Where once the implant had been, there were now areas containing only few cells (mostly fibroblasts and myeloid cells) and little extracellular matrix. (**Fig. 5.6f**). The rate of these bone marrow regeneration processes was slightly faster in the MAO group, showing a higher cell count at the original implant site (**Fig. 5.6h**). Adjacent to the former implant interface, both groups exhibited bone formation, producing comparatively unstructured woven bone with large osteocyte lacunae.

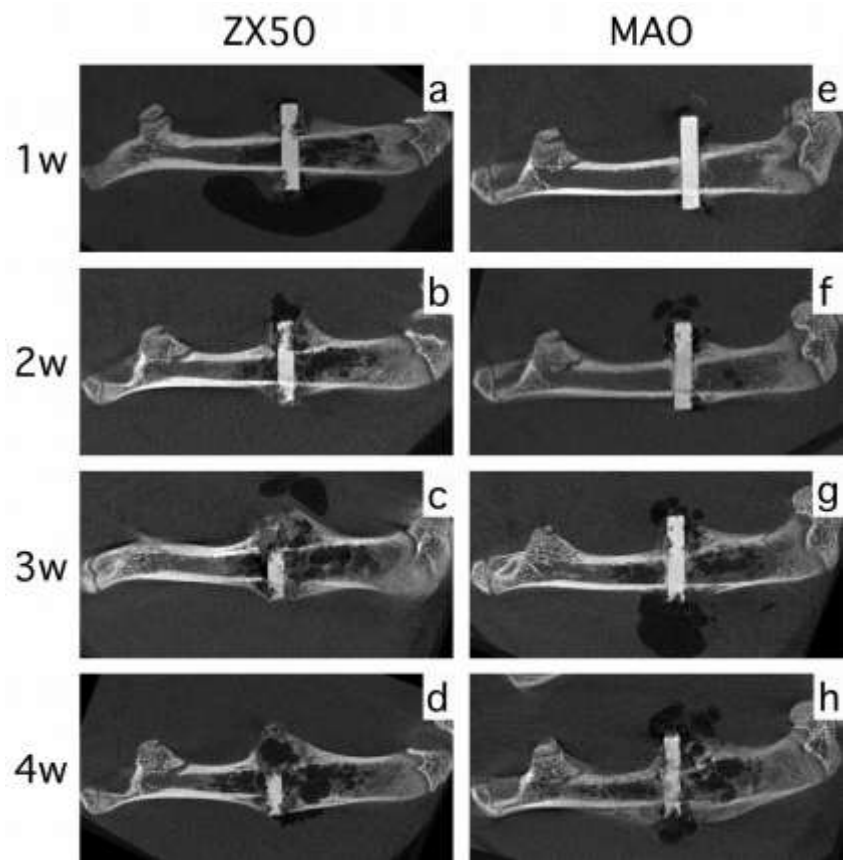

Figure 5.5: µCT reconstructions (2-D slices) illustrating the ZX50 and MAO degradation process, gas evolution and bone response in the early stages after implantation (weeks 1 to 4); ZX50 (a-d) and MAO (e-h).

After 24 weeks histological ground sections (**Figs. 5.6i-l**) showed notable tissue regeneration. Both ZX50 and MAO featured replacement of the drill hole with newly formed bone tissue (**Figs. 5.6i and k**). The bone marrow was also completely restored in both groups (**Figs. 5.6j and l**). Adipocytes predominate in the cell line of the bone marrow. In the MAO group, a few scattered bone tissue formations remained in the medullary cavity at this point (**Fig. 5.6l**).

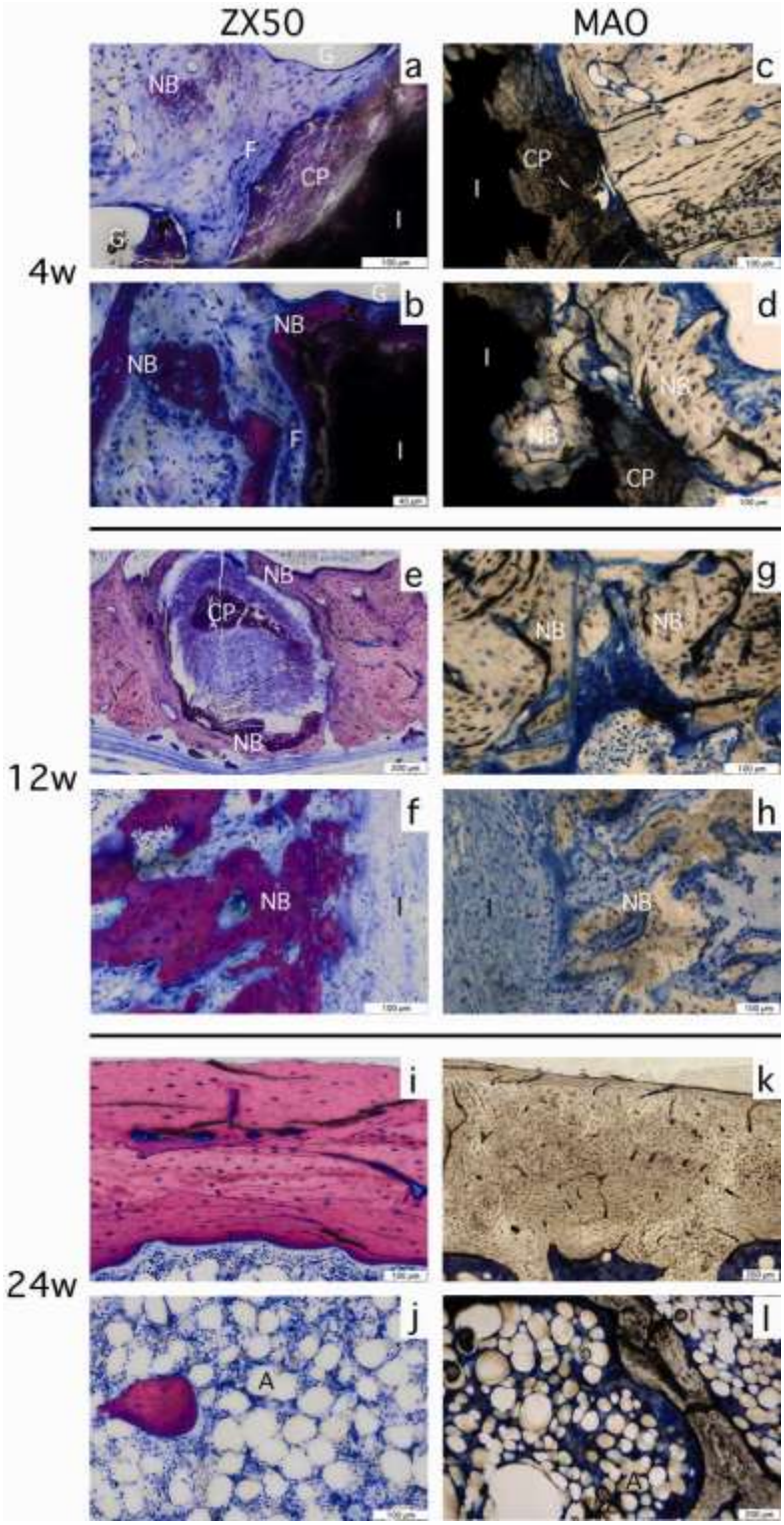

Figure 5.6: Histological thin slides of ZX50 and MAO pins in Levai–Laczko staining for ZX50 samples (left) and Toluidine Blue O for the MAO implants (right). Situation after 4 weeks (a-d), 12 weeks (e-h) and 24 weeks (i-l). I=implant/initial implant site, CP=corrosion products, G=hydrogen gas bubble, NB=new bone formation, F=fibroblast band, A=adipocytes.

5.4 Discussion

The electrochemical activity of Mg and Mg alloys in physiological solutions makes it necessary, for safe application in the human body, to control the corrosion rate. Development of suitable strategies to enhance the poor corrosion resistance of magnesium alloys is therefore important. Alloy compositions play a significant role as well as coatings and surface modifications. A number of preventive measures have been proposed and are being adopted to overcome corrosion problems [9, 14-16, 45, 49, 50]. While most of previous studies focused on the *in vitro* degradation of surface-modified magnesium [26, 30, 31, 51-53], this study evaluates the micro-arc oxidation surface treatment of Mg ZX50 alloys *in vivo*.

The growing rat model was selected because of the extensive emerging field of biodegradable implants in pediatric surgery, as the Elastic Stable Intramedullary Technique (ESIN) is the rising osteosynthetic technique for long bone fractures in children. For that reason a transcortical model was also chosen which enables investigation of biological responses of the cortical bone and of the bone marrow. Moreover, the animals can be easily observed by μCT over the whole growing process.

The evaluation of micro-arc oxidized magnesium implants revealed three major findings that are of great interest for the clinical application of biodegradable Mg implants: (i) Micro-arc oxidation inhibits the initial corrosion process; (ii) it enhances the corrosion process over time; and (iii) it improves the bone-implant interface. In the following sections we discuss these findings in detail.

5.4.1 Micro-arc oxidation inhibits the initial degradation process

The increased corrosion resistance is based on the formation of an oxide layer on the implant surface during the oxidation process. The layer acts as a more or less continuous barrier against charge transport and thus degradation [26, 44-47, 54]. It is well known that micro-arc coatings reduce the corrosion rate to a high degree, even up to 90% [26]. In fact, as shown in **Fig. 5.3a** and more clearly in **Fig. 5.3c** the volume loss and degradation rate, respectively, were significantly smaller for the MAO implants. During the first week after implantation the average degradation rate (DR) of MAO was about 0.25 mm a^{-1}, while for ZX50 it was on average 1.7 mm a^{-1}. Because of the fast degradation of ZX50 the effects of micro-arc coating could be seen clearly. Similar performance was observed for a Mg-2Zn-

0.2Ca alloy that exhibited an average DR of 1 mm a^{-1} over a period of 8 weeks, while a composite-coated version (micro-arc plus hydroxyapatite layer) showed a DR of only 0.13 mm a^{-1} [55].

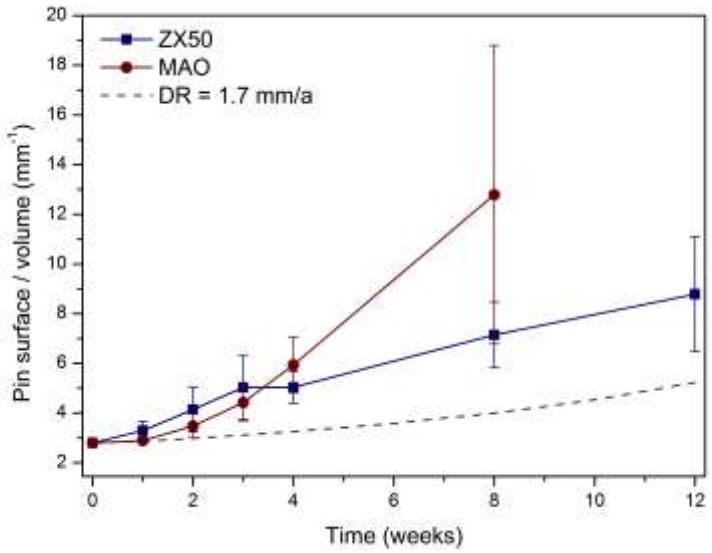

Figure 5.7: Surface-area to volume ratio as measure for the "topography" and "imperfection" of the pin. Large values suggest a rugged topography and/or fragmentation of the pin. For comparison the S/V values for homogeneous degradation with a DR of 1.7 mm a^{-1} are plotted.

5.4.2 Micro-arc oxidation enhances corrosion process over time

Figs. 5.3a and 5.3c reveal a pronounced acceleration of the MAO degradation between weeks 3 and 4. As mentioned in the results section, this phenomenon can be attributed to the occurrence of severe localized corrosion attacks. In the following we use the surface-area to volume ratio as a measurement for localized attack; we assume the implant surface topography to be very rugged and fragmented at high S_i/V_i values. **Fig. 5.7** shows the variation of the S/V ratio for MAO and ZX50. The figure also shows the theoretical S/V-value for homogeneous degradation with a degradation rate of 1.7 mm a^{-1} (initial degradation rate of ZX50; see **Fig. 5.3c**). Because higher S/V values than those for homogeneous degradation correspond to an increase in localized corrosion attacks, the change in the corrosion mode becomes clearly visible. ZX50 forms surface pits as early as week 1 (**Fig. 5.2b**) and the "inhomogeneity" of the degradation increases monotonically with time. MAO stays at low values for 1 to 2 weeks, while between weeks 3 and 4 a steep increase is observed. This corresponds to the moment of pronounced degradation rate acceleration. Such behavior was indirectly mentioned by Chen et al [55]. They report low degradation rates in the range of

0.13 mm a^{-1} during the first period of implantation but an increase by a factor of ten in the subsequent phase after a partial degradation of the composite coating.

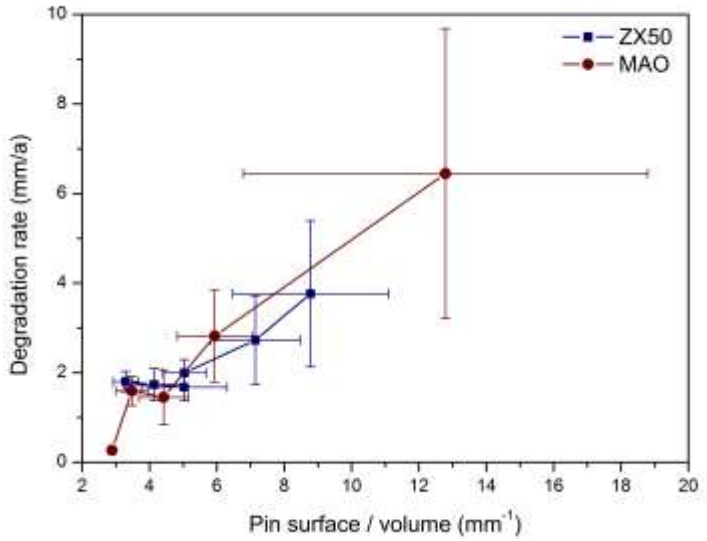

Figure 5.8: Degradation rate (DR) as function of the surface-area to volume ratio. DR increases proportionally with the surface-area to volume ratio.

From the above-mentioned facts it may be concluded that the degradation rate is somewhat dependent on the surface topography. **Fig. 5.8** illustrates that this is obviously the case for Mg-alloys in body fluid, where the degradation rate increases more or less linearly with the *S*/*V*-ratio. A detailed discussion of this observation is beyond the scope of this study. However, in literature several arguments are given that may help to find a convincing explanation [32, 56, 57]. They are all based on the description of chemical processes that occur inside of surface pits or pores, i.e. the formation of an autocatalytic corrosion cell, which results in a serious localized corrosion breakdown. While localized attack is a well-known phenomenon for non-surface-treated Mg alloys [56, 58] little is known about the long-term stable resistance to pronounced localized corrosion in body fluid of micro-arc treated samples. However, the rapid increase in degradation rate after an initial period observed in the present study and reported in [31, 55, 59] can be attributed to severe pit formation. In general, the protective layer is characterized by the presence of pores, calderas and cracks (**Fig. 5.1**). Such "weak spots" can be easily penetrated by the physiological solution and may act as nuclei for localized corrosion attack. Gu et al. [31] describe this mechanism using the example of micro-arc oxidation-treated AZ31 alloy in simulated body fluid. According to Wang et al. [59], the corrosion is also accelerated if the coating is destroyed locally. They

relate the rapid corrosion to the galvanic effect between the exposed substrate and the coated substrate that served as a cathode. To solve this "problem" at least to some degree, an improvement in the quality of the oxide layer and/or sealing is recommended, as undertaken for example by Chen et al.[55] and Lu et al. [52, 53].

5.4.3 Micro-arc oxidation improves the bone-implant interface

A tight contact between cells and implant surface reveals a good bone-to-implant interface. It shows that the implant is tolerated well by the organism and indicates that the surface is osteoconductive. The porous pin surface of the MAO implants and reduced gas evolution because of higher corrosion resistance may explain increased new bone formation around MAO-treated implants [60]. MAO also inhibited fast Mg ion release. While Mg ions enhance the osteoblast apposition on the implant and promote new bone formation [61, 62], excessive Mg concentrations and/or corresponding pH changes might reduce bone cell activity and result in less bone formation around the samples, as seen for ZX50 and reported in other studies [63]. In MAO we observed that irritations in bone healing were minimized in the very first stage of fracture healing. It has also been reported that MAO-treated Mg-alloys possesses improved blood compatibility compared to untreated Mg [64], which is of great importance clinically. We found that even when MAO delayed the start of implant corrosion for just one week the positive biological response remained for up to 4 weeks, where osteoblast adhesions were still observed on the implant surface (**Figs. 5.6c and d)**. Significantly increased cell numbers on MAO-treated Mg–Ca alloys compared with untreated ones were also found by Gu et al. [26]. Accompanied with an acceleration of the MAO implant degradation, a detachment between the former formed bone tissue and the implant surface occurred. Thereby bone cells lost the implant as an osteoconductive base frame. Further new bone formations were consequently formed as irregular scattered woven bones at various places in the medullar cavity **(Fig. 5.6f and h).** At the initial implant site loose tissue remained after entire implant degradation (**Fig. 5.6f and h**). It is certain that these cell poor tissue areas were present due to the very fast degradation of the basic Mg alloy, which generated enhanced gas evolution, pH-increase, and high cell osmolarity [5, 65, 66]. For less fast degrading alloys a preservation of cell integrity during implant degradation can be expected, as the mentioned irritating side-effects would be minimized [19].

After fulfilling its task of bone restoration, it is desirable, to avoid future inflammatory effects, that no implant debris or corrosion products remain inside bone tissue.

No substrate or oxide layer remnants were visible in our histological slides after 24 weeks. This indicates that the ZX50 alloy is not only completely degradable in body fluid but also is the oxide layer. At the end of the study (week 24) the cortical bone and the bone marrow both recovered *restitio ad integrum*. These findings concur with those of Kraus et al. [19], who found that bone recovered even where there was massive gas formation due to Mg degradation. Due to enhanced formation of new bone at the MAO surface right after pin implantation, a few scattered bone trabeculae remained in the bone marrow at week 24. These are expected to decompose in the subsequent weeks and do not affect the functionality of the bone.

Clinically, an Mg-based implant is required which possesses good biocompatibility, maintains its mechanical integrity during the reparative phase (4-16 weeks; depending on fracture configuration and location, status of the adjacent soft tissues, as well as patient characteristics (species, age, health status, concurrent injuries/diseases) [1]) to ensure solid healing of the fractured bone, and afterwards degrades entirely within a short period of time. Here MAO showed itself to be an effective way not only to improve the corrosion resistance of magnesium alloys in the initial fracture healing period, but also to increase these alloys' surface bioactivity and later to induce enhanced degradation rate.

The fast degrading alloy ZX50 used in the present study needs to be modified towards enhanced degradation resistance in order to preserve its mechanical integrity during the reparative phase. First results with ultra-high-pure ZX50 (reduction of trace elements Fe, Cu, Ni, Mn and Si from 500 ppm to < 5 ppm) are highly promising. In particular, the absence of RE and Al additions might make them very interesting for pediatric surgery applications.

5.5 Conclusions

Surface treatment of Mg-alloys via micro-arc oxidation appears to be very interesting for biodegradable implant applications. MAO treatment generates a protective oxide layer with a high level of porosity. The protective layer, on the one hand, delays the initial corrosion process and thus, due to reduced hydrogen evolution, enhances the primary neo-formation of bone around the implant. The porous surface, on the other hand, generates inhomogeneous degradation via severe localized corrosion attacks, which increase significantly with the degradation of the implant in the later stage due to an ever-increasing surface-area to volume ratio. In conclusion, the results of improved initial corrosion

resistance, accompanied by the immediate build-up of a stable bone-implant interface and followed by accelerated degradation in the later stage, make micro-arc oxidation a promising method for achieving the degradation properties required to fulfill clinical demands for the use of magnesium-implants in osteosynthetic applications.

Acknowledgements

The authors very much appreciate the support of the Laura Bassi Center of Expertise BRIC (Bioresorbable Implants for Children), FFG, Austria, and the Staub/Kaiser Foundation, Switzerland. We are also grateful to the Institute of Biomedical Research at the Medical University of Graz for the provision of infrastructure facilities to perform this animal study.

References

[1] Frost HM. The biology of fracture healing. An overview for clinicians. Part I. Clin Orthop Relat Res 1989:283-93.

[2] Saris NE, Mervaala E, Karppanen H, Khawaja JA, Lewenstam A. Magnesium. An update on physiological, clinical and analytical aspects. Clin Chim Acta 2000;294:1-26.

[3] Wolf F, Cittadini A. Chemistry and biochemistry of magnesium. Mol Aspects Med 2003;24:3–9.

[4] Huan ZG, Leeflang MA, Zhou J, Fratila-Apachitei LE, Duszczyk J. *In vitro* degradation behavior and cytocompatibility of Mg-Zn-Zr alloys. J Mater Sci Mater Med 2010;21:2623-35.

[5] Witte F, Hort N, Vogt C, Cohen S, Kainer KU, R. W. Degradable biomaterials based on magnesium corrosion. Curr Opin Solid State Mater Sci 2008;12:63-72.

[6] Krause A, von der Höh N, Bormann D, Krause C, Bach F-W, Windhagen H, et al. Degradation behaviour and mechanical properties of magnesium implants in rabbit tibiae. J Mater Sci Mater Med 2010;45:624-32.

[7] Claes L. Mechanical Characterization of Biodegradable Implants. Clinical Materials 1992;10:41-6.

[8] Staiger MP, Pietak AM, Huadmai J, Dias G. Magnesium and its alloys as orthopedic biomaterials: a review. Biomaterials 2006;27:1728-34.

[9] Gray J, Luan B. Protective coatings on magnesium and its alloys—a critical review. J Alloys Compendium 2002;(1–2):88–113.

[10] Yamamoto A, Watanabe A, Sugahara K, Tsubakino H, Fukumoto S. Improvment of corrosion resistance of magnesium alloys by vapor deposition. Scr Mater 2001;44:1039-44.

[11] Verbrugge J. L'utilisation du magnésium dans le traitement chirurgical des fractures. Bull Mém Soc Nat Cir 1937;59:813–23.

[12] Reifenrath J, Krause A, Bormann D, von Rechenberg B, Windhagen H, Meyer-Lindenberg A. Profound differences in the *in-vivo*-degradation and biocompatibility of two very similar rare-earth containing Mg-alloys in a rabbit model. Materialwissenschaft und Werkstofftechnik 2010;41:1054-61.

[13] Huehnerschulte TA, Reifenrath J, von Rechenberg B, Dziuba D, Seitz JM, Bormann D, et al. *In vivo* assessment of the host reactions to the biodegradation of the two novel magnesium alloys ZEK100 and AX30 in an animal model. Biomedical engineering online 2012;11:14.

[14] Gunde P, Hänzi A, Sologubenko A, Uggowitzer P. High-strength magnesium alloys for degradable implant applications. Materials Science and Engineering A 2011;A:1047-54.

[15] Zhang BP, Geng L, Huang LJ, Zhang XX, Dong CC. Enhanced mechanical properties in fine-grained Mg–1.0Zn–0.5Ca alloys prepared by extrusion at different temperatures. Scripta Materialia 2010;63:1024-7.

[16] Orlov D, Ralston KD, Birbilis N, Estrin Y. Enhanced corrosion resistance of Mg alloy ZK60 after processing by integrated extrusion and equal channel angular pressing. Acta Materialia 2011;59:6176-86.

[17] Zberg B, Uggowitzer PJ, Loffler JF. MgZnCa glasses without clinically observable hydrogen evolution for biodegradable implants. Nat Mater 2009;8:887-91.

[18] Castellani C, Lindtner RA, Hausbrandt P, Tschegg E, Stanzl-Tschegg SE, Zanoni G, et al. Bone-implant interface strength and osseointegration: Biodegradable magnesium alloy versus standard titanium control. Acta biomaterialia 2011;7:432-40.

[19] Kraus T, Fischerauer SF, Hanzi AC, Uggowitzer PJ, Loffler JF, Weinberg AM. Magnesium alloys for temporary implants in osteosynthesis: *in vivo* studies of their degradation and interaction with bone. Acta biomaterialia 2012;8:1230-8.

[20] Witte F, Kaese V, Haferkamp H, Switzer E, Meyer-Lindenberg A, Wirth CJ, et al. *In vivo* corrosion of four magnesium alloys and the associated bone response. Biomaterials 2005;26:3557-63.

[21] Tschegg EK, Lindtner RA, Doblhoff-Dier V, Stanzl-Tschegg SE, Holzlechner G, Castellani C, et al. Characterization methods of bone-implant-interfaces of bioresorbable and titanium implants by fracture mechanical means. Journal of the mechanical behavior of biomedical materials 2011;4:766-75.

[22] Von der Höh N, Bormann D, Lucas A, Denkena B, Hackenbroich C, Meyer-Lindenberg A. Influence of Different Surface Machining Treatments of Magnesium-based Resorbable Implants on the Degradation Behavior in Rabbits. Advanced Engineering Materials 2009;11:B47-B54.

[23] Revell PA, Damien E, Zhang XS, Evans P, Howlett CR. The Effect of Magnesium Ions on Bone Bonding to Hydroxyapatite Coating on Titanium Alloy Implants. Key Eng Mater 2004;254-256:447-50.

[24] Janning C, Willbold E, Vogt C, Nellesen J, Meyer-Lindenberg A, Windhagen H, et al. Magnesium hydroxide temporarily enhancing osteoblast activity and decreasing the osteoclast number in peri-implant bone remodelling. Acta biomaterialia 2010;6:1861-8.

[25] Stroganov G, Savitsky E, Mikhailovich T, Nina M, Terekhova V, Fedorovna V, et al. Magnesium-base alloys for use in bone surgery. US Patent no 3,687,1351972.

[26] Gu X, Li N, Zhou W, Zheng Y, Zhao X, Cai Y, et al. Corrosion resistance and surface biocompatibility of a microarc oxidation coating on a Mg–Ca alloy. Acta biomaterialia 2010;7:1880–9.

[27] Hornberger H, Virtanen S, Boccaccini AR. Biomedical coatings on magnesium alloys – A review. Acta biomaterialia.

[28] Huang Y-S, Liu H-W. TEM Analysis on Micro-Arc Oxide Coating on the Surface of Magnesium Alloy. Journal of Materials Engineering and Performance 2011;20:463-7.

[29] Shadanbaz S, Dias GJ. Calcium phosphate coatings on magnesium alloys for biomedical applications: a review. Acta biomaterialia 2012;8:20-30.

[30] Guo H, An M. Growth of ceramic coatings on AZ91D magnesium alloys by micro-arc oxidation in aluminate-fluoride solutions and evaluation of corrosion resistance. Applied Surface Science 2005;246:229-38.

[31] Gu Y, Chen C-f, Bandopadhyay S, Ning C, Zhang Y, Guo Y. Corrosion mechanism and model of pulsed DC microarc oxidation treated AZ31 alloy in simulated body fluid. Applied Surface Science 2012;258:6116-26.

[32] Zeng R-c, Zhang J, Huang W-j, Dietzel W, Kainer KU, Blawert C, et al. Review of studies on corrosion of magnesium alloys. Transactions of Nonferrous Metals Society of China 2006;16, Supplement 2:s763-s71.

[33] Zhang J, Gu Y, Guo Y, Ning C. Electrochemical behavior of biocompatible AZ31 magnesium alloy in simulated body fluid. J Mater Sci 2012;47:5197-204.

[34] Jo JH, Hong JY, Shin KS, Kim HE, Koh YH. Enhancing Biocompatibility and Corrosion Resistance of mg Implants via Surface Treatments. Journal of biomaterials applications 2011.

[35] Hanzi AC, Gerber I, Schinhammer M, Loffler JF, Uggowitzer PJ. On the *in vitro* and *in vivo* degradation performance and biological response of new biodegradable Mg-Y-Zn alloys. Acta biomaterialia 2010;6:1824-33.

[36] Hanzi AC, Sologubenko AS, Uggowitzer PJ. Design strategy for new biodegradable Mg–Y–Zn alloys for medical applications. Int J Mat Res 2009;100:1127-36.

[37] http://www.ahc-surface.com/en/surface-treatment/processes/magoxid-coat®

[38] Feldkamp LA, Goldstein SA, Parfitt AM, Jesion G, Kleerekoper M. The direct examination of three-dimensional bone architecture *in vitro* by computed tomography. J Bone Miner Res 1989;4:3-11.

[39] Kothari M, Keaveny TM, Lin JC, Newitt DC, Genant HK, Majumdar S. Impact of spatial resolution on the prediction of trabecular architecture parameters. Bone 1998;22:437-43.

[40] Balto K, Muller R, Carrington DC, Dobeck J, Stashenko P. Quantification of periapical bone destruction in mice by micro-computed tomography. J Dent Res 2000;79:35-40.

[41] Wong H, Yeung K, Lam K, Tam V, Chu P, Luk K. Biodegradable polymer-based coating to control the performance of magnesium alloy orthopedic implants. Biomaterials 2010;31:2084–96.

[42] Donath K. Die Trenn-Dünnschliff-Technik zur Herstellung histologischer Präparate von nicht schneidbaren Geweben und Materialien. Deutsche Zeitschrift für Mund-Kiefer Gesichtschirurgie 1988:197-206.

[43] Kieswetter K, Schwartz Z, Dean DD, Boyan BD. The role of implant surface characteristics in the healing of bone. Critical reviews in oral biology and medicine: an official publication of the American Association of Oral Biologists 1996;7:329-45.

[44] Blawert C, Heitmann V, Dietzel W, Nykyforchyn HM, Klapkiv MD. Influence of process parameters on the corrosion properties of electrolytic conversion plasma coated magnesium alloys. Surface and Coatings Technology 2005;200:68-72.

[45] Bala Srinivasan P, Blawert C, Dietzel W. Effect of plasma electrolytic oxidation coating on the stress corrosion cracking behaviour of wrought AZ61 magnesium alloy. Corrosion Science 2008;50:2415-8.

[46] Ryu HS, Hong S-H. Corrosion Resistance and Antibacterial Properties of Ag-Containing MAO Coatings on AZ31 Magnesium Alloy Formed by Microarc Oxidation. Journal of The Electrochemical Society 2010;157:C131-C6.

[47] Blawert C, Dietzel W, Ghali E, Song G. Anodizing Treatments for Magnesium Alloys and Their Effect on Corrosion Resistance in Various Environments. Advanced Engineering Materials 2006;8:511-33.

[48] Pourbaix M. Atlas of electrochemical equilibria in aqueous solutions: National Association of Corrosion Engineers; 1974.

[49] Sathiyanarayanan S, Azim SS, Venkatachari G. Corrosion resistant properties of polyaniline–acrylic coating on magnesium alloy. Applied Surface Science 2006;253:3113-2117.

[50] He YD, Fu HF, Li XG, Gao W. Microstructure and properties of mechanical attrition enhanced electroless Ni–P plating on magnesium alloy. Scripta Materialia 2008;58:504-7.

[51] Lu P, Cao L, Xu X, Wu X. Evaluation of magnesium ions release, biocorrosion and hemocompatibility of MAO/PLLA-modified magnesium alloy WE42. Journal of Biomedical Materials Research B, Applied Materials 2010;96B:101-9.

[52] Lu P, Cao L, Liu Y, Xu X, Wu X. Evaluation of magnesium ions release, biocorrosion, and hemocompatibility of MAO/PLLA-modified magnesium alloy WE42. Journal of Biomedical Materials Research Part B: Applied Biomaterials 2011;96B:101-9.

[53] Lu P, Liu Y, Guo M, Fang H, Xu X. Corrosion and drug release properties of EN-plating/PLGA composite coating on MAO film. Materials Science and Engineering: C 2011;31:1285-9.

[54] Curran J, Clyne T. Thermo-physical properties of plasma electrolytic oxide coatings on aluminium. Surface & Coatings Technology 199 (2005) 168– 176 2005;199:168– 76.

[55] Chen S, Guan S, Li W, Wang H, Chen J, Wang Y, et al. *In vivo* degradation and bone response of a composite coating on Mg–Zn–Ca alloy prepared by microarc oxidation and electrochemical deposition. Journal of Biomedical Materials Research Part B: Applied Biomaterials 2012;100B:533-43.

[56] Tunold R, Holtan H, Berge M-BH, Lasson A, Steen-Hansen R. The corrosion of magnesium in aqueous solution containing chloride ions. Corrosion Science 1977;17:353-65.

[57] Song G, Atrens A, Dargusch M. Influence of microstructure on the corrosion of diecast AZ91D. Corrosion Science 1998;41:249-73.

[58] Song G. Corrosion of Magnesium Alloys: Woodhead Publishing; 2011.

[59] Wang YQ, Zheng MY, Wu K. Microarc oxidation coating formed on SiCw/AZ91 magnesium matrix composite and its corrosion resistance. Materials Letters 2005;59:1727-31.

[60] Paul W, Sharma CP. Nanoceramic Matrices: Biomedical Applications. Am J Biochem Biotech 2006;2:41-8.

[61] Zreiqat H, Howlett CR, Zannettino A, Evans P, Schulze-Tanzil G, Knabe C, et al. Mechanisms of magnesium-stimulated adhesion of osteoblastic cells to commonly used orthopaedic implants. J Biomed Mater Res 2002;62:175-84.

[62] Ajroud K, Sugimori T, Goldmann WH, Fathallah DM, Xiong JP, Arnaout MA. Binding Affinity of Metal Ions to the CD11b A-domain Is Regulated by Integrin Activation and Ligands. The Journal of biological chemistry 2004;279:25483-8.

[63] Serre CM, Papillard M, Chavassieux P, Voegel JC, Boivin G. Influence of magnesium substitution on a collagen-apatite biomaterial on the production of a calcifying matrix by human osteoblasts. J Biomed Mater Res 1998;42:626-33.

[64] Wang D-W, Cao Y, Qiu H, Bi Z-G. Improved blood compatibility of Mg-1.0Zn-1.0Ca alloy by micro-arc oxidation. Journal of Biomedical Materials Research Part A 2011;99A:166-72.

[65] Song GL, Atrens A. Corrosion Mechanisms of Magnesium Alloys. Advanced Engineering Materials 1999;1:11-33.

[66] Song G. Control of biodegradation of biocompatible magnesium alloy. Corrosion Science 2007;49:1696-701.

[67] Gunde P. Biodegradable magnesium alloys for osteosynthesis – alloy development and surface modifications [PhD thesis]: ETH Zurich; 2010.

6 Summary, Discussion and Outlook

The development process of a functional biodegradable implant requires a multidisciplinary approach to bring material properties and biological realities in accordance with each other. This thesis featured efficient methods to explore the major biological material properties related to biodegradation, bone-implant-interface, biocompatibility, and biofunctionality in a development process of Mg-based implants designated for osteosynthetic application. In each field, a high specific knowledge was acquired and high standard methodologies were established.

In vivo study methods have been used, as the complexity of a living organism and its mutual interference with the biomaterial is hardly reproducible in an in vitro setting. Especially in Mg-testing, the majority of studies that have systematically compared Mg-alloys in vivo and in vitro showed significant differences between the degradation behavior [1-4]. Over the last years, the complex corrosion process of Mg in a relatively harsh environment like the human body (pH values between 7.4 and 7.6 at temperature of ~37, biological fluids with a salt content of~0.9 wt.%, chloride ions at levels of 150mmol/L, dissolved oxygen, sodium, potassium, calcium, magnesium, phosphate, sulphate ions, amino acids, proteins, plasma and several other substances [5, 6]) and its multifaceted reactions became better understood. Consequently, in vitro testing protocols have been significantly adjusted and are nowadays used for effective screening of suitable materials, thus reducing the need of animal testing dramatically [7]. However, many biofunctional investigations including systemic reactions or fracture-healing properties related to an implant material will so far remain a domain of in vivo testing.

Many studies, including the works of this thesis, attested Mg excellent biomechanical, electrochemical, and biofunctional properties, which make the material appropriate for orthopaedic applications. The key benefits of Mg as an osteosynthetic device and its potential drawbacks are listed in **Table 6.1** and **6.2**.

Table 6.1:Key benefits of Mg as osteosynthetic implant (modified from Kirkland [7])

Benefit	Description
Low density and reduction of stress shielding	Mg density (1.738 g/cm3) [8] and elastic modulus (~45) GPa is similar to that of cortical bone (1.75-2.1 g/cm3; ~20 GPa) [9, 10]. Current orthopaedic implants like Ti alloy (110-120 Gpa) or stainless steel (210 GPa) can cause implant failure due to a much higher elastic modulus, density, and yield strength than that of bone. This process is called stress shielding by which bone mass and density will decrease in proximity of an implant with a higher stiffness, as it transfers the load away from adjacent bone [11]. As mechanical properties of pure Mg are very close to natural bone, stress shielding related problems can be greatly reduced.
High damping capacity	Mg has the highest dumping capacity of any metal [12]. This shock- and vibration-absorbing ability could provide benefits especially in load-bearing applications.
Machinability and dimensional stability	Mg is easy to machine and stable complex shapes can be easily produced [13].
Biocompatibility and osteogenesis	Mg is considered biocompatible [14-17] and has been shown to possess osteoconductive and osteoinductive properties [16, 18, 19]. Mg ions are intimately involved in the formation of biological apatites and thus have a positive influence on bone fragility and strength [16].
Safe degradation	Mg's ion release in the body is dealt with effectively and eventually corrosion results in complete degradation [14-16]. Despite the applicability as a temporary implant, safe wear particles metabolisation and limited exposure to a "foreign" object minimises the appearance of acute inflammation and eventually implant failure [20].

Table 5.2: Potential drawbacks of Mg as osteosynthetic implant (modified from Kirkland [7])

Drawback	Description
Low elastic modulus	The low elastic modulus of Mg can lead to mechanical failure in load-bearing applications when compressive loads exceed 3.500 N [21].
Fast degradation	Mg purity and allying elements have been used to control the degradation of Mg. Rapid degradation and consecutively high evolution of hydrogen gas can still be an issue [22, 23].
Resorption problems	Too quickly release of Mg and other element ions can cause adverse biological reactions. Corrosion controlling alloying elements must be selected with non-toxicity.
Hydrogen gas	At high degradation the amount of hydrogen gas release can exceed the resorption ability of the surrounding tissues (tolerable rates of hydrogen evolution <0.01 ml/cm^2/day, depending on the location of the implant and its surrounding environment [22]). An accumulation of gas in cysts may cause separation of tissue and/or tissue layers [24], delay healing, lead to necrosis of surrounding tissue [25], and in a worst case scenario, block the blood stream, causing death [26].

Mechanical and biological properties determine the success rate of a biomaterial in its clinical application. Any implant that has been designed for osteosynthetic applications has to sustain its load without deformation. Maintenance of mechanical support is crucial throughout the entire healing phase until the bone regains its functionality. As corrosion processes influence the mechanical integrity of the material significantly, it is desired to design an implant that initiates degradation not before fracture consolidation occurs. On the

other hand, implant degradation after fracture consolidation is favored in a homogenous manner with a releasing rate of element ions that can be appropriately dealt by the body (e.g. excess of Mg excreted via kidneys or hydrogen gas absorbed via soft tissues). Furthermore, to ensure absolute biocompatibility, complete degradability and full absorbability, the use of toxic or exogenous alloying elements must be avoided.

Concerns about the implantation of exogenous alloying elements have been increased recently, as zirconium has been reported to reduce the healing properties [27], aluminium remains in the organism and can lead to unpredictable effects, the application of silver might result in a silver-disease [28], yttrium remains local, even for years [29] and can have negative effects on the immunological system [30], and as quotable literature focusing on the toxic long-term effects of rare earth elements (REE) in the organism is still not available. Hence, the applications of the mentioned alloying elements have to be insistently refused, especially for an application in children.

Therefore, current research focuses on the development of REE- and yttrium-free Mg-alloys that only consist of natural occurring human elements. Ultra-high purification processes and the combination of Mg-Zn-Ca alloys have already shown promising preliminary results. Also surface modification and coatings of Mg-alloys is gaining increasing interest to further improve the implant biofunctionalities (e.g. implementation of anti-inflammatory properties and anti-bacterial or bone stimulating additives. These developments will be the focus of the magnesium research community in upcoming years. Today, the specifications, a Mg-based implant material has to fulfil as a temporary osteosynthetic device for successful clinical application, are defined as:

- Mechanical properties of yield strength > 240MPa, tensile strength > 300MPa, and elongation to fracture > 20% (similar to human bone).
- Maintenance of mechanical integrity for four to six weeks during healing phase.
- Direct bone-implant-interface during healing phase.
- Highly purification with trace elements in sum < 20 ppm.
- Implant degradation rate per year: $0.25 < Pm < 2.5$ mm y^{-1}.
- Total degradation process within a time frame of 1.5 years, with respect to the turn over of the skeleton.
- Biocompatibility of all alloying elements.
- Biofunctional interference with fracture consolidation and restitution ad integrum.

Their realization will be the future challenge for a multidisciplinary research community.

References

[1] Li Z, Gu X, Lou S, Zheng Y. The development of binary Mg-Ca alloys for use as biodegradable materials within bone. Biomaterials 2008;29:1329-44.

[2] Witte F, Fischer J, Nellesen J, Crostack HA, Kaese V, Pisch A, et al. In vitro and in vivo corrosion measurements of magnesium alloys. Biomaterials 2006;27:1013-8.

[3] Zhang S, Zhang X, Zhao C, Li J, Song Y, Xie C, et al. Research on an Mg–Zn alloy as a degradable biomaterial. Acta biomaterialia 2010;6:626-40.

[4] Ren Y, Wang H. Study of biodegradation of pure magnesium. Key Eng Mater 2007;342-343:601-4.

[5] Kamachimudali U, Sridhar TM, Raj B. Corrosion of bio implants. Sadhana 2003;28:601-37.

[6] Ivanova EP, Bazaka K, Crawford RJ. 7 - Bioinert ceramic biomaterials: advanced applications. In: Ivanova EP, Bazaka K, Crawford RJ, editors. New Functional Biomaterials for Medicine and Healthcare: Woodhead Publishing; 2014. p. 173-86.

[7] Kirkland NT, Birbilis N. Magnesium Biomaterials: Design, Testing, and Best Practice: Springer International Publishing; 2013.

[8] TAFST D. Magnesium alloys. The American Foundry Society, Schaumburg 2006.

[9] Richards AM, Coleman NW, Knight TA, Belkoff SM, Mears SC. Bone density and cortical thickness in normal, osteopenic, and osteoporotic sacra. Journal of osteoporosis 2010;2010.

[10] Staiger MP, Pietak AM, Huadmai J, Dias G. Magnesium and its alloys as orthopedic biomaterials: a review. Biomaterials 2006;27:1728-34.

[11] Pietrzak WS, Sarver D, Verstynen M. Bioresorbable implants: practical considerations. Bone 1996;19:109S-19S.

[12] Avedesian M, Baker H. Magnesium and magnesium alloys. ASM Int 1999.

[13] Emley EF. Principles of Magnesium Technology: Elsevier Science & Technology; 1966.

[14] Saris NE, Mervaala E, Karppanen H, Khawaja JA, Lewenstam A. Magnesium. An update on physiological, clinical and analytical aspects. Clin Chim Acta 2000;294:1-26.

[15] Vormann J. Magnesium: nutrition and metabolism. Mol Aspects Med 2003;24:27-37.

[16] Okuma T. Magnesium and bone strength. Nutrition 2001;17:679–80.

[17] Wolf F, Cittadini A. Chemistry and biochemistry of magnesium. Mol Aspects Med 2003;24:3–9.

[18] Revell PA, Damien E, Zhang XS, Evans P, Howlett CR. The Effect of Magnesium Ions on Bone Bonding to Hydroxyapatite Coating on Titanium Alloy Implants. Key Eng Mater 2004;254-256:447-50.

[19] Zreiqat H, Howlett CR, Zannettino A, Evans P, Schulze-Tanzil G, Knabe C, et al. Mechanisms of magnesium-stimulated adhesion of osteoblastic cells to commonly used orthopaedic implants. J Biomed Mater Res 2002;62:175-84.

[20] Bach FW. Development of biocompatible magnesium alloys and investigation of the degradation behaviour. Sustainable bioresorbable and permanent implants of metallic and ceramic materials. University of Hanover2006.

[21] Davis KG, Marras WS, Waters TR. Evaluation of spinal loading during lowering and lifting. Clinical biomechanics (Bristol, Avon) 1998;13:141-52.

[22] Baker H, Committee ASMIH. ASM Specialty Handbook: Magnesium and Magnesium Alloys: ASM International; 1999.

[23] Witte F, Hort N, Vogt C, Cohen S, Kainer KU, R. W, et al. Degradable biomaterials based on magnesium corrosion. Curr Opin Solid State Mater Sci 2008;12:63-72.

[24] Song G. Control of biodegradation of biocompatible magnesium alloys. Corrosion Science 2007;49:1696-701.

[25] Meyer-Lindenberg A, Windhugen H. US 200410241036.

[26] Zeng R, Dietzel W. Progress and challenge for magnesium alloys as biomaterials. Adv Eng Mater 2008;10:B3-B14.

[27] Martinelli E, Fischerauer SF. PHAs as bioresorbable implants? – A study in a living rat model. Proceedings of the 24th International Symposium on Pediatric Surgical Research 2011.

[28] Sudmann E, Vik H, Rait M, Todnem K, Andersen KJ, Julsham K, et al. Systemic and local silver accumulation after total hip replacement using silver-impregnated bone cement. Medical progress through technology 1994;20:179-84.

[29] Amerstorfer F, Fischerauer SF, Eichler J, Draxler J, Zitek A, Löffler J, et al. Long-term in vivo degradation behavior and element distribution of the magnesium alloys WZ21 and ZX50. Acta biomaterialia 2015:(under Review).

[30] Pichler K, Fischerauer SF, Ferlic P, Martinelli E, Brezinsek H, Uggowitzer PJ, et al. Immunological Response to Biodegradable Magnesium Implants. JOM 2014;66:573-9.

7 Appendix

CURRICULUM VITAE

Name:	Stefan Franz Fischerauer
Date of birth:	6 August 1982, Heiligenkreuz am Waasen (Austria)
Nationality:	Austria
Email:	stefan.fischerauer@medunigraz.at

Education

Mag. rer. nat. (equivalent to M.Sc.) 2014
- University of Graz, Faculty of Environmental, Regional and Educational Sciences, Institute of Sports Sciences
- Diploma thesis: Kinetic and Kinematic Differences Between Idiopathic and Neurologic Toe-walkers

Dr. med. univ. (equivalent to MD) 2010
- Medical University of Graz, Department of Pediatric and Adolescent Surgery
- Diploma thesis: In Vivo Micro-CT Exploration of Bioresorbable Magnesium Implants – Evaluation in a Transcortical Rat Model

Academic Honor

Scholarship funded by the James H. & Myra Hume Jones International House Program at the Jacksonville State University, AL 2001/02

Further Education

Extracurricular courses taken at the Medical University of Graz

Basismodule: Teaching at the Medical University of Graz	2014
Professional University Didactic	2013
Motivational Lecturing	2013
How to Master Difficult Situations in Conversations	2012
Effectuation – Future-orientated Actions	2012
Leadership: The Personality Factor	2012
Presentation Techniques and Rhetoric	2012
Advanced Statistics	2012
Basic Statistics	2012
Medical Writing Course – Preparing 2 Publish	2009
Massage Therapist Training	2003
Mandatory Military Service	2002
Fitness Instructor Training	2001

Clinical History

Residency

University Hospital Graz, Department of Trauma Surgery since 2015	2015-
University Hospital Graz, Department of Orthopedics	2013/14
AUVA Trauma Hospital Graz	2013

Internships

University Hospital Graz, Department of Internal Medicine	2009/10
State Hospital Bruck/Mur, Emergency Room	2009/10
Residency at Dr. Pösinger's office, Weiz	2009
Sigmund Freud Hospital Graz, Paediatric and Adolescent Psychiatry	2009
University Hospital Graz, Department of Paediatric and Adolescent	2009
University Hospital Graz, Department of Neurology	2009
University Hospital Graz, Department of Paediatric and Adolescent Surgery	2009
AUVA Trauma Hospital Graz	2008
University Hospital Graz, Department of Trauma Surgery	2006

Affiliations

Resident for Orthopedics and Traumatology,	
University Hospital Graz, Department of Trauma Surgery	2015-
University Hospital Graz, Department of Orthopedics	2013/14
AUVA Trauma Hospital Graz	2013
Lecturer of Anatomy at University of Graz, Insitute of Sport Science	2013-15
Lecturer of Anatomy and Physiology at College of Education Graz	2013-15
Graduate researcher, PhD-student at Medical University Graz, Laura Bassi Center of Expertise BRIC - Bioresorbable Implants for Children Mentor: Assoz. Prof. Priv.-Doz. Dr. Annelie Weinberg	2010-13
Massage Therapist and Sports Medical Instructor "Graz 99ers", national hockey league team	2007-10
Undergraduate Researcher Human Performance Research Center Graz Under the guidance of Univ. Prof. Mag. Dr. Wolfram Müller	2009

Research career

Publications

Amerstorfer F, Fischerauer SF, Eichler J, Draxler J, Zitek A, Löffler J, et al. Long-term in vivo degradation behavior and element distribution of the magnesium alloys WZ21 and ZX50. Acta biomaterialia 2015:(under Review).

Fischerauer, SF; Berger, L; Eichler, J; Weiß, B; Rosmarin, W; Tschegg, E; Weinberg, AM; Castellani, C. ESIN for lower extremity fractures in children – is interlocking essential to prevent loss of stabilisation? A biomechanical analysis in an ovine tibia model. J of Trauma: (under review).

Berger, L; Fischerauer, SF; Weiß, B; Celarek, A; Castellani, C; Weinberg, AM; Tschegg, E. Unlocked and locked elastic stable intramedullary nailing in an ovine tibia fracture model: A biomechanical study. Mater Sci Eng C Mater Biol Appl. 2014; 40: 267-274.

Kraus, T; Moszner, F; Fischerauer, SF; Fiedler, M; Martinelli, E; Eichler, J; Witte, F; Willbold, E; Schinhammer, M; Meischel, M; Uggowitzer, PJ; Löffler, JF; Weinberg, AM. Biodegradable Fe-based alloys for use in osteosynthesis: Outcome of an in vivo study after 52 weeks. Acta Biomater. 2014; 10(7):3346-3353.

Pichler, K; Fischerauer, SF; Ferlic, P; Martinelli, E; Brezinsek, HP; Uggowitzer, PJ; Löffler, JF; Weinberg, AM. Immunological response to biodegradable magnesium implants. J of Metals (JOM). 2014; 66: 573 – 579.

Celarek, A; Fischerauer, SF; Weinberg, AM; Tschegg, EK. Fracture patterns of the growth plate and surrounding bone in the ovine kneejoint at different ages. J Mech Behav Biomed Mater. 2013; 29C: 286-294.

Fischerauer, SF; Kraus, T; Wu, X; Tangl, S; Sorantin, E; Uggowitzer, PJ; Hänzi, AC; Löffler, JF; Weinberg, AM; In Vivo Degradation Performance of Micro-Arc Oxidized Magnesium Implants: A Micro-CT Study in Rats. Acta Biomater. 2013; 2: 5411- 5420.

Heidari, N; Kraus, T; Fischerauer, SF; Tesch, N; Weinberg, AM; Do the Presence of Pathologic Changes and the Level of Operator Experience Alter the Rate of Intra-Articular Injection of the First Metatarsophalangeal Joint?: A Cadaver Study. J Am Podiatr Med Assoc. 2013; 103(3): 204-207.

Celarek, A; Kraus, T; Tschegg, EK; Fischerauer, SF; Stanzl-Tschegg, S; Uggowitzer, PJ; Weinberg, AM; PHB, crystalline and amorphous magnesium alloys: Promising candidates for bioresorbable osteosynthesis implants? Mater Sci Eng C. 2012; 32(6): 1503-1510.

Kraus, T; Fischerauer, SF; Hänzi, AC; Uggowitzer, PJ; Löffler, JF; Weinberg, AM; Magnesium alloys for temporary implants in osteosynthesis: in vivo studies of their degradation and interaction with bone. Acta Biomater. 2012; 8(3): 1230-1238.

Tschegg, EK; Celarek, A; Fischerauer, SF; Stanzl-Tschegg, S; Weinberg, AM; Fracture properties of growth plate cartilage compared to cortical and trabecular bone in ovine femora. Journal of the Mechanical Behavior of Biomedical Materials. 2012; 14(11): 119-129.

Wessels, V; Le Mene, G; Fischerauer, SF; Kraus, T; Weinberg, AM; Uggowitzer, PJ; Loffler, JF; In Vivo Performance and Structural Relaxation of Biodegradable Bone Implants Made from Mg-Zn-Ca Bulk Metallic Glasses. Adv Eng Mater. 2012; 14(6): B357-B364.

Oral Presentations (excerpt)

Basic Anatomies of Bone, Muscle, and Joint. Doctoral School, Medical University of Graz; 07.04.2014; Graz, Austria.

Ultra-pure magnesium alloys for use as biodegradable pediatric osteosynthetic material. 33rd Annual Meeting. 2014; European Paediatric Ortopaedic Society ; 02.04.2014 - 05.04.2014; Bruges, Belgium.

Biomechanical comparison of fatigue and load-bearing performance of locked and unlocked elastic stable intramedullary nailing. 33rd Annual Meeting. 2014; European Paediatric Ortopaedic Society ; 02.04.2014 - 05.04.2014; Bruges, Belgium.

Biomaterials. Ausbildungsseminar der ÖGO - Grundlagen der Orthopädie; 07.10.2013 - 08.10.2013 and 07.10.2014; Graz, Austria.

Magnesium alloys for temporary implants in Micro-arc oxidation of biodegradable magnesium implant surface approaches degradation performance to fracture consolidation. EFORT; 23.05.2012 - 25.05.2012; Berlin, Germany.

In-vivo effects of micro-arc oxidation on magnesium-based implants. 33rd SICOT Orthopaedic Conference; 28.11.2012-30.11.2012; Dubai, United Arab Emirates.

Micro-Arc oxidation of biodegradable Magnesium implant: In vivo findings of a rat study. 4th Symposium on Biodegradable Metals; 27.08.-01.09.2012; Maratea, Italy.

Use of Magensium-Based Biodegradable Implants for ESIN in Children. 31st Annual Meeting European Paediatric Orthopaedic Society; 18.04.2012 - 21.04.2012; Helsinki, Finland.

Biodegradation of magnesium implants ZX50 and WZ21 in a transepiphyseal rat model. Jahrestagung der deutschen Gesellschaft für Biomaterialien; 01.11.2012 - 03.11.2012; Hamburg, Germany.

Magnesium Alloys for Temporary Implants in Osteosynthesis: In-vivo Studies of their Degradation and Interaction with Bone. Proceedings of the 24th International Symposium on Pediatric Surgical Research. 24th International Symposium on Pediatric Surgical Research; 08.09.2011 - 10.09.2011; Graz, Austria.

Online Micro-CT Monitoring of the in vivo Degradation of Mg Pin Implants in the Growing Rat Skeleton. 17th Global Congress on Health & Medicine in Sport; 23.07.2011 - 31.07.2011; Manchester, UK.